Bose-Einstein Condensation in Low-Dimensional Trapped Gases

ACADEMISCH PROEFSCHRIFT

ter verkrijging van de graad van doctor
aan de Universiteit van Amsterdam,
op gezag van de Rector Magnificus
prof. mr. P.F. van der Heijden
ten overstaan van een door het college voor promoties ingestelde
commissie, in het openbaar te verdedigen in de Aula der Universiteit
op woensdag 9 april 2003 te 14:00 uur

door

Dmitry Sergeevich Petrov

geboren te Moskou, Rusland

Promotiecommissie:

Promotor:	Prof. dr. J. T. M. Walraven
Co-promotor:	Prof. dr. G. V. Shlyapnikov
Overige Leden:	Prof. dr. H. J. Bakker Prof. dr. H. B. van Linden van den Heuvell Prof. dr. A. M. M. Pruisken Prof. dr. C. Salomon Prof. dr. S. Stringari Prof. dr. B. J. Verhaar
Faculteit:	Faculteit der Natuurwetenschappen, Wiskunde en Informatica

The work described in this thesis was part of the research program of the
Stichting voor Fundamenteel Onderzoek der Materie (FOM),
which is financially supported by the
Nederlandse Organisatie voor Wetenschappelijk Onderzoek (NWO)
and was carried out at the

FOM Institute AMOLF
Kruislaan 407,
1098 SJ, Amsterdam,
The Netherlands

Contents

This Thesis is based on the following papers:

Chap. 3 D.S. Petrov, M. Holzmann, and G.V. Shlyapnikov, *Bose-Einstein condensation in quasi-2D trapped gases*, Phys. Rev. Lett. **84**, 2551 (2000)

D.S. Petrov, M.A. Baranov, and G.V. Shlyapnikov, *Superfluid transition in quasi-2D Fermi gases*, accepted for publication in Phys. Rev. A

Chap. 4 D.S. Petrov and G.V. Shlyapnikov, *Interatomic collisions in a tightly confined Bose gas*, Phys. Rev. A **64**, 012706 (2001)

I. Bouchoule, M. Morinaga, C. Salomon, and D.S. Petrov, *Cesium gas strongly confined in one dimension: Sideband cooling and collisional properties*, Phys. Rev. A **65**, 033402 (2002)

Chap. 5 D.S. Petrov, G.V. Shlyapnikov, and J.T.M. Walraven, *Regimes of quantum degeneracy in trapped 1D gases*, Phys. Rev. Lett. **85**, 3745 (2000)

Chap. 6 D.S. Petrov, G.V. Shlyapnikov, and J.T.M. Walraven, *Phase-fluctuating 3D Bose-Einstein condensates in elongated traps*, Phys. Rev. Lett. **87**, 050404 (2001)

S. Dettmer, D. Hellweg, P. Ryytty, J.J. Arlt, W. Ertmer, K.Sengstock, D.S. Petrov, G.V. Shlyapnikov, H. Kreutzmann, L. Santos, and M. Lewenstein, *Observation of phase fluctuations in elongated Bose-Einstein condensates*, Phys. Rev. Lett **87**, 160406 (2001)

Other papers to which the author contributed:

- M.A. Baranov and D.S. Petrov, *Critical temperature and Ginzburg-Landau equation for a trapped Fermi gas*, Phys. Rev. A **58**, R801 (1998)
- M.A. Baranov and D.S. Petrov, *Low-energy collective excitations in a superfluid trapped Fermi gas*, Phys. Rev. A **62**, 041601(R) (2000)
- P. Rosenbusch, D.S. Petrov, S. Sinha, F. Chevy, V. Bretin, Y. Castin, G.V. Shlyapnikov, and J. Dalibard, *Critical rotation of a harmonically trapped Bose gas*, Phys. Rev. Lett. **88**, 250403 (2002)
- I. Shvarchuck, Ch. Buggle, D.S. Petrov, K. Dieckmann, M. Zielonkowski, M. Kemmann, T.G. Tiecke, W. von Klitzing, G.V. Shlyapnikov, and J.T.M. Walraven, *Bose-Einstein condensation into non-equilibrium states studied by condensate focusing*, Phys. Rev. Lett. **89**, 270404 (2002)
- D.S. Petrov, *Three-body problem in Fermi gases with short-range interparticle interaction*, Phys. Rev. A **67**, 010703(R) (2003)

Chapter 1 Introduction

1.1 Background

Nature provides us with three spatial coordinates to describe various phenomena which happen in our daily life. We often do not use all the coordinates as it is sufficient to build a description or a model in 2-dimensional or even in 1-dimensional terms using either symmetry or necessity considerations. Low-dimensional systems were always used as textbook examples aimed to make the description of phenomena technically easier and the phenomena themselves physically transparent. This does not mean, however, that all low-dimensional problems are only poor dependent relatives of the rich family of colorful and challenging 3D physics. Dilute low-dimensional gases present an example of many-body systems that stand by themselves and for which the dimensionality is essential.

Bose-Einstein condensation (BEC) is a quantum statistics phenomenon which occurs in a 3D system of bosons (particles with an integer spin) when the characteristic thermal de Broglie wavelength of particles exceeds the mean interparticle separation. Under this condition it is favorable for particles to occupy a single ground state, and below a critical temperature the population of this state becomes macroscopic. This phenomenon has been predicted as a result of the work of Bose [1] and Einstein [2] in the mid twenties. Since that time, a number of phenomena have been considered as manifestations of BEC: superfluidity in liquid helium, high-T_c superconductivity in some materials, condensation of hypothetical Higgs particles, BEC of pions and so on. Bose-Einstein condensation in dilute gases has been observed in 1995 in pioneering experiments with clouds of magnetically trapped alkali atoms at JILA [3], MIT [4] and RICE [5].

Since then the field of ultracold quantum gases has developed from the point of proof of principle to a mature field, and hundreds of BEC experiments with different atoms, atom numbers, temperatures, interatomic interactions and trapping geometries have been performed. Many experiments focus attention on creating quasi2D and quasi1D trapped gases by tightly confining the particle motion to zero point oscillations in one or two directions. Then, kinematically the gas is 2D or 1D, and the difference from purely 2D or 1D gases is only related to the value of the interparticle interaction which now depends on the tight confinement. The presence of a shallow confinement in the other direction(s) allows one to speak of a trapped 1D(2D) gas. Recently, several groups have realized quasi2D and quasi1D regimes for trapped condensates [6; 7; 8; 9]. One-dimensional systems of bosons become especially interesting in view of ongoing experiments on atom lasers and atom chip interferometry. These experiments deal with very elongated atomic clouds where the problem of phase coherence is of fundamental importance.

Uniform purely 1D and 2D many-body systems are relatively well understood and described. However, the presence of the trapping potential adds new features to the well-known problems and attracts our attention to the low-dimensional systems again. The trapping geometry introduces a finite size of the system and significantly modifies the

structure of energy levels. The effective interparticle interaction plays an important role in low dimensions and in trapped gases it strongly depends on the tight confinement. A number of questions arise naturally: How do these features modify the well-known conclusions about the BEC phase transition, superfluidity and phase coherence properties of the low-dimensional quantum gases? What are the regimes of quantum degeneracy in these novel low-dimensional systems?

Trying to find answers to these questions we rely on a long prehistory of the subject. In uniform low-dimensional Bose systems the true BEC and long-range order are absent at finite temperatures [10; 11]. At sufficiently low temperatures the density fluctuations are suppressed as in the 3D case. However, long-wave fluctuations of the phase of the boson field provide a power law decay of the density matrix in 2D and an exponential decay in 1D (see [12] for review). The characteristic radius of phase fluctuations exceeds the healing length, and locally the system is similar to a true condensate. This state of the system is called *quasicondensate* or *condensate with fluctuating phase* (see [13]).

The presence of the quasicondensate is coupled to the phenomenon of superfluidity. In uniform 2D systems one has the Kosterlitz-Thouless superfluid phase transition associated with the formation of bound pairs of vortices below a critical temperature. The Kostelitz-Thouless transition has been observed in monolayers of liquid helium [14; 15]. Recently, the observation of KTT in the 2D gas of spin-polarized atomic hydrogen on liquid-helium surface has been reported [16]. BEC of excitons – electron-hole bound pairs in semiconductors – has been discussed for a long time (see [17; 18; 19; 20] for review). There are now promising prospects for reaching quantum degeneracy in quasi2D trapped exciton gases [21; 22; 23; 24]. Bose-Einstein condensation of composite bosons formed out of tightly bound pairs of electrons (bipolaron mechanism) is one of the explanations of the high critical temperature in superconducting copper-oxide layers and other HTSC materials [25]. Non-BCS mechanisms of superconductivity have been reported in quasi1D wires [26].

From a theoretical point of view, the situation in dilute gases is unique compared with liquids or HTSC materials. In a gas the characteristic radius of interaction between particles, R_e, is much smaller than the mean interparticle separation, giving rise to a small parameter (gaseous parameter). In the ultra-cold limit, collisions are dominated by the s-wave scattering and the scattering amplitude is characterized by a single parameter of the dimension of length. In low dimensions this quantity is an analog of the 3D scattering length and replaces the full knowledge of the interaction potential. The existence of the small gaseous parameter allows an *ab initio* theoretical description of gases and makes the physical picture more transparent than in phenomenological theories of liquids.

1.2 This Thesis

In this Thesis we develop a theory for describing regimes of quantum degeneracy and BEC in ultra-cold low-dimensional trapped gases. The main emphasis is put on the phase coherence and on the role of interparticle interaction in trapped degenerate gases. The results of the Thesis are linked to the ongoing and future experimental studies.

In Chapter 2 we introduce fundamental concepts related to BEC in low dimensions and give a brief overview of literature on low-dimensional quantum gases.

In Chapter 3 we investigate the interparticle interaction in the quasi2D regime and discuss the influence of the tight confinement on the properties of degenerate quasi2D Bose and Fermi gases. The first section is dedicated to the mean-field interaction in quasi2D Bose gases. We show that it is sensitive to the strength of the tight confinement, and one can even switch the sign of the interaction by changing the confinement frequency. We find that well below the BEC transition temperature T_c the equilibrium state of a quasi2D Bose gas is a true condensate, whereas at intermediate temperatures $T < T_c$ one can have a quasicondensate.

After the recent progress in cooling 3D Fermi gases to well below the temperature of quantum degeneracy, achieving superfluidity is a challenging goal and it may require much lower temperatures. In the second section we show that quasi2D atomic Fermi gases are promising for achieving superfluid regimes: the regime of BCS pairing for weak attraction between atoms, and the regime of strong coupling resulting in the formation of weakly bound quasi2D bosonic dimers. For the BCS limit, we calculate the transition temperature T_c and discuss how to increase the ratio of T_c to the Fermi energy. In the other extreme, we analyze the stability of a Bose condensate of the quasi2D dimers.

Active studies on achieving the quasi2D regime [27; 28; 29; 30; 31; 6; 7] for cold gases raise a subtle question of how 3D collisions and interactions transform into 2D. In a nondegenerate gas, the crossover from 3D to 2D should take place when the level spacing for the tightly confining potential becomes comparable with the mean kinetic energy of particles. In Chapter 4 we develop a theory of pair interatomic collisions at an arbitrary energy in the presence of tight confinement in one direction. We identify regimes in which collisions can be no longer regarded as three-dimensional and the 2D nature of the particle motion is important. We describe the collision-induced energy exchange between the axial and radial degrees of freedom and analyze the recent experiments on kinetic properties, thermalization and spin relaxation in a tightly confined gas of Cs atoms [27; 28; 29; 30].

Chapter 5 is dedicated to quasi1D trapped Bose gases. We discuss the regimes of quantum degeneracy and obtain the diagram of states for this system. We identify three regimes: the BEC regimes of a true condensate and quasicondensate, and the regime of a trapped Tonks gas (gas of impenetrable bosons). We show that the presence of a sharp cross-over to the BEC regime requires extremely small interaction between particles.

The phase coherence in a degenerate 3D Bose gas depends on the geometry. If the sample is sufficiently elongated, long-wave thermal fluctuations of the phase in the axial direction acquire 1D character and can destroy BEC. In Chapter 6 we show that in very elongated 3D trapped Bose gases, even at temperatures far below the BEC transition temperature T_c, the equilibrium state is a quasicondensate. At very low temperatures the phase fluctuations are suppressed and the quasicondensate turns into a true condensate.

A simple and efficient method of observing phase fluctuations in an elongated trapped Bose-condensed gas has been recently demonstrated in Hannover. The method relies on the measurement of the density distribution after releasing the gas from the trap. In the second section of Chapter 6 we analyze this experiment and show how the phase fluctuations in an elongated BEC transform into the density modulations in the course of free expansion.

Chapter 2 Overview

In this chapter we give a brief overview of literature on low-dimensional gases and introduce important concepts and methods used in this Thesis.

2.1 BEC of an ideal gas in 1D and 2D harmonic traps

The analysis of trapped gases has been extended mostly to the noninteracting case. Bagnato and Kleppner [32] have found that in a harmonically trapped ideal 2D Bose gas occupation of the ground state becomes macroscopic (ordinary BEC transition) below a critical temperature which depends on the number of particles and trap frequencies. Ketterle and van Druten have shown that the BEC-like behavior is also present in an ideal trapped 1D gas [33].

We start with thermodynamic description of an ideal 1D or 2D gas of N bosons trapped in a harmonic external potential. The gas sample is assumed to be in thermal equilibrium at temperature T. We will calculate thermodynamic averages for the grand canonical ensemble, where the system is characterized by a fixed chemical potential μ and fluctuating number of particles N. In the thermodynamic limit ($N \to \infty$) this is equivalent to the description in the canonical ensemble (fixed N and fluctuating μ).

Generally, in an arbitrary trap of any dimension the system is characterized by a set of eigenenergies of an individual atom, $\{\epsilon_\nu\}$. The (average) total number of particles N is then related to the temperature and chemical potential by the equation

$$N = \sum_\nu N\left((\epsilon_\nu - \mu)/T\right), \tag{2.1.1}$$

where $N(z) = 1/(\exp z - 1)$ is the Bose occupation number (we use the convention $k_B = 1$). The population of the ground state ($\epsilon_0 = 0$) is

$$N_0 = \frac{1}{\exp(-\mu/T) - 1}, \tag{2.1.2}$$

and in the thermodynamic limit can become macroscopic (comparable with N) only if $\mu = 0$. For a large but finite number of particles in a trap, N_0 becomes comparable with N and one has a crossover to the BEC regime at a small but finite μ.

We now determine the temperature of the BEC crossover for a 2D Bose gas confined in a circularly symmetric harmonic trap. In this case the index ν corresponds to the pair of quantum numbers $\{n_x, n_y\}$ in such a way that $\epsilon_{n_x,n_y} = \hbar\omega(n_x + n_y)$, where ω is the trap frequency. This particular level structure allows one to rewrite the sum in Eq. (2.1.1) in the form of an integral

$$N = N_0 + \int_0^\infty N((\epsilon - \mu)/T)\rho(\epsilon)\mathrm{d}\epsilon. \tag{2.1.3}$$

Here $\rho(\epsilon) = \epsilon/(\hbar\omega)^2$ is the density of states of the system and we have separated the ground state population. The transformation from the sum to the integral is justified by the inequality $\hbar\omega \ll T$ and by the fact that the relative contribution of several low-energy states is negligible (the density of states goes to zero). For a large population of the ground state Eq. (2.1.2) gives $-\mu/T \approx 1/N_0 \ll 1$. Then the first two leading terms in the expansion of the integral in Eq. (2.1.3) are

$$\int_0^\infty N((\epsilon-\mu)/T)\rho(\epsilon)\mathrm{d}\epsilon \approx \left(\frac{T}{\hbar\omega}\right)^2 \left(\frac{\pi^2}{6} - \frac{1+\ln N_0}{N_0}\right), \tag{2.1.4}$$

and Eq. (2.1.3) reduces to the form

$$N\left[1-(T/T_c)^2\right] = N_0 - (T/\hbar\omega)^2\,(1+\ln N_0)/N_0, \tag{2.1.5}$$

where

$$T_c = \sqrt{6N/\pi^2}\hbar\omega\,. \tag{2.1.6}$$

From Eq. (2.1.4) one clearly sees that there is a sharp crossover to the BEC regime at $T \approx T_c$ [32; 34]. Below T_c we can neglect the last term in Eq. (2.1.5). Then we obtain the occupation of the ground state $N_0 \approx N\left[1-(T/T_c)^2\right]$ similar to that in the 3D case. Above T_c the first term in the rhs of Eq. (2.1.5) can be neglected compared to the second one. Note that at T_c the de Broglie wavelength of particles $\lambda \sim \sqrt{\hbar^2/mT_c}$ becomes comparable with the mean interparticle separation $\sim (Nm\omega^2/T_c)^{-1/2}$. In the crossover region between the two regimes all terms in Eq. (2.1.5) are equally important and we estimate the width of the crossover region as

$$\frac{\Delta T}{T_c} \sim \sqrt{\frac{\ln N}{N}}. \tag{2.1.7}$$

Solutions of Eq. (2.1.5) for various N are presented in Fig. 2.1.1.

For a large number of particles the relative width of the crossover region is very small. Therefore, one can speak of an ordinary BEC transition in an ideal harmonically trapped 2D gas.

In the 1D case the spectrum is $\epsilon_n = \hbar\omega n$ and the density of states is $\rho(\epsilon) = 1/\hbar\omega$. Here the integral representation Eq. (2.1.3) fails as the integral diverges for $-\mu/T \to 0$ and we should correctly take into account the lowest energy levels [33]. In the limit $\{-\mu,\, \hbar\omega\} \ll T$ we rewrite Eq. (2.1.1) in the form

$$N = N_0 + \frac{T}{\hbar\omega}\sum_{n=1}^{M}\frac{1}{n-\mu/\hbar\omega} + \sum_{n=M+1}^{\infty}\frac{1}{\exp(\hbar\omega n/T - \mu/T) - 1}, \tag{2.1.8}$$

where the number M satisfies the inequalities $1 \ll M \ll T/\hbar\omega$. The first sum is

$$\sum_{n=1}^{M}\frac{1}{n-\mu/\hbar\omega} = \psi(M+1-\mu/\hbar\omega) - \psi(1-\mu/\hbar\omega) \approx -\psi(1-\mu/\hbar\omega) + \ln(M-\mu/\hbar\omega), \tag{2.1.9}$$

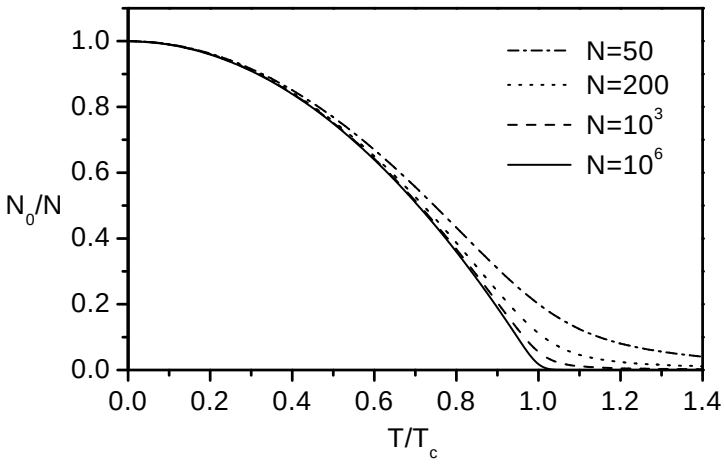

Figure 2.1.1: The ground state population in a 2D trap versus temperature. The curves are calculated from Eq. (2.1.5) for various N.

where ψ is the digamma function. The second sum in Eq. (2.1.8) can be transformed to an integral

$$\sum_{n=M+1}^{\infty} \frac{1}{\exp\frac{\hbar\omega n-\mu}{T}-1} \approx \frac{T}{\hbar\omega}\int_{\hbar\omega M/T}^{\infty} \frac{\mathrm{d}x}{\exp(x-\mu/T)-1} \approx -\frac{T}{\hbar\omega}\ln\frac{\hbar\omega(M-\mu/\hbar\omega)}{T}.$$

Finally, eliminating the chemical potential by using the equality $-\mu \approx T/N_0$, we reduce Eq. (2.1.8) to the form

$$N-\frac{T}{\hbar\omega}\ln\frac{T}{\hbar\omega} = N_0 - \frac{T}{\hbar\omega}\psi\left(1+\frac{T}{\hbar\omega N_0}\right). \tag{2.1.10}$$

As in the 2D case, we have two regimes, with the border between them at T_c determined by $N \approx (T_c/\hbar\omega)[\ln(T_c/\hbar\omega)+0.577]$. Indeed, below this temperature the first term in the rhs of Eq. (2.1.10) greatly exceeds the second one and the ground state population behaves as $N_0 \approx N-(T/\hbar\omega)\ln(T/\hbar\omega)$. The crossover region is determined as the temperature interval where both terms are equally important:

$$\Delta T/T_c \sim 1/\ln N. \tag{2.1.11}$$

The crossover temperature in a 1D trap is $T_c \approx N\hbar\omega/\ln N$ and, in contrast to 3D and 2D cases, is much lower than the degeneracy temperature $T_d \approx N\hbar\omega$. In Fig. 2.1.2 we present $N_0(T)$ calculated from Eq. (2.1.10).

The crossover region in the 1D case is much wider than in 2D. This is not surprising as the crossover itself is present only due to the discrete structure of the trap levels. The quasiclassical calculation does not lead to any crossover [32].

Note that an ideal 2D Bose gas in a finite box has the density of states independent of energy, just like a harmonically trapped 1D gas. Therefore, it is characterized by a similar crossover to the BEC regime [35; 33].

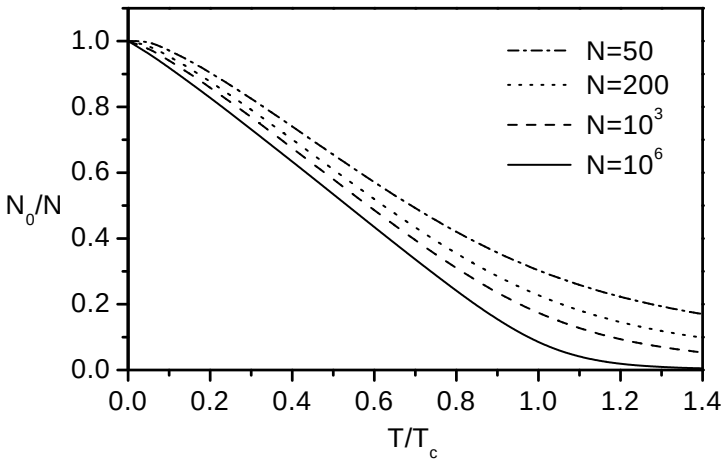

Figure 2.1.2: The ground state population in a 1D trap versus temperature. The curves are calculated from Eq. (2.1.10) for various N.

2.2 Interacting Bose gas

We now consider an interacting d-dimensional Bose gas in a trap with the potential $U(\mathbf{r})$. The Hamiltonian of the system in the second quantization reads (see [36])

$$\hat{H} = \int_{\mathbf{r}} \hat{\Psi}^\dagger(\mathbf{r}) \left(-\frac{\hbar^2 \nabla^2}{2m} + U(\mathbf{r}) \right) \hat{\Psi}(\mathbf{r}) + \frac{1}{2} \iint_{\mathbf{r},\,\mathbf{r}'} V(|\mathbf{r}-\mathbf{r}'|) \hat{\Psi}^\dagger(\mathbf{r}) \hat{\Psi}^\dagger(\mathbf{r}') \hat{\Psi}(\mathbf{r}) \hat{\Psi}(\mathbf{r}'), \quad (2.2.1)$$

where $V(\mathbf{r})$ is the potential of interaction between two atoms and $\hat{\Psi}(\mathbf{r})$, $\hat{\Psi}^\dagger(\mathbf{r})$ are the Boson field operators satisfying the commutation relations

$$[\hat{\Psi}(\mathbf{r}), \hat{\Psi}(\mathbf{r}')] = 0, \;\; [\hat{\Psi}(\mathbf{r}), \hat{\Psi}^\dagger(\mathbf{r}')] = \delta(\mathbf{r}-\mathbf{r}'). \quad (2.2.2)$$

In the Heisenberg representation the time derivative of $\hat{\Psi}(\mathbf{r})$ is given by

$$i\hbar \frac{\partial \hat{\Psi}}{\partial t} = -[\hat{H}, \hat{\Psi}] = \left(-\frac{\hbar^2 \nabla^2}{2m} + U(\mathbf{r}) + \int_{\mathbf{r}'} V(|\mathbf{r}-\mathbf{r}'|) \hat{\Psi}^\dagger(\mathbf{r}') \hat{\Psi}(\mathbf{r}') \right) \hat{\Psi}. \quad (2.2.3)$$

Using the commutation relations (2.2.2) we rewrite Eq. (2.2.3) in the form

$$i\hbar \frac{\partial \hat{\Psi}}{\partial t} + V(0)\hat{\Psi} = -\frac{\hbar^2 \nabla^2}{2m} \hat{\Psi} + U(\mathbf{r})\hat{\Psi} + \hat{\Psi} \int_{\mathbf{r}'} V(|\mathbf{r}-\mathbf{r}'|) \hat{\Psi}^\dagger(\mathbf{r}') \hat{\Psi}(\mathbf{r}'). \quad (2.2.4)$$

The term $V(0)\hat{\Psi}$ gives only a trivial time dependence and can be eliminated by the substitution $\hat{\Psi} \to \hat{\Psi} \exp(iV(0)t/\hbar)$. Let us now turn to the density-phase representation of the field operators

$$\hat{\Psi} = \exp(i\hat{\phi})\sqrt{\hat{n}}, \;\; \hat{\Psi}^\dagger = \sqrt{\hat{n}} \exp(-i\hat{\phi}), \quad (2.2.5)$$

where the density and phase operators are real and satisfy the commutation relation

$$[\hat{n}(\mathbf{r}), \hat{\phi}(\mathbf{r}')] = i\delta(\mathbf{r} - \mathbf{r}'). \tag{2.2.6}$$

Substituting Eqs. (2.2.5) into Eq. (2.2.4) and separating real and imaginary parts, we get the coupled continuity and Euler hydrodynamic equations for the density and velocity $\hat{\mathbf{v}} = (\hbar/m)\nabla\hat{\phi}$:

$$-\hbar\frac{\partial\hat{n}}{\partial t} = \frac{\hbar^2}{m}\nabla(\nabla\hat{\phi}\,\hat{n})\,, \tag{2.2.7}$$

$$-\hbar\frac{\partial\hat{\phi}}{\partial t} = \frac{\hbar^2}{2m}(\nabla\hat{\phi})^2 - \frac{\hbar^2}{2m}\frac{\nabla^2\sqrt{\hat{n}}}{\sqrt{\hat{n}}} + U(\mathbf{r}) + \int_{\mathbf{r}'} V(|\mathbf{r}' - \mathbf{r}|)\hat{n}(\mathbf{r}')\,. \tag{2.2.8}$$

Eqs. (2.2.7-2.2.8) are obtained from the Hamiltonian (2.2.1) without any approximations and, in principle, should describe any property of an interacting Bose gas. At the same time, these equations are nonlinear and very complicated. However, in a dilute ultra-cold weakly interacting gas we can use a number of simplifications. The short-range character of the interatomic potential[1] allows us to rewrite the integral in Eq. (2.2.8) as

$$\int_{\mathbf{r}'} V(|\mathbf{r}' - \mathbf{r}|)\hat{n}(\mathbf{r}') \approx g\hat{n}(\mathbf{r}), \tag{2.2.9}$$

where the mean-field coupling constant g can also depend on density or on average momentum of particles (see Chapters 3 and 4).

We further simplify Eqs. (2.2.7-2.2.8) assuming small fluctuations of the density. In this case, Eq. (2.2.7) shows that fluctuations of the phase gradient are also small. Representing the density operator as $\hat{n}(\mathbf{r}) = n_0(\mathbf{r}) + \delta\hat{n}(\mathbf{r})$ and shifting the phase by $-\mu t/\hbar$ we then linearize Eqs. (2.2.7-2.2.8) with respect to $\delta\hat{n}$, $\nabla\hat{\phi}$ around the stationary solution $\hat{n} = n_0$, $\nabla\hat{\phi} = 0$. The zero order terms give the Gross-Pitaevskii equation for n_0:

$$-\frac{\hbar^2}{2m}\frac{\nabla^2\sqrt{n_0}}{\sqrt{n_0}} + U(\mathbf{r}) + gn_0 = \mu\,, \tag{2.2.10}$$

and the chemical potential μ follows from the normalization condition

$$\int_{\mathbf{r}} n_0(\mathbf{r}) = N\,. \tag{2.2.11}$$

The first order terms provide equations for the density and phase fluctuations:

$$\hbar\,\partial(\delta\hat{n}/\sqrt{n_0})/\partial t = (-\hbar^2\nabla^2/2m + U(\mathbf{r}) + gn_0 - \mu)(2\sqrt{n_0}\,\hat{\phi})\,, \tag{2.2.12}$$

$$-\hbar\,\partial(2\sqrt{n_0}\,\hat{\phi})/\partial t = (-\hbar^2\nabla^2/2m + U(\mathbf{r}) + 3gn_0 - \mu)(\delta\hat{n}/\sqrt{n_0})\,. \tag{2.2.13}$$

Solutions of Eqs. (2.2.12-2.2.13) are obtained by representing $\delta\hat{n}$, $\nabla\hat{\phi}$ in terms of elementary excitations:

$$\delta\hat{n}(\mathbf{r}) = n_0(\mathbf{r})^{1/2}\sum_\nu i f_\nu^-(\mathbf{r})e^{-i\epsilon_\nu t/\hbar}\,\hat{a}_\nu + \text{H.c.}\,, \tag{2.2.14}$$

$$\hat{\phi}(\mathbf{r}) = [4n_0(\mathbf{r})]^{-1/2}\sum_\nu f_\nu^+(\mathbf{r})e^{-i\epsilon_\nu t/\hbar}\,\hat{a}_\nu + \text{H.c.}\,. \tag{2.2.15}$$

[1] In this Thesis we do not consider dipolar or charged gases with long-range interatomic forces.

From Eqs. (2.2.14-2.2.15) we then find equations for the eigenenergies ϵ_ν and eigenfunctions $f_\nu^\pm$ of the excitations:

$$\left(-\hbar^2\nabla^2/2m + U(\mathbf{r}) + gn_0 - \mu\right) f_\nu^+ = \epsilon_\nu f_\nu^- \,, \tag{2.2.16}$$

$$\left(-\hbar^2\nabla^2/2m + U(\mathbf{r}) + 3gn_0 - \mu\right) f_\nu^- = \epsilon_\nu f_\nu^+ \,. \tag{2.2.17}$$

The commutation relation (2.2.6) ensures that the functions $f_\nu^\pm$ are normalized by the condition

$$\frac{1}{2}\int_{\mathbf{r}} \left(f_\nu^+(\mathbf{r}) f_\nu^{-*}(\mathbf{r}) + f_\nu^-(\mathbf{r}) f_\nu^{+*}(\mathbf{r}) \right) = 1 \,. \tag{2.2.18}$$

Equations (2.2.16-2.2.17) are exactly the same as the Bogolyubov-de Gennes equations[2] for elementary excitations of a Bose-Einstein condensate with the density profile $n_0(\mathbf{r})$. The functions $f_\nu^\pm$ are related to the well-known Bogolyubov u, v functions by $f_\nu^\pm = u \pm v$. We thus see that the assumption of small density fluctuations is sufficient for having the Bogolyubov spectrum of the excitations, irrespective of the presence or absence of a true condensate.

The spectrum of elementary excitations of a trapped Bose-condensed gas has been intensively discussed in literature. In a vast majority of experiments the number of particles is very large and the chemical potential μ greatly exceeds the level spacing in the trap. In this case the kinetic energy term in Eq. (2.2.10) is much smaller than the nonlinear term and can be neglected. This approach is called the Thomas-Fermi (TF) approximation, and in a harmonic trap the density profile n_0 takes the well-known parabolic shape

$$n_0 = [\mu - U(\mathbf{r})]/g. \tag{2.2.19}$$

In this case, the low-energy excitations ($\epsilon_\nu \ll \mu$) can be found analytically [38; 39; 40]. The dependence of the excitation spectrum on the trapping geometry has been extensively studied for 3D TF condensates (see [41] for review). For example, in very elongated cigar-shaped condensates the spectrum of low lying axial excitations reads $\epsilon_j = \hbar\omega_z\sqrt{j(j+3)}/2$ [40; 42]. Stringari [42] has found the spectrum for very anisotropic pancake-shaped condensates. The spectrum of low-energy excitations has also been found for purely 2D and 1D Thomas-Fermi clouds [43].

In a homogeneous Bose gas the chemical potential $\mu = gn_0$ and Eqs. (2.2.16-2.2.18) give the well-known spectrum and wavefunctions:

$$\epsilon(k) = \sqrt{E(k)\left[E(k) + 2\mu\right]} \,, \tag{2.2.20}$$

$$f_{\mathbf{k}}^\pm = \frac{1}{\sqrt{V}} \left(\frac{\epsilon(k)}{E(k)} \right)^{\pm 1/2} e^{i\mathbf{k}\cdot\mathbf{r}} \,, \tag{2.2.21}$$

where $E(k) = \hbar^2 k^2/2m$ is the free-particle spectrum, and V is the d-dimensional volume of the system. The Bogolyubov spectrum (2.2.20) is phonon-like, with $\epsilon(k) \approx c_s\hbar k$, for energies of the order of or smaller than μ. This corresponds to momenta $k \lesssim 1/l_c$, where the healing length $l_c = \hbar/\sqrt{m\mu}$. The speed of sound is $c_s = \sqrt{\mu/m}$. For larger momenta the spectrum (2.2.20) is particle-like, with $\epsilon(k) \approx E(k) + \mu$.

[2] Similar equations have been found by de Gennes [37] for inhomogeneous superconductors.

The chemical potential μ is an approximate border between two classes of excitations. In order to analyze the role of these two classes let us separate the operator of the density fluctuations into two parts: $\delta\hat{n} = \delta\hat{n}_s + \delta\hat{n}_p$, where the indices s and p stand for the phonon ($\epsilon < \mu$) and free-particle ($\epsilon > \mu$) parts respectively. We now use Eq. (2.2.14) and calculate the density-density correlation function $\langle \delta\hat{n}_s(\mathbf{r}_1)\delta\hat{n}_s(\mathbf{r}_2)\rangle$, where the symbol $\langle ...\rangle$ denotes the statistical average. A straightforward calculation yields

$$\langle \hat{n}'_s(\mathbf{r}_1)\hat{n}'_s(\mathbf{r}_2)\rangle = \frac{n_0}{V}\sum_{\epsilon(k)<\mu}\frac{E(k)}{\epsilon(k)}\left[2N(\epsilon(k)/T)+1\right]\cos\mathbf{k}\cdot(\mathbf{r}_1-\mathbf{r}_2)\,. \tag{2.2.22}$$

Here we used the equality $\langle \hat{a}^\dagger_{\mathbf{k}}\hat{a}_{\mathbf{k}}\rangle = N(\epsilon(k)/T)$ for the equilibrium occupation number of excitations. Taking into account that this number is always smaller than $T/\epsilon(k)$ we obtain

$$\langle \hat{n}'_s(\mathbf{r}_1)\hat{n}'_s(\mathbf{r}_2)\rangle/n_0^2 \lesssim (\mu/T_d)^{d/2}\max\{(T/\mu),1\}, \tag{2.2.23}$$

where d is the dimension of the system, and the temperature of quantum degeneracy is $T_d = \hbar^2 n_0^{2/d}/m$. We then see that well below T_d in 2D and 3D weakly interacting gases the phonon-induced density fluctuations are small and can be neglected. To ensure that they are small in the one-dimensional gas we require $T \ll (\mu T_d)^{1/2}$ in 1D. Then, omitting fluctuations originating from the high-energy part ($\epsilon > \mu$) of the spectrum, we represent the field operator Ψ in the form

$$\hat{\Psi} = \sqrt{n_0}\exp\left(i\hat{\phi}_s\right)\,, \tag{2.2.24}$$

In order to make sure that fluctuations coming from high-energy excitations can be omitted, we *a priori* assume that they are small and can be evaluated by linearizing the field operator $\hat{\Psi} = \exp(i\hat{\phi})\sqrt{\hat{n}}$ with regard to the high-energy part. This is equivalent to writing the preexponential factor in Eq. (2.2.24) as $(\sqrt{n_0}+\hat{\Psi}')$ instead of just $\sqrt{n_0}$. The operator $\hat{\Psi}'$ accounts for both density and phase fluctuations and reads

$$\hat{\Psi}' = i\sum_{\epsilon(k)>\mu} u_{\mathbf{k}}(\mathbf{r})\hat{a}_{\mathbf{k}}e^{-i\epsilon(k)t/\hbar} - v_{\mathbf{k}}(\mathbf{r})\hat{a}^\dagger_{\mathbf{k}}e^{i\epsilon(k)t/\hbar}\,. \tag{2.2.25}$$

At energies significantly larger than μ the function $v_{\mathbf{k}} = (f^+_{\mathbf{k}} - f^-_{\mathbf{k}})/2 \to 0$, and $u_{\mathbf{k}} = (f^+_{\mathbf{k}} + f^-_{\mathbf{k}})/2 \to V^{-1/2}\exp(i\mathbf{k}\cdot\mathbf{r})$. The energy itself is $\epsilon(k) \approx E(k) + \mu$ and, hence, the operator $\hat{\Psi}'$ describes an ideal gas of Bose particles with chemical potential equal to $-\mu$. One thus sees that high-energy Bogolyubov excitations correspond to the incoherent non-condensed part of the gas. The density of this gas is exponentially small at $T < \mu$ and for $T \gtrsim \mu$ it is equal to

$$\langle \hat{\Psi}'^\dagger\hat{\Psi}'\rangle \approx \int_{\epsilon(k)>\mu} N\left[\epsilon(k)/T\right]\frac{\mathrm{d}^d k}{(2\pi)^d} \sim n_0 \times \begin{cases} (T/T_d)^{3/2}\,, & \text{in 3D} \\ (T/T_d)\ln(T/\mu)\,, & \text{in 2D} \\ T\,(\mu T_d)^{-1/2}\,, & \text{in 1D.} \end{cases} \tag{2.2.26}$$

At temperatures $T \ll T_d$ ($T \ll (\mu T_d)^{1/2}$ in the 1D case) the quantity $\langle \hat{\Psi}'^{\dagger} \hat{\Psi}' \rangle$ is really small, which justifies Eq. (2.2.24) for the field operator.

Equation (2.2.24) allows us to calculate correlation functions at low temperatures to zero order in perturbation theory. For obtaining perturbative corrections, one should expand Eqs. (2.2.12-2.2.13) up to quadratic terms in $\delta\hat{n}$ and $\hat{\phi}$. This provides a correction for the stationary solution and for the chemical potential as a function of density. One should then include the low-energy density fluctuations and the high-energy fluctuations in the expression for the field operator. This is equivalent to proceeding along the lines of the perturbation theory developed by Popov (see [12]).

2.3 Phase fluctuations and quasicondensates in a uniform gas

Bose-Einstein condensation in a uniform gas is associated with the long-range order in the system, i.e. with the finite value of the one-particle density matrix $\rho(\mathbf{r}_1, \mathbf{r}_2) = \langle \hat{\Psi}^{\dagger}(\mathbf{r}_1) \hat{\Psi}(\mathbf{r}_2) \rangle$ at $|\mathbf{r}_1 - \mathbf{r}_2| \to \infty$. Using Eq. (2.2.24) the density matrix at low temperatures can be written in the form [12]

$$\rho(\mathbf{r}_1, \mathbf{r}_2) = n_0 \left\langle e^{-i\left[\hat{\phi}_s(\mathbf{r}_1) - \hat{\phi}_s(\mathbf{r}_2)\right]} \right\rangle = n_0 \, e^{-\frac{1}{2}\left\langle \left[\hat{\phi}_s(\mathbf{r}_1) - \hat{\phi}_s(\mathbf{r}_2)\right]^2 \right\rangle} . \tag{2.3.1}$$

The phase correlator is obtained from Eqs. (2.2.15) and (2.2.21). It reads

$$\left\langle \left[\hat{\phi}_s(\mathbf{r}) - \hat{\phi}_s(\mathbf{0})\right]^2 \right\rangle = \frac{1}{2n_0 V} \sum_{\epsilon(k)<\mu} \frac{\epsilon(k)}{E(k)} \left[2N(\epsilon(k)/T) + 1\right] (1 - \cos \mathbf{k} \cdot \mathbf{r}) , \tag{2.3.2}$$

In the 3D case this correlator is small even at temperatures larger than μ, where it is approximately equal to $T/(\pi^2 T_d n_0^{1/3} l_c)$.

The two-dimensional vacuum fluctuations of the phase are negligible and in 2D one has a true condensate at zero temperature. At finite temperatures the correlator (2.3.2) takes the form (see [44])

$$\left\langle \left[\hat{\phi}_s(\mathbf{r}) - \hat{\phi}_s(\mathbf{0})\right]^2 \right\rangle \approx T/(\pi T_d) \ln(r/l_c) . \tag{2.3.3}$$

This result means that the long-wave fluctuations of the phase of the boson field provide a power law decay of $\rho(\mathbf{r})$ at $r \to \infty$ in contrast to the 3D case. This was first found by Kane and Kadanoff [44] and is consistent with the Bogolyubov theorem [10; 11] indicating the absence of a true condensate at finite temperatures in 2D. The power law behavior of $\rho(\mathbf{r})$ is qualitatively different from the exponential decay at large distances in a classical gas, which indicates a possibility of phase transition at sufficiently low T. The existence of a superfluid phase transition in 2D gases (liquids) has been proved by Berezinskii [45; 46]. Kosterlitz and Thouless [47; 48] found that this transition is associated with the formation of bound pairs of vortices below a critical temperature T_{KT} which is of the order of T_d. Recently, the exact value of this temperature has been found using Monte Carlo simulations [49; 50].

Earlier theoretical studies of 2D systems have been reviewed in [12] and have led to the conclusion that below the Kosterlitz-Thouless transition (KTT) temperature the Bose liquid (gas) is characterized by the presence of a quasicondensate, which is a condensate with fluctuating phase (see [13]). Indeed, from Eqs. (2.3.1) and (2.3.3) we see that the density matrix decays on a length scale $R_\phi \approx l_c \exp(\pi T_d/T) \gg l_c$. In this case the system can be divided into blocks with a characteristic size greatly exceeding the healing length l_c but smaller than the radius of phase fluctuations R_ϕ. Then, there is a true condensate in each block but the phases of different blocks are not correlated with each other.

The situation is similar in the 1D gas at temperatures $T \ll (\mu T_d)^{1/2}$, except for the presence of a true condensate at $T = 0$. Eq. (2.3.2) gives

$$\left\langle \left[\hat{\phi}_s(r) - \hat{\phi}_s(0)\right]^2 \right\rangle \approx \frac{T}{\sqrt{\mu T_d}} \frac{r}{l_c} + \frac{1}{\pi}\sqrt{\frac{\mu}{T_d}} \ln \frac{r}{l_c}\,, \tag{2.3.4}$$

where the first term in the rhs comes from the thermal part and the second one from the vacuum part of the phase fluctuations. Thus, at zero temperature the density matrix undergoes a power-law decay [51; 52; 12], and there is no true Bose-Einstein condensate. This is consistent with a general analysis of 1D Bose gases at $T = 0$ [53]. At finite temperatures the long-range order is destroyed by long-wave fluctuations of the phase leading to an exponential decay of the one-particle density matrix at large distances [44; 12].

In this Thesis we mostly concentrate on the properties of a trapped 1D Bose gas in the weakly interacting regime, where the healing length $l_c = \hbar/\sqrt{mng}$ greatly exceeds the mean interparticle separation $1/n$. This corresponds to small values of the parameter $\gamma = mg/\hbar^2 n$. Our previous discussions of the uniform 1D interacting gas in this chapter were related to this particular regime. In general, the 1D Bose gas with repulsive short-range interactions characterized by the coupling constant $g > 0$ is integrable by using the Bethe Ansatz at any g and n and has been a subject of extensive theoretical studies [54; 55; 56; 57]. The equation of state and correlation functions depend crucially on the parameter γ. The weakly interacting regime ($\gamma \ll 1$) is realized at comparatively large densities (or small g). For sufficiently small densities (or large g), the parameter $\gamma \gg 1$ and one has a gas of impenetrable bosons (Tonks gas), where the wavefunction strongly decreases when particle approach each other. In this respect the system acquires fermionic properties.

2.4 Realization of BEC's in lower dimensions

In commonly studied BEC's in 3D harmonic traps the mean-field interaction greatly exceeds the level spacings. In this case the Thomas-Fermi approximation can be used and the shape of the condensate density profile is given by Eq. (2.2.19). For the Thomas-Fermi condensate the chemical potential equals

$$\mu_{3D} = \left(\frac{15 N_0 g m^{3/2} \bar{\omega}^3}{\pi 2^{9/2}}\right)^{2/5}\,, \tag{2.4.1}$$

where $\bar{\omega}^3 = \omega_x\omega_y\omega_z$, N_0 is the number of condensed particles, and $g = 4\pi\hbar^2 a/m$ is the 3D coupling constant with a being the 3D scattering length.

In order to reach quasi-1D or quasi-2D regimes for BEC in harmonic traps one has to satisfy the condition $\mu \ll \hbar\omega_0$, where ω_0 is the frequency of the tight confinement. In cylindrically symmetric traps ($\omega_x = \omega_y = \omega_\perp$) the approximate crossover to quasi-1D or quasi-2D, defined by $\mu_{3D} = \hbar\omega_0$, occurs if the number of condensate particles becomes

$$N_{1D} = \sqrt{\frac{32\hbar}{225ma^2}}\sqrt{\frac{\omega_\perp}{\omega_z^2}}; \quad N_{2D} = \sqrt{\frac{32\hbar}{225ma^2}}\sqrt{\frac{\omega_z^3}{\omega_\perp^4}}.$$

Görlitz et al. [6] have explored the crossover from 3D to 1D and 2D in a ^{23}Na BEC by reducing the number of the condensed atoms. The scattering length for sodium is relatively small, $a \approx 28$Å , and the traps in this experiment feature extreme aspect ratios resulting in high numbers $N_{1D} > 10^4$ and $N_{2D} > 10^5$.

For the 1D case, the condition $\mu = \hbar\omega_\perp$ yields a linear density $\tilde{n}_{1D} \approx 1/4a$, implying that the linear density of a 1D condensate is limited to less than one atom per scattering length independent of the radial confinement. Therefore, tight transverse confinement, as may be achievable in small magnetic waveguides [58; 59; 60; 61; 62; 63] or hollow laser beam guides [64; 65], is by itself not helpful to increase the number of atoms in a 1D condensate. Large 1D numbers may be achieved only at the expense of longer condensates or if the scattering length is smaller.

In anisotropic traps, a primary indicator of crossing the transition temperature for Bose-Einstein condensation is a sudden change of the aspect ratio of the ballistically expanding cloud, and an abrupt change in its energy. The transition to lower dimensions is a smooth cross-over, but has similar indicators. In the 3D Thomas-Fermi limit the degree of anisotropy of a BEC is independent of the number of atoms N_0, whereas in 1D and 2D the aspect ratio depends on N_0. Similarly, the release energy in 3D depends on N_0 [41] while in lower dimensions it saturates at the zero-point energy of the tightly confining dimension(s).

A trapped 3D condensate has a parabolic shape and its radius and half-length are given by $R_\perp = \sqrt{2\mu_{3D}/m\omega_\perp^2}$ and $R_z = \sqrt{2\mu_{3D}/m\omega_z^2}$, resulting in an aspect ratio of $R_\perp/R_z = \omega_z/\omega_\perp$. When the 2D regime is reached by reducing the atom number, the condensate assumes a Gaussian shape with the width $l_z = \sqrt{\hbar/m\omega_z}$ along the axial direction, but retains the parabolic shape radially. The radius of a trapped 2D condensate decreases with N_0 as $R_{\perp 2D} = (128N_0^2a^2\hbar^3\omega_z/\pi m^3\omega_\perp^4)^{1/8}$ (see Section 3.1). Similarly, the half-length of a trapped 1D condensate is $R_{z2D} = (3N_0a\hbar\omega_\perp/m\omega_z^2)^{1/3}$ (see Chapter 5).

In a ballistically expanding cloud the size in the direction(s) of shallow confinement practically does not change in time compared to a fast expansion in the direction(s) of tight confinement. In the case of pancake Thomas-Fermi condensates the latter equals b_zR_z, where the parameter b_z is governed by the scaling equation [66; 67; 68]

$$\ddot{b}_z = \omega_z^2/b_z^2. \tag{2.4.2}$$

At long times of flight $t \gg 1/\omega_z$ Eq. (2.4.2) predicts $b_z \approx \sqrt{2}\,\omega_z t$. Therefore, the aspect ratio is $b_z(t)R_z/R_\perp \approx \sqrt{2}\,\omega_\perp t$.

If the cloud is in the quasi-2D regime, the scaling parameter equals $b_z(t) \approx \omega_z t$ and the aspect ratio is $b_z(t)l_z/R_{\perp 2D} \approx (\pi\hbar\omega_z^3/128mN_0^2a^2\omega_\perp^4)^{1/8}\omega_\perp t$, which is larger than in the Thomas-Fermi regime. Görlitz et al. [6] have observed the crossover in the change of the aspect ratio by decreasing the number of particles in the condensate.

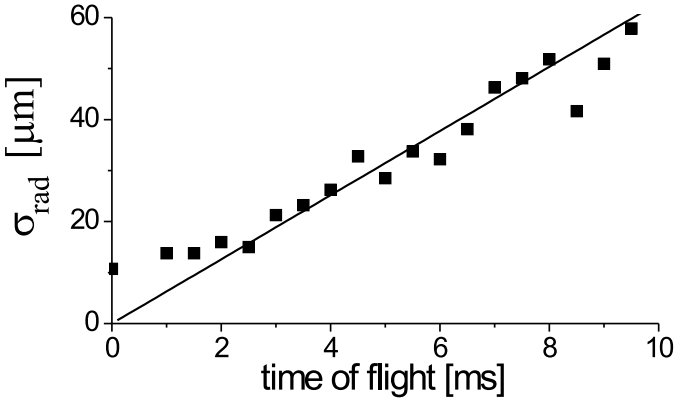

Figure 2.4.1: Signature of 1D condensate. Radial size of expanding condensates with 10^4 atoms as a function of time of flight. The straight line is the expected behavior for the expansion of the ground state radial harmonic oscillator with $\omega_\perp/2\pi = 4\,\mathrm{kHz}$

In cigar-shaped Thomas-Fermi condensates at $t \gg 1/\omega_\perp$ the aspect ratio equals $R_\perp b_\perp(t)/R_z \approx \omega_z t$. In the quasi-1D regime the radial size expands differently and the aspect ratio reads $\sqrt{\hbar/m\omega_\perp}\, b_\perp(t)/R_{z1D} \approx (\hbar\omega_\perp/9N_0^2a^2m\omega_z^2)^{1/6}\omega_z t$ and is larger than in the Thomas-Fermi case. In both cases the scaling parameter is $b_\perp(t) \approx \omega_\perp t$ (see [66]). The change in the aspect ratio with the decrease of the particle number has been observed in Ref. [6]. Schreck et al. [8] have reached the quasi-1D regime in a ^{7}Li condensate taking advantage of the small scattering length. Their measurements of the radial size of the cloud agree with the time evolution of the radial ground state wave function (see Fig. 2.4.1).

An efficient way to reach the quasi-2D and quasi-1D regimes in trapped condensates is to apply a periodic potential of an optical lattice to a 3D condensate initially prepared in a usual magnetic trap. In this way an array of quasi-2D Rb condensates has been obtained by Burger et al. [7]. Greiner et al. [9] realized an array of quasi-1D Rb condensates in a two-dimensional periodic dipole force potential, formed by a pair of standing wave laser fields.

Advantages of this method are obvious: First, an optical lattice can confine a large array of 2D or 1D systems, which allows measurements with a much higher number of involved atoms with respect to a single confining potential. Second, the macroscopic population of a single quantum state in the initial 3D trap naturally transfers the whole system into 2D or 1D systems well below the degeneracy temperature.

Chapter 3 Quantum degenerate quasi-2D trapped gases

3.1 Bose-Einstein condensation in quasi-2D trapped gases

We discuss BEC in quasi-2D trapped gases and find that well below the transition temperature T_c the equilibrium state is a true condensate, whereas at intermediate temperatures $T < T_c$ one has a quasicondensate (condensate with fluctuating phase). The mean-field interaction in a quasi-2D gas is sensitive to the frequency ω_0 of the (tight) confinement in the "frozen" direction, and one can switch the sign of the interaction by changing ω_0. Variation of ω_0 can also reduce the rates of inelastic processes. This offers promising prospects for tunable BEC in trapped quasi-2D gases.

The influence of dimensionality of the system of bosons on the presence and character of Bose-Einstein condensation (BEC) and superfluid phase transition has been a subject of extensive studies in spatially homogeneous systems. In 2D a true condensate can only exist at $T = 0$, and its absence at finite temperatures follows from the Bogolyubov k^{-2} theorem and originates from long-wave fluctuations of the phase (see, e.g., [69; 12]). However, as was first pointed out by Kane and Kadanoff [44] and then proved by Berezinskii [45; 46], there is a superfluid phase transition at sufficiently low T. Kosterlitz and Thouless [47; 48] found that this transition is associated with the formation of bound pairs of vortices below the critical temperature $T_{KT} = (\pi\hbar^2/2m)n_s$ (m is the atom mass, and n_s the superfluid density just below T_{KT}). Earlier theoretical studies of 2D systems have been reviewed in [12] and have led to the conclusion that below the Kosterlitz-Thouless Transition (KTT) temperature the Bose liquid (gas) is characterized by the presence of a quasicondensate, that is a condensate with fluctuating phase (see [13]). In this case the system can be divided into blocks with a characteristic size greatly exceeding the healing length but smaller than the radius of phase fluctuations. Then, there is a true condensate in each block but the phases of different blocks are not correlated with each other.

The KTT has been observed in monolayers of liquid helium [14; 15]. The only dilute atomic system studied thus far was a 2D gas of spin-polarized atomic hydrogen on liquid-helium surface (see [70] for review). Recently, the observation of KTT in this system has been reported [16].

BEC in trapped 2D gases is expected to be qualitatively different. The trapping potential introduces a finite size of the sample, which sets a lower bound for the momentum of excitations and reduces the phase fluctuations. Moreover, for an ideal 2D Bose gas in a harmonic potential Bagnato and Kleppner [32] found a macroscopic occupation of the ground state of the trap (ordinary BEC) at temperatures $T < T_c \approx N^{1/2}\hbar\omega$, where N is the number of particles, and ω the trap frequency. Thus, there is a question of

whether an interacting trapped 2D gas supports the ordinary BEC or the KTT type of a cross-over to the BEC regime[1]. However, the critical temperature will be always comparable with T_c of an ideal gas: On approaching T_c from above, the gas density is $n_c \sim N/R_{T_c}^2$, where $R_{T_c} \approx \sqrt{T_c/m\omega^2}$ is the thermal size of the cloud, and hence the KTT temperature is $\sim \hbar^2 n_c/m \sim N^{1/2}\hbar\omega \approx T_c$.

The discovery of BEC in trapped alkali-atom clouds [3; 4; 5] stimulated a progress in optical cooling and trapping of atoms. Present facilities allow one to tightly confine the motion of trapped particles in one direction and to create a (quasi-)2D gas. In other words, kinematically the gas is 2D, and in the "frozen" direction the particles undergo zero point oscillations. This requires the frequency of the tight confinement ω_0 to be much larger than the gas temperature T and the mean-field interparticle interaction $n_0 g$ (n_0 is the gas density, and g the coupling constant). Recent experiments [72; 73; 27; 28; 74; 75] indicate a realistic possibility of creating quasi-2D trapped gases and achieving the regime of quantum degeneracy in these systems. The character of BEC will be similar to that in purely 2D trapped gases, and the main difference is related to the sign and value of the coupling constant g.

In this section we discuss BEC in quasi-2D trapped gases and arrive at two key conclusions. First, well below T_c the phase fluctuations are small, and the equilibrium state is a true condensate. At intermediate temperatures $T < T_c$ the phase fluctuates on a distance scale smaller than the Thomas-Fermi size of the gas, and one has a quasicondensate (condensate with fluctuating phase). Second, in quasi-2D the coupling constant g is sensitive to the frequency of the tight confinement ω_0 and, for a negative 3D scattering length a, one can switch the mean-field interaction from attractive to repulsive by increasing ω_0. Variation of ω_0 can also reduce the rates of inelastic processes. These findings are promising for tunable BEC.

In a weakly interacting Bose-condensed gas the correlation (healing) length $l_c = \hbar/\sqrt{mn_0 g}$ ($g > 0$) should greatly exceed the mean interparticle separation. In (quasi-)2D the latter is $\sim 1/\sqrt{2\pi n_0}$, and we obtain a small parameter of the theory, $(mg/2\pi\hbar^2) \ll 1$ (see [13]).

We first analyze the character of BEC in a harmonically trapped 2D gas with repulsive interparticle interaction, relying on the calculation of the one-particle density matrix. Similarly to the spatially homogeneous case [69; 12], at sufficiently low temperatures only phase fluctuations are relevant. Then the field operator can be written as $\hat{\Psi}(\mathbf{R}) = n_0^{1/2}(\mathbf{R}) \exp\{i\hat{\phi}(\mathbf{R})\}$, where $\hat{\phi}(\mathbf{R})$ is the operator of the phase fluctuations, and $n_0(\mathbf{R})$ the condensate density at $T = 0$. The one-particle density matrix takes the form [12]

$$\langle \hat{\Psi}^\dagger(\mathbf{R})\hat{\Psi}(0)\rangle = \sqrt{n_0(\mathbf{R})n_0(0)}\, \exp\{-\langle(\delta\hat{\phi}(\mathbf{R}))^2\rangle/2\}. \tag{3.1.1}$$

Here $\delta\hat{\phi}(\mathbf{R}) = \hat{\phi}(\mathbf{R}) - \hat{\phi}(0)$, and $\mathbf{R} = 0$ at the trap center. Formula (3.1.1) is a generalization of Eq. (2.3.1) for the inhomogeneous case. For a trapped gas the operator $\hat{\phi}(\mathbf{R})$ is given by (we count only phonon excitations (see Overview))

$$\hat{\phi}(\mathbf{R}) = \sum_{\nu:\ \epsilon_\nu < n_0 g} [4n_0(\mathbf{R})]^{-1/2} f_\nu^+ \hat{a}_\nu + \text{h.c.}, \tag{3.1.2}$$

[1] Indications of a BEC-type of phase transition in a weakly interacting trapped 2D Bose gas were obtained in [71].

where $\hat{a}_\nu$ is the annihilation operator of an elementary excitation with energy ϵ_ν, and $f_\nu^{\pm} = u_\nu \pm v_\nu$ are the Bogolyubov u, v functions of the excitations.

In the Thomas-Fermi regime the density $n_0(\mathbf{R})$ has the parabolic shape, with the maximum value $n_{0m} = n_0(0) \approx (Nm/\pi g)^{1/2}\omega$, and the radius $R_{TF} \approx (2\mu/m\omega^2)^{1/2}$. The chemical potential is $\mu = n_{0m}g$, and the ratio $T_c/\mu \approx (\pi\hbar^2/mg)^{1/2} \gg 1$. For calculating the mean square fluctuations of the phase, we explicitly found the (discrete) spectrum and wavefunctions of excitations with energies $\varepsilon_\nu \ll \mu$ by using the method developed for 3D trapped condensates [38; 39; 40]. For excitations with higher energies we used the WKB approach. At distances R greatly exceeding l_c near the trap center, for $T \gg \mu$ we obtain

$$\langle(\delta\hat{\phi}(\mathbf{R}))^2\rangle \approx \frac{mT}{\pi\hbar^2 n_{0m}} \ln(R/\lambda_T), \tag{3.1.3}$$

where λ_T is the wavelength of thermal excitations ($\varepsilon_\nu \approx T$). Eq. (3.1.3) holds at any T for a homogeneous gas of density n_{0m}, where at $T \ll \mu$ it reproduces the well-known result (see [12]). Strictly speaking, for $T \gg \mu$ we should put the healing length l_c instead of λ_T under the logarithm. However, this gives only a small correction at temperatures significantly lower than T_c. In a trapped gas for $T \ll \mu$, due to the contribution of low-energy excitations, Eq. (3.1.3) acquires a numerical coefficient ranging from 1 at $R \ll R_{TF}$ to approximately 3 at $R \approx R_{TF}$.

The character of the Bose-condensed state is determined by the phase fluctuations at $R \sim R_{TF}$. With logarithmic accuracy, from Eq. (3.1.3) we find

$$\langle(\delta\phi(R_{TF}))^2\rangle \approx \left(\frac{T}{T_c}\right)\left(\frac{mg}{4\pi\hbar^2}\right)^{1/2} \ln N. \tag{3.1.4}$$

In quasi-2D trapped alkali gases one can expect a value $\sim 10^{-2}$ or larger for the small parameter $mg/2\pi\hbar^2$, and the number of trapped atoms N ranging from 10^4 to 10^6. For $T \gtrsim \mu$ the quantity $n_{0m}\lambda_T^2 \approx (\pi\hbar^2/m/g)(\mu/T)$ and $\ln N$ is always significantly larger than $\ln(n_{0m}\lambda_T^2)$.

Then, from Eq. (3.1.4) we identify two BEC regimes. At temperatures well below T_c the phase fluctuations are small, and there is a true condensate. For intermediate temperatures $T < T_c$ the phase fluctuations are large and, as the density fluctuations are suppressed, one has a quasicondensate (condensate with fluctuating phase).

The characteristic radius of the phase fluctuations $R_\phi \approx \lambda_T \exp(\pi\hbar^2/mT)$, following from Eq. (3.1.3) under the condition $\langle(\delta\hat{\phi}(\mathbf{R}))^2\rangle \sim 1$, greatly exceeds the healing length. Therefore, the quasicondensate has the same Thomas-Fermi density profile as the true condensate. Correlation properties at distances smaller than R_ϕ and, in particular, local density correlators are also the same. Hence, one expects the same reduction of inelastic decay rates as in 3D condensates [13]. However, the phase coherence properties of a quasicondensate are drastically different. For example, in the MIT type [76] of experiment on interference of two independently prepared quasicondensates the interference fringes can significantly differ from the case of pure condensates.

We now calculate the mean-field interparticle interaction in a quasi-2D Bose-condensed gas, relying on the binary approximation. The coupling constant g is influenced by the trapping field in the direction z of the tight confinement. For a harmonic tight confinement, the motion of two atoms interacting with each other via the potential $V(r)$ can be

still separated into their relative and center of mass motion. The former is governed by $V(r)$ together with the potential $V_H(z) = m\omega_0^2 z^2/4$ originating from the tight harmonic confinement. Then, similarly to the 3D case (see, e.g. [77]), to zero order in perturbation theory the coupling constant is equal to the vertex of interparticle interaction in vacuum at zero momenta and frequency[2] $E = 2\mu$. For low $E > 0$ this vertex coincides with the amplitude of scattering at energy E and, hence, is given by (see [36], pp. 501-502)

$$g = f(E) = \int d\mathbf{r}\psi(\mathbf{r})V(r)\psi_f^*(\mathbf{r}). \tag{3.1.5}$$

The wavefunction of the relative motion of a pair of atoms, $\psi(\mathbf{r})$, satisfies the Schrödinger equation

$$\left[-\frac{\hbar^2}{m}\Delta + V(\mathbf{r}) + V_H(z) - \frac{\hbar\omega_0}{2}\right]\psi(\mathbf{r}) = E\psi(\mathbf{r}). \tag{3.1.6}$$

The wavefunction of the free x, y motion $\psi_f(\mathbf{r}) = \varphi_0(z)\exp(i\mathbf{q}\boldsymbol{\rho})$, with $\varphi_0(z)$ being the ground state wavefunction for the potential $V_H(z)$, $\boldsymbol{\rho}$= $\{x, y\}$, and $q = (mE/\hbar^2)^{1/2}$. As the vertex of interaction is an analytical function of E, the coupling constant for $\mu < 0$ is obtained by analytical continuation of $f(E)$ to $E < 0$.

The possibility to omit higher orders in perturbation theory requires the above criterion $(mg/2\pi\hbar^2) \ll 1$.

The solution of the quasi-2D scattering problem from Eq. (3.1.6) contains two distance scales: the extension of $\psi(\mathbf{r})$ in the z direction, $l_0 = (\hbar/m\omega_0)^{1/2}$, and the characteristic radius R_e of the potential $V(r)$. In alkalis it ranges from 20 Å for Li to 100 Å for Cs. At low energies ($qR_e \ll 1$) the amplitude $f(E)$ is determined by the scattering of the s-wave for the motion in the x, y plane.

We first consider the limiting case $l_0 \gg R_e$. Then the relative motion of atoms in the region of interatomic interaction is not influenced by the tight confinement, and $\psi(\mathbf{r})$ in Eq. (3.1.5) differs only by a normalization coefficient from the 3D wavefunction:

$$\psi(r) = \eta\varphi_0(0)\psi_{3D}(r). \tag{3.1.7}$$

At $r \gg R_e$ we have $\psi_{3D} = 1 - a/r$. Hence, for $R_e \ll r \ll l_0$, Eq. (3.1.7) takes the form $\psi = \psi_{\rm as}(r) = \eta\varphi_0(0)(1 - a/r)$. This expression serves as a boundary condition at $r \to 0$ for the solution of Eq. (3.1.6) with $V(r) = 0$ ($r \gg R_e$). The latter can be expressed through the Green function $G(\mathbf{r}, \mathbf{r}')$ of this equation:

$$\psi(\mathbf{r}) = \varphi_0(z)\exp(i\mathbf{q}\cdot\boldsymbol{\rho}) + AG(\mathbf{r}, 0), \tag{3.1.8}$$

The coefficients A and η are obtained by matching the solution (3.1.8) at $r \to 0$ with $\psi_{\rm as}(r)$.

Similarly to the case of a purely 1D harmonic oscillator (see, e.g., [78]), we have

$$G(\mathbf{r}, 0) = \frac{1}{l_0}\int_0^\infty dt \frac{\exp\{i(z^2\cot t/4l_0^2 - q^2 l_0^2 t - t/2 + \rho^2/4tl_0^2)\}}{t\sqrt{(4\pi i)^3\sin t}}.$$

[2]For an inhomogeneous density profile in the x, y plane, μ should be replaced by $n_0(\mathbf{R})g$.

Under the condition $ql_0 \ll 1$ ($\mu \ll \hbar\omega_0$) at $r \ll l_0$ we obtain

$$G \approx \frac{1}{4\pi r} + \frac{1}{2(2\pi)^{3/2} l_0} \left[\ln\left(\frac{1}{\pi q^2 l_0^2}\right) + i\pi \right]. \tag{3.1.9}$$

Omitting the imaginary part of G (3.1.9) and comparing Eq. (3.1.8) with $\psi_{\rm as}$, we immediately find

$$\eta = -\frac{A}{4\pi a \varphi_0(0)} = \left[1 + \frac{a}{\sqrt{2\pi} l_0} \ln\left(\frac{1}{\pi q^2 l_0^2}\right) \right]^{-1}. \tag{3.1.10}$$

In Eq. (3.1.5) one can put $\psi_f = \varphi_0(0) = (1/2\pi l_0^2)^{1/4}$. Then, using the well-known result $\int d\mathbf{r} \psi_{3D}(r) V(r) = 4\pi\hbar^2 a/m$, Eqs. (3.1.5), (3.1.7) and (3.1.10) lead to the coupling constant

$$g = \frac{2\sqrt{2\pi}\hbar^2}{m} \frac{1}{l_0/a + (1/\sqrt{2\pi}) \ln(1/\pi q^2 l_0^2)}. \tag{3.1.11}$$

For $\mu < 0$, analytical continuation of Eqs. (3.1.9) and (3.1.11) to $E = \hbar^2 q^2/m < 0$ leads to the replacement $E \to |E| = 2|\mu|$ in the definition of q.

The coupling constant in quasi-2D depends on $q = (2m|\mu|/\hbar^2)^{1/2}$ and, hence, on the condensate density. In the limit $l_0 \gg |a|$ the logarithmic term in Eq. (3.1.11) is not important, and g becomes density independent. In this case the quasi-2D gas can be treated as a 3D condensate with the density profile $\propto \exp(-z^2/l_0^2)$ in the z direction.

As follows from Eq. (3.1.11), for repulsive mean-field interaction in 3D ($a > 0$) the interaction in quasi-2D is also repulsive. For $a < 0$ the dependence of g (and the scattering amplitude f) on l_0 has a resonance character (cf. Fig. 3.1.1): The coupling constant changes sign from negative (attraction) at very large l_0 to positive for $l_0 < l_* = (|a|/\sqrt{2\pi}) \ln(1/\pi q^2 l_0^2)$. The resonance originates from the fact that the modulus of energy coincides with the binding energy of a pair of atoms in the quasi-2D geometry at $l_0 \approx l_*$. This should describe the case of Cs, where $a \lesssim -600$ Å [79; 80; 81; 73; 27; 28] and the condition $l_0 \gg R_e$ assumed in Eq. (3.1.11) is satisfied at $l_0 < l_*$. Near the resonance point l_* the quantity $(m|g|/2\pi\hbar^2)$ becomes large, which violates the perturbation theory for a Bose-condensed gas and makes Eqs. (3.1.5) and (3.1.11) invalid.

For $l_0 \lesssim R_e$ (except for very small l_0) we used directly Eqs. (3.1.5) and (3.1.6) and calculated numerically the coupling constant g for Li, Na, Rb, and Cs. The potential $V(r)$ was modeled by the Van der Waals tail, with a hard core at a distance $R_0 \ll R_e$ selected to support many bound states and reproduce the scattering length a. The numerical results differ slightly from the predictions of Eq. (3.1.11). For Rb and Cs both are presented in Fig. 3.1.1.

The nature of the $g(l_0)$ dependence in quasi-2D can be understood just relying on the values of g in the purely 2D and 3D cases. In 2D at low energies the mean-field interaction is always repulsive. This striking difference from the 3D case can be found from the solution of the 2D scattering problem in [36] and originates from the 2D kinematics: At distances, where $R_e \ll \rho \ll q^{-1}$ ($q \to 0$), the solution of the Schrödinger equation for the (free) relative motion in a pair of atoms reads $\psi \propto \ln(\rho/d)/\ln(1/qd)$ ($d > 0$). We always have $|\psi|^2$ increasing with ρ, unless we touch resonances corresponding to the presence of a bound state with zero energy ($d \to \infty$). This means that it is favorable for particles to be at larger ρ, i.e. they repel each other.

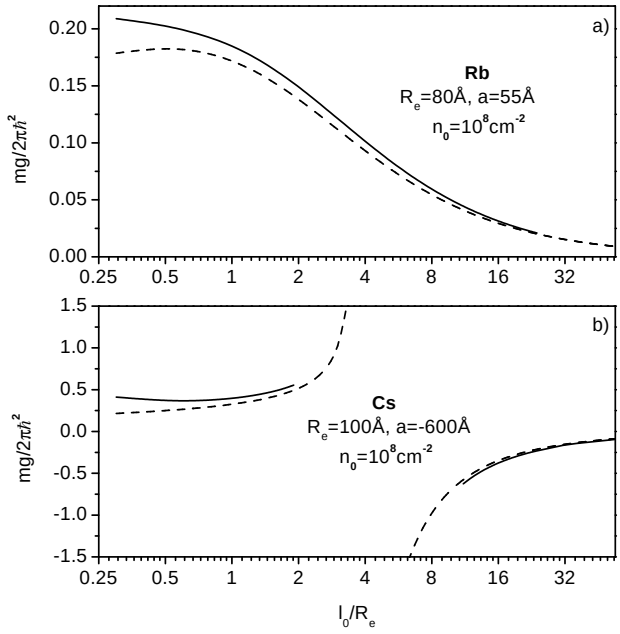

Figure 3.1.1: The parameter $mg/2\pi\hbar^2$ versus l_0/R_e at fixed n_0 for Rb (a) and Cs (b). Solid curves correspond to the numerical results, dashed curves to Eq. (3.1.11). The dotted curve in (b) shows the result of Eq. (3.1.11) in the region where $m|g|/2\pi\hbar^2 \sim 1$.

In quasi-2D for very large l_0 the sign of the interparticle interaction is the same as in 3D. With decreasing l_0, the 2D features in the relative motion of atoms become pronounced, which is described by the logarithmic term in Eq. (3.1.11). Hence, for $a > 0$ the interaction remains repulsive, whereas for $a < 0$ the attraction turns to repulsion.

The obtained results are promising for tunable BEC in quasi-2D gases, based on variations of the tight confinement and, hence, l_0. However, as in the MIT studies of tunable 3D BEC by using Feshbach resonances [82], an "underwater stone" concerns inelastic losses: Variation of l_0 can change the rates of inelastic processes. For optically trapped atoms in the lowest Zeeman state the most important decay process is 3-body recombination[3].

This process occurs at interparticle distances $r \lesssim \max\{R_e, |a|\}$ [84; 85]. We will restrict ourselves to the case where $l_0 \gtrsim |a|$ and is also significantly larger than R_e. Then the character of recombination collisions remains 3-dimensional, and one can treat them in a similar way as in a 3D gas with the density profile $(n_0/\sqrt{\pi}l_0)\exp(-z^2/l_0^2)$.

However, the normalization coefficient of the wavefunction in the incoming channel will be influenced by the tight confinement. Relying on the Jastrow approximation, we write this wavefunction as a product of the three wavefunctions $\psi(\mathbf{r}_{ik})$, each of them being a solution of the binary collision problem Eq. (3.1.6). In our limiting case the

[3]Three-body recombination to a weakly bound quasi-2D molecular state was discussed in [83].

solution is given by Eq. (3.1.7) divided by $\varphi_0(0)$ to reconstruct the density profile in the z direction. The outgoing wavefunction remains the same as in 3D, since one has a molecule and an atom with very large kinetic energies.

Thus, in the Jastrow approach we have an additional factor η^3 for the amplitude and η^6 for the probability of recombination in a quasi-2D gas compared to the 3D case. Averaging over the density profile in the z direction, we can relate the quasi-2D rate constant α to the rate constant in 3D (see [85] for a table of α_{3D} in alkalis):

$$\alpha = (\eta^6/\pi l_0^2)\alpha_{3D}. \tag{3.1.12}$$

As η is given by Eq. (3.1.10), for $a > 0$ the dependence $\alpha(l_0)$ is smooth. For $a < 0$ the rate constant α peaks at $l_0 \approx l_*$ and decreases as $l_0^4/(l_* - l_0)^6$ at smaller l_0. This indicates a possibility to reduce recombination losses while maintaining a repulsive mean-field interaction ($g > 0$). For Cs already at $l_0 \approx 200$ Å ($l_* \approx 500$Å) we have $\alpha \sim 10^{-17}$ cm^4/s, and at densities 10^8 cm^{-2} the life-time $\tau > 1$ s.

The predicted possibility to modify the mean-field interaction and reduce inelastic losses by varying the frequency of the tight confinement opens new handles on tunable BEC in quasi-2D gases. These experiments can be combined with measurements of non-trivial phase coherence properties of condensates with fluctuating phase.

3.2 Superfluid transition in quasi-2D Fermi gases

We show that atomic Fermi gases in quasi-2D geometries are promising for achieving superfluidity. In the regime of BCS pairing for weak attraction, we calculate the critical temperature T_c and analyze possibilities of increasing the ratio of T_c to the Fermi energy. In the opposite limit, where a strong coupling leads to the formation of weakly bound quasi-2D dimers, we find that their Bose-Einstein condensate will be stable on a long time scale.

Recent progress in trapping and cooling of Fermi isotopes of K [86; 87; 88; 89] and Li [90; 8; 91; 92; 93; 94] has shown the ability to go far below the temperature of quantum degeneracy and to manipulate independently the trapping geometry, density, temperature and interparticle interaction. The Duke experiment [95] presents intriguing results on the possibility of achieving a superfluid phase transition in the two-component Fermi gas of ^{6}Li.

Two-dimensional Fermi gases have striking features not encountered in 3D. In the superfluid state, thermal fluctuations of the phase of the order parameter strongly modify the phase coherence properties. The interaction strength depends logarithmically on the relative energy of the colliding atoms. For degenerate Fermi gases this energy is of the order of the Fermi energy ε_F which is proportional to the 2D density n. Accordingly, the exponential dependence of the BCS transition temperature on the interaction strength transforms into a power law dependence on the density: $T_c \propto n^{1/2}$ [96; 97; 98; 99]. This suggests a unique possibility to cross the critical point by adiabatically expanding a degenerate Fermi gas. Since the ratio T/ε_F remains unchanged, the temperature scales as n and decreases with density faster than T_c.

Experimentally it is possible to achieve the quasi-2D regime by confining the atoms in one direction so tightly that the corresponding level spacing exceeds the Fermi energy. Under this condition the degenerate Fermi gas is kinematically two-dimensional. Thus far, this regime has been reached for Cs atoms [73; 27; 74; 75; 30; 31] and for Bose-Einstein condensates of Na [6] and Rb [7].

In the quasi-2D regime the mean-field interaction between particles exhibits a similar logarithmic dependence on the particle energy as in the purely 2D case (see Section 3.1 and Chapter 4). The amplitude of the s-wave scattering turns out to be sensitive to the strength of the tight confinement. This opens new handles on manipulations of the interparticle interaction and superfluid pairing.

In this section we show that atomic Fermi gases in quasi-2D geometries can become strong competitors of 3D gases in achieving superfluidity. The ability to increase the interparticle interaction by tuning the trap frequencies gives an opportunity to realize a transition from the standard BCS pairing in the case of weak attraction to the limit of strong interactions and pairing in coordinate space. In the latter case one eventually gets a dilute system of weakly bound quasi-2D dimers of fermionic atoms, which can undergo Bose-Einstein condensation. For the BCS case, we calculate the critical temperature T_c to second order in perturbation theory and discuss possibilities of increasing the ratio T_c/ε_F. In the other extreme, we find that the interaction between the quasi-2D dimers is repulsive, and their collisional relaxation and decay are strongly suppressed. This allows us to conclude that BEC of these composite bosons will be stable on a long time scale.

We consider an ultracold two-component Fermi gas in the quasi-2D regime and confine ourselves to the s-wave interaction and superfluid pairing between atoms of different components. We assume that the characteristic radius of the interaction potential is much smaller than the harmonic oscillator length in the tightly confined direction, $l_0 = (\hbar/m\omega_0)^{1/2}$, where m is the atom mass, and ω_0 is the confinement frequency. Then the interaction problem involves two length scales: l_0 and the 3D scattering length a. For $a < 0$ and $|a| \ll l_0$, there is a peculiar quasi-2D weakly bound s-state of two particles, with the binding energy (see Chapter 4)

$$\varepsilon_0 = 0.915(\hbar\omega_0/\pi)\exp\left(-\sqrt{2\pi}l_0/|a|\right) \ll \hbar\omega_0. \tag{3.2.1}$$

In this case the coupling constant for the intercomponent interaction takes the form $g = (4\pi\hbar^2/m)\ln^{-1}(\varepsilon_0/\varepsilon)$, where the relative collision energy ε is assumed to be either much smaller or much larger than ε_0 (see Chapter 4). As in degenerate Fermi gases one has $\varepsilon \sim \varepsilon_F$, the interaction is attractive ($g < 0$) if the density is sufficiently high and one satisfies the inequality

$$\varepsilon_0/\varepsilon_F \ll 1. \tag{3.2.2}$$

Thus, the inequality (3.2.2) is the necessary condition for the BCS pairing. For finding the critical temperature T_c below which the formation of Cooper pairs becomes favorable, we go beyond the simple BCS approach and proceed along the lines of the theory developed by Gor'kov and Melik-Barkhudarov for the 3D case [100].

The critical temperature T_c is determined as the highest temperature for which the linearized equation for the order parameter (gap) $\Delta = \langle g\hat{\Psi}\hat{\Psi}\rangle$ has a nontrivial solution [101]. Assuming that the quasi-2D gas is uniform in two in-plane directions, the gap

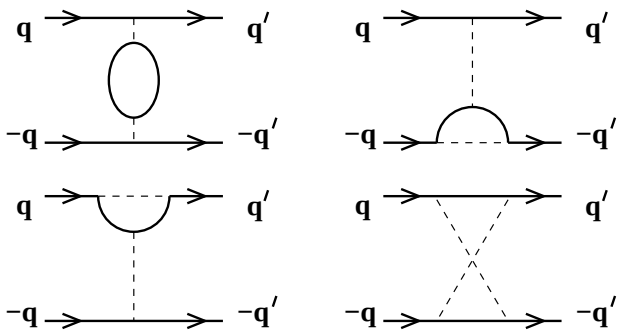

Figure 3.2.1: The leading contributions to $\delta V(\mathbf{q}, \mathbf{q}')$.

equation in the momentum space takes the 2D form

$$\Delta(\mathbf{q}) \approx -\int \left\{ \frac{\hbar^2}{m} f(z, \mathbf{q}, \mathbf{q}') \left[K(q') + \frac{1}{z - \xi(q') + i0} \right] + \delta V(\mathbf{q}, \mathbf{q}') K(q') \right\} \Delta(\mathbf{q}') \frac{\mathrm{d}^2 q'}{(2\pi)^2}, \tag{3.2.3}$$

where $K(q) = (1/2\xi(q)) \tanh(\xi(q)/2T)$, $\xi(q) = \hbar^2 q^2/2m - \mu$, $\mu \approx \varepsilon_F = \pi\hbar^2 n/m$ is the chemical potential, and n is the total density of the two equally populated components. The first term in the rhs of Eq. (3.2.3) results from the direct interaction between particles, and we renormalized the interaction potential in terms of the scattering amplitude f (vertex function). The latter is a solution of the quasi-2D scattering problem. The parameter z has a meaning of the total energy of colliding particles in their center of mass reference frame. It is of the order of ε_F and drops out of the final answer. The term $\delta V(\mathbf{q}, \mathbf{q}')$ describes the modification of the interparticle interaction due to the presence of other particles (many-body effects). The leading contributions to this term are second order in the scattering amplitude. They are shown in Fig. 3.2.1 and correspond to an indirect interaction between two particles when one of them interacts with a particle-hole pair virtually created from the ground state (filled Fermi sea) by the other particle. These second order contributions are important for the absolute value of the critical temperature (preexponential factor in the 3D case), whereas higher order terms involving more interaction events can be neglected.

The amplitude f is independent of the momenta $\mathbf{q}, \mathbf{q}'$ and we will use the 2D relation (see [12])

$$f = 4\pi \ln^{-1}\{\varepsilon_0/(-z)\}. \tag{3.2.4}$$

The last term in the rhs of Eq. (3.2.3) is a small correction, since $\delta V \sim f^2$. Accordingly, the quantity $|f|$ represents a small parameter of the theory. In the quasi-2D regime ($z \ll \hbar\omega_0$) the motion of particles in the tightly confined direction provides a correction to Eq. (3.2.4), which is $\sim (z/\hbar\omega_0) f^2$ (see Chapter 4). It is much smaller than δV and will be omitted.

Equations (3.2.3) and (3.2.4) show that the momentum dependence of the order parameter appears only due to the second order term that contains many-body contributions to the interparticle interaction δV. The latter is a function of $p = |\mathbf{q} + \mathbf{q}'|$ and

rapidly decays for $p > 2q_F$, where $q_F = \sqrt{2m\mu}/\hbar$ is the Fermi momentum. For $p \leq 2q_F$ the quantity δV is almost constant. Therefore, one has $\Delta(\mathbf{q}') \approx \Delta(q_F)$ in a wide momentum range near the Fermi surface. Then, for $q = q_F$ a direct integration of Eq. (3.2.3) yields

$$\Delta(q_F) = -\frac{f(z)}{4\pi}\Delta(q_F)\ln\left(-\frac{2\mu z}{\pi^2 T^2}e^{2\gamma}\right) - \delta V(q_F, q_F)\frac{m}{2\pi\hbar^2}\ln\left(C\frac{\mu}{T}\right)\Delta(q_F),$$

where $\gamma \approx 0.5772$ is the Euler constant, and C is a numerical factor determined by the momentum dependence of Δ and δV. The calculation of $\delta V(q_F, q_F)$ is straightforward and gives $\delta V(q_F, q_F) = (\hbar^2/2\pi m) f^2(2\mu)$. Then, using Eq. (3.2.4) we obtain the critical temperature

$$T_c \approx (2\mu/\pi)\exp\left(\gamma - 1 - |2\pi \mathrm{Re} f^{-1}(2\mu)|\right).$$

The exponent in this equation should be large and the quantity $\mathrm{Re} f^{-1}(2\mu)$ should be negative. As the chemical potential is $\mu \approx \varepsilon_F$, from Eq. (3.2.4) one sees that these requirements are reached under the condition (3.2.2). Using Eqs. (3.2.1) and (3.2.4) the critical temperature takes the form

$$T_c = \frac{\gamma\sqrt{2\varepsilon_0\varepsilon_F}}{\pi e} = 0.16\sqrt{\varepsilon_F\hbar\omega_0}\exp\left(-\sqrt{\frac{\pi}{2}}\frac{l_0}{|a|}\right) \ll \varepsilon_F. \tag{3.2.5}$$

The relative correction to this result is of the order of $1/|\ln(\varepsilon_0/\varepsilon_F)| \ll 1$.

Note that Eq. (3.2.5) predicts by a factor of e smaller value for the critical temperature than a simple BCS calculation[4]. This means that the attractive interaction between particles becomes weaker once we take into account the polarization of the medium.

The ratio T_c/ε_F is not necessarily very small. For example, using Feshbach resonances the scattering length is tunable over a wide interval of negative values [86; 87; 91; 92; 93; 94]. Keeping the exponential term equal to 0.05 in Eq. (3.2.5), with $\omega_0 \sim 100$ kHz we obtain $T_c/\varepsilon_F \sim 0.1$ for 2D densities $n \sim 10^9$ cm^{-2} ($T_c \sim 40$ nK).

As in the purely 2D case [96; 97; 98; 99], the transition temperature $T_c \propto n^{1/2}$ and the ratio T_c/ε_F increases with decreasing density as $n^{-1/2}$. This is a striking difference from the 3D case, where this ratio decreases exponentially with density. In the presence of the in-plane confinement, one can approach the BCS transition in a degenerate Fermi gas by adiabatically expanding the quasi-2D trap in the in-plane direction(s). As the degeneracy parameter T/ε_F is conserved in the course of the adiabatic expansion, the ratio T/T_c will decrease as $n^{1/2}$. Equations (3.2.1) and (3.2.5) also show that one can increase ε_0 and T_c/ε_0 by tuning $|a|$ to larger values or by making the tight confinement stronger and thus decreasing l_0.

What happens if ε_0 and ε_F become comparable with each other, i.e. one reaches the quasi-2D resonance for two-body collisions? Then Eq. (3.2.5) leads to $T_c \sim \varepsilon_F$ and is no longer valid. In fact, for $\varepsilon_0 > \varepsilon_F$ the formation of bound quasi-2D dimers of distinguishable fermions becomes energetically favorable and one encounters the problem of Bose-Einstein condensation of these bosonic molecules. Thus, an increase of the ratio $\varepsilon_0/\varepsilon_F$ from small to large values is expected to provide a transformation of the BCS pairing to molecular BEC. This type of crossover has been discussed in literature in

[4]For the purely 2D case see this calculation in [96; 102; 103].

the context of superconductivity [104; 105; 106; 102; 97; 98; 99] and in relation to superfluidity in 2D films of ^{3}He [96; 103]. The idea of using a Feshbach resonance for achieving a superfluid transition in the BCS-BEC crossover regime in ultracold 3D Fermi gases has been proposed in refs. [107; 108].

We will not consider the crossover regime and confine ourselves to the limiting case of molecular BEC ($\varepsilon_0 \gg \varepsilon_F$). A subtle question is related to the stability of the expected condensate, which depends on the interaction between the molecules. For the repulsive interaction one will have a stable molecular BEC, and the attractive interaction should cause a collapse.

The molecule-molecule scattering is a 4-body problem described by the Schrödinger equation

$$\left[-\frac{\hbar^2}{m}\left(\nabla^2_{\mathbf{r}_1}+\nabla^2_{\mathbf{r}_2}+\frac{\nabla^2_{\mathbf{R}}}{2}\right)+U(r_1)+U(r_2)+\sum_{\pm}U\left(\frac{\mathbf{r}_1+\mathbf{r}_2}{2}\pm\mathbf{R}\right)-E\right]\Psi(\mathbf{r}_1,\mathbf{r}_2,\mathbf{R})=0. \tag{3.2.6}$$

Here $\mathbf{r}_1$ is the distance between two given distinguishable fermions, $\mathbf{r}_2$ is the distance between the other two, $\mathbf{R}$ is the distance between the centers of mass of these pairs, and U is the interatomic potential. The total energy is $E=-2\varepsilon_0+\varepsilon$, with ε being the relative molecule-molecule kinetic energy.

The interaction between molecules is present only at intermolecular distances of the order of or smaller than the size of a molecule $d_*=\hbar/\sqrt{m\varepsilon_0}$. Therefore, at energies $\varepsilon \ll \varepsilon_0$ the scattering between molecules is dominated by the s-wave channel and can be analyzed on the basis of the solution of Eq. (3.2.6) for $\varepsilon = 0$. For large R the corresponding wavefunction is $\Psi(\mathbf{r}_1,\mathbf{r}_2,\mathbf{R}) \approx K_0(r_1/d_*)K_0(r_2/d_*)\ln(\alpha R/d_*)$, where the decaying Bessel function $K_0(r_{1,2}/d_*)$ represents the 2-body bound state. The parameter α is a universal constant which can be found by matching the quantity $\ln(\alpha R/d_*)$ with the solution of Eq. (3.2.6) at short distances. Finally, matching $\ln(\alpha R/d_*)$ with the wavefunction of free relative motion of two molecules at distances $d_* \ll R \ll \Lambda_\varepsilon$, where $\Lambda_\varepsilon=\hbar/\sqrt{m\varepsilon}$ is their de Broglie wavelength, we obtain the coupling constant (scattering amplitude) for the interaction between molecules:

$$g_m=(2\pi\hbar^2/m)\ln^{-1}(2\alpha^2e^{-2\gamma}\varepsilon_0/\varepsilon)>0; \quad \varepsilon\ll\varepsilon_0. \tag{3.2.7}$$

A precise value of α is not important as it gives rise to higher order corrections in Eq. (3.2.7). However, in order to make sure that this constant is neither anomalously large nor anomalously small we have integrated Eq. (3.2.6) numerically. For this purpose, it is convenient to transform Eq. (3.2.6) into an integral equation for a function which depends only on three independent coordinates. This has been done by using the method of ref. [109]. Our calculations lead to $\alpha \approx 1.6$. They show the absence of 4-body weakly bound states and confirm an intuitive picture that the interaction between two molecules can be qualitatively represented by means of a purely repulsive potential with the range $\sim d_*$. For the interaction between Bose-condensed dimers, in Eq. (3.2.7) one has $\varepsilon = 2n_m g_m \ll \varepsilon_0$, where n_m is the density of the dimers (see Section 3.1). We thus conclude that a Bose condensate of these weakly bound dimers is stable with respect to collapse.

The 2D gas of bosons becomes Bose-condensed below the Kosterlitz-Thouless transition temperature T_{KT} [47; 48] which depends on the interaction between particles.

According to the recent quantum Monte Carlo simulations [49; 50], for the 2D gas with the coupling constant (3.2.7) the Kosterlitz-Thouless temperature is given by

$$T_{KT} = (\pi\hbar^2 n_m/m) \ln^{-1}\left[(\eta/4\pi)\ln\left(1/n_m d_*^2\right)\right], \tag{3.2.8}$$

where the numerical factor $\eta \approx 380$. For $\varepsilon_F \ll \varepsilon_0$, the density of dimers $n_m \approx n/2$ and the parameter $(1/n_m d_*^2) \approx 2\pi\varepsilon_0/\varepsilon_F$. Then, for $\varepsilon_0/\varepsilon_F = 10$, Eq. (3.2.8) gives $T_{KT}/\varepsilon_F \approx 0.1$ and at densities 10^8 cm^{-2} the transition temperature in the case of ^{6}Li is $T_{KT} \approx 30$ nK.

The weakly bound dimers that we are considering are molecules in the highest rovibrational state and they can undergo collisional relaxation and decay. The relaxation process occurs in pair dimer-dimer or dimer-atom collisions. It produces diatomic molecules in deep bound states and is accompanied by a release of the kinetic energy. The size of these deeply bound molecules is of the order of the characteristic radius of the interatomic potential $R_e \ll l_0$, and their internal properties are not influenced by the tight confinement. Therefore, the relaxation can be treated as a 3D process and it requires the presence of at least three fermionic atoms at distances $\sim R_e$ between them. Since at least two of them are identical, the relaxation probability acquires a small factor $(kR_e)^2$ compared to the case of bosons, where $k \sim 1/d_* = \sqrt{\varepsilon_0/\hbar\omega_0}/l_0$ is a characteristic momentum of atoms. The 3D density of atoms in the quasi-2D geometry is $\sim n/l_0$. Thus, qualitatively, the inverse relaxation time can be written as $\tau_{\rm rel}^{-1} \sim \alpha_{\rm rel} n (R_e/l_0)^2 (\varepsilon_0/\hbar\omega_0)/l_0$, where $\alpha_{\rm rel}$ is the relaxation rate constant for the highest rovibrational states of 3D molecules of two bosonic atoms. We estimate $\tau_{\rm rel}$ keeping in mind the recent measurements for Rb_2 molecules [110] which give $\alpha_{\rm rel} \approx 3 \times 10^{-11}$ cm^3/s. For l_0 in the interval from 10^{-5} to 10^{-4} cm, the suppression factor $(R_e/l_0)^2(\varepsilon_0/\hbar\omega_0)$ ranges from 10^{-3} to 10^{-5} and at 2D densities $n \sim 10^8$ cm^{-2} we find the relaxation time $\tau_{\rm rel}$ of the order of a second or larger.

Dimer-dimer pair collisions can lead to the formation of bound trimers, accompanied by a release of one of the atoms. The formation of deeply bound trimer states will be suppressed at least in the same way as the relaxation process discussed above. Therefore, it is important that there are no weakly bound trimers in (quasi-)2D. Just as in 3D [111; 112] (see also ref. [109]), this can be established by using the zero-range approach ($R_e \to 0$). We have performed this analysis along the lines of the 3D work [109]. Qualitatively, the symmetry of the 3-fermion system containing two identical fermions provides a strong centrifugal repulsion that does not allow the presence of 3-body bound states. This is in contrast to 2D bosons where one has two fully symmetric trimer bound states [113].

Thus, the life-time of quasi-2D dimers of fermionic atoms is rather long and one easily estimates that it greatly exceeds the characteristic time of elastic collisions. One can even think of achieving BEC in the initially non-condensed gas of dimers produced out of a non-superfluid atomic Fermi gas under a decrease of n or l_0.

In conclusion, we have found the temperature of superfluid phase transition in two-component quasi-2D Fermi gases. Our results are promising for achieving this transition in both the regime of BCS pairing and the regime of BEC of weakly bound dimers.

Chapter 4 Interatomic collisions in a tightly confined Bose gas

We discuss pair interatomic collisions in a Bose gas tightly confined in one (axial) direction and identify two regimes of scattering. In the quasi-2D regime, where the confinement frequency ω_0 greatly exceeds the gas temperature T, the scattering rates exhibit 2D features of the particle motion. At temperatures $T \sim \hbar\omega_0$ one has a confinement-dominated 3D regime, where the confinement can change the momentum dependence of the scattering amplitudes. We describe the collision-induced energy exchange between the axial and radial degrees of freedom and analyze recent experiments on thermalization and spin relaxation rates in a tightly (axially) confined gas of Cs atoms.

4.1 Introduction

Collisional properties of ultra-cold gases strongly confined in one direction attract a great deal of interest since the start of active studies of spin-polarized atomic hydrogen. In the latter case the interest was related to recombination and spin relaxation collisions and to elastic scattering in the (quasi-)2D gas of atomic hydrogen adsorbed on liquid He surface (see [70] for review). The discovery of Bose-Einstein condensation in trapped alkali-atom clouds [3; 4; 5] stimulated a progress in evaporative and optical cooling and in trapping of neutral atoms. Present facilities make it possible to (tightly) confine the motion of particles in one direction to zero point oscillations. Then, kinematically the gas is 2D, and the only difference from the purely 2D case is related to the value of the interparticle interaction which now depends on the tight confinement. Thus, one now has many more opportunities to create (quasi-)2D gases. In the recent experiments with optically trapped Cs [73; 27; 74; 75; 29; 30] about 90% of atoms are accumulated in the ground state of the harmonic oscillator potential in the direction of the tight confinement.

In this chapter we consider a Bose gas tightly confined in one (axial) direction and discuss how the axial confinement manifests itself in pair elastic and inelastic collisions. We identify two regimes of scattering. At temperatures $T \ll \hbar\omega_0$ (ω_0 is the axial frequency) only the ground state of the axial harmonic oscillator is occupied, and one has a quasi-2D regime. In this case, the 2D character of the relative motion of particles at large separation between them, manifests itself in a logarithmic energy dependence of the scattering amplitude. For a negative 3D scattering length a, we observe resonances in the dependence of the elastic scattering rate on a. This is quite different from the 3D case where the scattering rate always increases with a^2. The presence of these resonances in quasi-2D follows from the analysis given in Section 3.1 and finds its origin in increasing role of the 2D kinematics of the particle motion with increasing ratio $|a|/l_0$, where $l_0 = (\hbar/m\omega_0)^{1/2}$ is the axial extension of the atom wavefunction, and m the atom mass.

At temperatures $T \sim \hbar\omega_0$ we have a confinement-dominated 3D regime of scattering, where the 2D character of the particle motion is no longer pronounced in the scattering process, but the axial confinement can strongly influence the energy (temperature) dependence of the scattering rate. Treating collisions as three-dimensional, the wavevector p of the relative motion of colliding atoms does not decrease with T. The atoms undergo zero-point oscillations in the axial direction and this corresponds to $p \sim 1/l_0$. If the 3D scattering amplitude is momentum-dependent at these p, which is the case for $|a| \gtrsim l_0$, then the temperature dependence of the elastic collisional rate becomes much weaker. This means that for a large 3D scattering length the tight axial confinement suppresses a resonant enhancement of the collisional rate at low energies. In many of the current experiments with ultra-cold gases one tunes a to large positive or negative values by varying the magnetic field and achieving Feshbach resonances [114; 115; 116; 82; 117; 28; 118; 119; 120]. In the unitarity limit ($|a| \to \infty$) the 3D elastic cross section is $\sigma = 8\pi/p^2$ and the rate of 3D elastic collisions strongly increases with decreasing temperature. The tight confinement of the axial motion makes the scattering rate practically temperature independent at $T \sim \hbar\omega_0$. We obtain a similar suppression of resonances for inelastic collisions, where the resonant temperature dependence in 3D is related to the energy dependence of the initial wavefunction of colliding atoms. We analyze the Stanford and ENS experiments on elastic [27; 29; 30] and spin relaxation [27] collisions in a tightly axially confined gas of cesium atoms and discuss the origin of significant deviations of the observed collisional rates from the 3D behavior.

We develop a theory to describe the collision-induced energy exchange between axial and radial degrees of freedom of the particle motion. We establish selection rules for transitions between particle states in the axial harmonic potential and calculate the corresponding transition amplitudes. This allows us to consider temperatures $T \gtrsim \hbar\omega_0$ and analyze thermalization rates in non-equilibrium clouds. In the Stanford and ENS experiments these clouds were created by means of degenerate Raman sideband cooling [73; 27; 74; 75; 29; 30] which effectively leads to a gas with different axial (T_z) and radial (T_ρ) temperatures. After the cooling is switched off, the temperatures T_z and T_ρ start to approach each other, and ultimately the gas reaches the equilibrium temperature. At sufficiently low T only a few axial states are occupied and the temperature dependence of the corresponding thermalization rates should deviate from the 3D behavior, thus exhibiting the influence of the axial confinement on the scattering process. We calculate the thermalization rates and establish the conditions under which this influence is pronounced.

The minimum energy exchange between the radial and axial degrees of freedom of two colliding atoms is equal to $2\hbar\omega_0$. This follows from the symmetry of the interatomic potential with respect to simultaneous inversion of the axial coordinates of the two atoms, which ensures the conservation of parity of their wavefunction under this operation. Accordingly, the sum of two (axial) vibrational quantum numbers can be changed only by an even value. The rate of energy transfer from the radial to axial motion is proportional to the difference between the radial and axial temperatures $\Delta T = T_\rho - T_z$, if they are close to each other. As the total energy of colliding particles should exceed $2\hbar\omega_0$ in order to enable the energy transfer, the rate of this process at temperatures $T < \hbar\omega_0$ becomes exponentially small: $\Delta\dot{E} \propto \Delta T \exp(-2\hbar\omega_0/T)$. Due to the presence of the energy gap

$\hbar\omega_0$ in the excitation spectrum of the axial harmonic oscillator, the heat capacity of the axial degree of freedom is $dE_z/dT_z \sim \exp(-\hbar\omega_0/T)$, which leads to a thermalization rate $\Delta\dot{T}/\Delta T \propto \exp(-\hbar\omega_0/T)$. This exponential temperature dependence shows that the thermalization is suppressed at very low temperatures. One can deeply cool the axial motion, but radially the cloud remains "hot" on a very long time scale.

4.2 2D scattering problem

First, we discuss the purely 2D elastic scattering in pair collisions of ultra-cold atoms interacting via a short-range potential $U(\rho)$. At interparticle distances $\rho \to \infty$ the wavefunction of colliding atoms is represented as a superposition of the incident plane wave and scattered circular wave [36]:

$$\psi(\boldsymbol{\rho}) \approx e^{i\mathbf{q}\cdot\boldsymbol{\rho}} - f(q,\phi)\sqrt{\frac{i}{8\pi q\rho}}e^{iq\rho}. \tag{4.2.1}$$

The quantity $f(q,\phi)$ is the scattering amplitude, q is the relative momentum of the atoms, and ϕ the scattering angle. Note that $f(q,\phi)$ in Eq. (4.2.1) differs by a factor of $-\sqrt{8\pi q}$ from the 2D scattering amplitude defined in [36].

Similarly to the 3D case, the scattering amplitude is governed by the contribution of the s-wave scattering if the relative momentum q satisfies the inequality $qR_e \ll 1$, where R_e is the characteristic radius of interaction. In the case of alkali atoms, the radius R_e is determined by the Van der Waals tail of the potential $U(\rho)$ and ranges from 20 Å for Li to 100 Å for Cs. The s-wave scattering amplitude is independent of the scattering angle ϕ. The probability $\alpha(q)$ for a scattered particle to pass through a circle of radius ρ per unit time is equal to the intensity of the scattered wave multiplied by $2\pi\rho v$, where $v = 2\hbar q/m$ is the relative velocity of colliding atoms. From Eq. (4.2.1) we have

$$\alpha(q) = \frac{\hbar}{2m}|f(q)|^2. \tag{4.2.2}$$

The velocity v is equal to the current density in the incident wave of Eq. (4.2.1). The ratio of $\alpha(q)$ to this quantity is the 2D cross section which has the dimension of length:

$$\sigma(q) = |f(q)|^2/4q. \tag{4.2.3}$$

For the case of identical bosons Eqs. (4.2.2) and (4.2.3) have an extra factor 2 in the rhs.

The quantity $\alpha(q)$ is nothing else than the rate constant of elastic collisions at a given q. The average of $\alpha(q)$ over the momentum distribution of atoms, multiplied by the number of pairs of atoms in a unit area, gives the number of scattering events in this area per unit time.

For finding the s-wave scattering amplitude one has to solve the Schrödinger equation for the s-wave of the relative motion of colliding atoms at energy $\varepsilon = \hbar^2q^2/m$:

$$\left[-\frac{\hbar^2}{m}\Delta_\rho + U(\rho)\right]\psi_s(q,\rho) = \frac{\hbar^2q^2}{m}\psi_s(q,\rho). \tag{4.2.4}$$

At distances $\rho \gg R_e$ the relative motion is free and one can omit the interaction between atoms. Then the solution of Eq. (4.2.4), which for $q\rho \gg 1$ gives the partial s-wave of $\psi(\boldsymbol{\rho})$ (4.2.1), takes the form

$$\psi_s(q,\rho) = J_0(q\rho) - \frac{if(q)}{4} H_0(q\rho), \quad \rho \ll R_e, \tag{4.2.5}$$

where J_0 and H_0 are the Bessel and Hankel functions.

On the other hand, at distances $\rho \ll 1/q$ one can omit the relative energy of particles in Eq. (4.2.4). The resulting (zero energy) solution depends on the momentum q only through a normalization coefficient. In the interval of distances where $R_e \ll \rho \ll 1/q$, the motion is free and this solution becomes $\psi_s \propto \ln(\rho/d)$, where $d > 0$ is a characteristic length that depends on a detailed shape of the potential $U(\rho)$ and has to be found from the exact solution of Eq. (4.2.4) with $q = 0$. This logarithmic expression serves as a boundary condition for $\psi_s(q,\rho)$ (4.2.5) at $q\rho \ll 1$, which immediately leads to the scattering amplitude [36]

$$f(q) = \frac{2\pi}{\ln(1/qd_*) + i\pi/2}, \tag{4.2.6}$$

where $d_* = (d/2)\exp C$ and $C \approx 0.577$ is the Euler constant.

It is important to mention that the condition $qR_e \ll 1$ is sufficient for the validity of Eq. (4.2.6). This equation also holds for the case of resonance scattering, where the potential $U(\rho)$ supports a weakly bound s-level. In this case the spatial shape of $\psi_s(q,\rho)$ at distances where $R_e \ll \rho \ll 1/q$, is the same as the shape of the wavefunction of the weakly bound state. This gives $d_* = \hbar/\sqrt{m\varepsilon_0}$, where ε_0 is the binding energy. We thus have the inequality $d_* \gg R_e$, and the quantity qd_* in Eq. (4.2.6) can be both small and large. The rate constant $\alpha(q)$ peaks at $q = 1/d_*$ and decreases as $1/[1 + (4/\pi^2)\ln^2(qd_*)]$ with increasing or decreasing q. Note that the 2D resonance is actually a resonance in the logarithmic scale of energies. The decrease of α by factor 2 from its maximum value requires a change of energy $\varepsilon = \hbar^2 q^2/m$ by factor 20.

For $qd_* \ll 1$ one may omit the imaginary part in Eq. (4.2.6), and the scattering amplitude becomes real and positive[1]. The positive sign of $f(q)$ has a crucial consequence for the mean-field interparticle interaction in purely 2D Bose gases. In the ultra-cold limit where $qR_e \ll 1$, the scattering amplitude is related to the energy of interaction in a pair of particles (coupling constant g). For a short-range potential $U(\rho)$, the energy of the mean-field interaction in a weakly interacting gas is the sum of all pair interactions. In a uniform Bose-condensed gas the coupling constant g for condensate atoms is equal to the amplitude of scattering (with an extra factor $\hbar^2/m$ for our definition of f) at the energy of the relative motion $\varepsilon = \hbar^2 q^2/m = 2\mu$, where μ is the chemical potential[2]. Hence, we

[1]For interatomic potentials which have a shallow well (spin-polarized atomic hydrogen), the bound state with an exponentially small binding energy ε_0, characteristic for shallow 2D potential wells [36], does not exist due to the presence of a strong repulsive core [121]. For potentials with a deep well (alkali atoms) the situation is similar to that in 3D: There are many bound states and only accidentally one can encounter a very weakly bound s-level ($d_* \to \infty$). Thus, for realistic momenta of particles in ultracold gases we always have the inequality $qd_* \ll 1$.

[2]This is easily established by comparing the relation for the vertex of elastic interaction, obtained to zero order in perturbation theory [77], with the expression for the scattering amplitude [36]. In the case of an inhomogeneous density profile one should replace μ by $n_0 g$, where n_0 is the coordinate-dependent condensate density.

have

$$g = \frac{\hbar^2}{m} f(q_c) = \frac{2\pi\hbar^2}{m} \frac{1}{\ln(1/q_c d_*)} > 0; \quad q_c d_* \ll 1, \tag{4.2.7}$$

where $q_c = \sqrt{2m\mu}/\hbar$ is the inverse healing length. In a dilute thermal 2D gas, due to the logarithmic dependence of f on q, the thermal average of the mean-field interaction leads to the coupling constant $g = (\hbar^2/m)f(q_T)$, where $q_T = \sqrt{mT}/\hbar$ is the thermal momentum of particles. At sufficiently low temperatures, where $q_T d_* \ll 1$, we again have $g > 0$.

Thus, in an ultra-cold purely 2D gas the coupling constant for the mean-field interaction is always positive in the dilute limit and, hence, the interaction is repulsive. This striking difference from the 3D case is a consequence of the 2D kinematics. For low energies, at interparticle distances $\rho \gg R_e$, the (free) relative motion of a pair of atoms is governed by the wavefunction $\psi_s \propto \ln(\rho/d)$. The probability density $|\psi_s|^2$ of finding two atoms at a given separation increases with ρ as the condition $\rho > d$ is always reached, unless the atoms have a bound state with energy $\varepsilon \to 0$ ($d \to \infty$). This means that it is favorable for particles to be at larger ρ, i.e. they repel each other.

4.3 Scattering in axially confined geometries. General approach

In this section we discuss elastic scattering of atoms (tightly) confined in the axial (z) direction, assuming that the motion in two other (x, y) directions is free. We analyze how the scattering is influenced by the confinement and calculate a complete set of scattering amplitudes corresponding to collision-induced transitions between particle states in the confining potential. We still call this scattering elastic as the internal states of atoms are not changing.

For a harmonic axial confinement, the motion of two atoms interacting with each other via the potential $V(r)$ can be still separated into their relative and center-of-mass motion. The latter drops out of the scattering problem. The relative motion is governed by the potential $V(r)$ and by the potential $V_H(z) = m\omega_0^2 z^2/4$ originating from the axial confinement with frequency ω_0. For the incident wave characterized by the wavevector $\mathbf{q}$ of the motion in the x, y plane and by the quantum number ν of the state in the potential $V_H(z)$, the wavefunction of the relative motion satisfies the Schrödinger equation

$$\left[-\frac{\hbar^2}{m}\Delta + V(r) + V_H(z) - \frac{\hbar\omega_0}{2}\right] \psi(\mathbf{r}) = \varepsilon\psi(\mathbf{r}), \tag{4.3.1}$$

where $\varepsilon = \hbar^2 q^2/m + \nu\hbar\omega_0$.

The scattering depends crucially on the relation between the radius of interatomic interaction R_e and the characteristic de Broglie wavelength of particles $\tilde{\Lambda}_\varepsilon$. The latter is introduced qualitatively, as the motion along the z axis is tightly confined. Accounting for the zero point axial oscillations one can write $\tilde{\Lambda}_\varepsilon \sim \hbar/\sqrt{m\tilde{\varepsilon}}$, with $\tilde{\varepsilon} = \varepsilon + \hbar\omega_0/2$. We will consider the ultra-cold limit where

$$\tilde{\Lambda}_\varepsilon \gg R_e. \tag{4.3.2}$$

Eq. (4.3.2) immediately leads to the inequality $qR_e \ll 1$, as the de Broglie wavelength for the motion in the x, y plane is $\sim 1/q$. For small ν the harmonic oscillator length $l_0 = (\hbar/m\omega_0)^{1/2}$ plays the role of the axial de Broglie wavelength of atoms. Therefore, the ultra-cold limit (4.3.2) also requires the condition $l_0 \gg R_e$. For large ν, the axial de Broglie wavelength is $\sim l_0/\sqrt{\nu}$ and, according to Eq. (4.3.2), this quantity should be much larger than R_e.

Under the condition $qR_e \ll 1$, the scattering amplitudes are determined by the contribution of the s-wave for the motion in the x, y plane. In the case of identical bosons, the s-wave scattering requires even values of ν and ν' as the wavefunction ψ should conserve its sign under the transformation $z \to -z$. The quantum numbers ν and ν' should be even also for distinguishable particles. Otherwise at distances of interatomic interaction, $r \lesssim R_e$, the wavefunction ψ will be small at least as R_e/l_0, ensuring the presence of this small parameter in the expressions for the scattering amplitudes.

The scattering amplitudes corresponding to transitions from the initial state ν (of the relative motion in the potential $V_H(z)$) to final states ν' are defined through the asymptotic form of the wavefunction ψ at an infinite separation ρ in the x, y plane:

$$\psi(\mathbf{r}) \approx \varphi_\nu(z) e^{i\mathbf{q}\cdot\boldsymbol{\rho}} - \sum_{\nu'} f_{\nu\nu'}(\varepsilon)\varphi_{\nu'}(z)\sqrt{\frac{i}{8\pi q_{\nu'}\rho}}e^{iq_{\nu'}\rho}, \tag{4.3.3}$$

where $\varphi_\nu(z)$ and $\varphi_{\nu'}(z)$ are the (real) eigenfunctions of the states ν and ν'. For each of the scattered circular waves the value of the momentum $q_{\nu'}$ follows from the energy conservation law $\hbar^2 q_{\nu'}^2/m = \varepsilon - \hbar\omega_0\nu' > 0$.

Relying on the condition (4.3.2), we develop a method that allows us to express the scattering amplitudes through the 3D scattering length. At interparticle distances $r \gg R_e$ the relative motion in the x, y plane is free, and the motion along the z axis is governed only by the harmonic oscillator potential $V_H(z)$. Then, the solution of Eq. (4.3.1) with $V(r) = 0$ can be expressed through the Green function $G_\varepsilon(\mathbf{r}, \mathbf{r}')$ of this equation. Retaining only the s-wave for the motion in the x, y plane, we have

$$\psi(\mathbf{r}) = \varphi_\nu(z) J_0(q\rho) + A_\nu G_\varepsilon(\mathbf{r}, 0), \tag{4.3.4}$$

and the expression for the Green function $G_\varepsilon(\mathbf{r}, 0)$ reads

$$G_\varepsilon(\mathbf{r}, 0) = \sum_{\nu'} \varphi_{\nu'}(z)\varphi_{\nu'}(0) \times \begin{cases} iH_0^{(1)}(q_{\nu'}\rho)/4;\ q_{\nu'}^2 > 0 \\ K_0(|q_{\nu'}|\rho)/2\pi;\ q_{\nu'}^2 < 0 \end{cases} \tag{4.3.5}$$

Here the summation is also performed over closed scattering channels for which $q_{\nu'}^2 < 0$. The function $K_0(x) = (i\pi/2)H_0(ix)$ and it decays as $\sqrt{\pi/2x}\,\exp(-x)$ at $x \gg 1$. Thus, for $\rho \to \infty$ the terms corresponding to the closed channels vanish. Then, comparing Eq. (4.3.4) at $\rho \to \infty$ with Eq. (4.3.3), we find a relation between the scattering amplitudes and the coefficients A_ν:

$$f_{\nu\nu'} = -A_\nu \varphi_{\nu'}(0)\theta(\varepsilon - \hbar\omega_0\nu'), \tag{4.3.6}$$

where θ is the step function.

The condition $l_0 \gg R_e$ ensures that the relative motion of atoms in the region of interatomic interaction is not influenced by the axial (tight) confinement. Therefore, the wavefunction $\psi(\mathbf{r})$ in the interval of distances where $R_e \ll r \ll \tilde{\Lambda}_\varepsilon$, differs only by a normalization coefficient from the 3D wavefunction of free motion at zero energy. Writing this coefficient as $\varphi_\nu(0)\eta$, we have

$$\psi(r) \approx \varphi_\nu(0)\eta(1 - a/r). \tag{4.3.7}$$

Eq. (4.3.7) contains the 3D scattering length a and serves as a boundary condition for $\psi(\mathbf{r})$ (4.3.4) at $r \to 0$.

For $r \to 0$, a straightforward calculation of the sum in Eq. (4.3.5) yields

$$G_\varepsilon(r, 0) \approx \frac{1}{4\pi r} + \frac{1}{2(2\pi)^{3/2} l_0} w\left(\frac{\varepsilon}{2\hbar\omega_0}\right), \tag{4.3.8}$$

where the complex function $w(x)$ is given by

$$w(x) = \lim_{N\to\infty} \left[2\sqrt{\frac{N}{\pi}} \ln\frac{N}{e^2} - \sum_{j=0}^{N} \frac{(2j-1)!!}{(2j)!!} \ln(j - x - i0) \right]. \tag{4.3.9}$$

With the Green function (4.3.8), the wavefunction (4.3.4) at $r \to 0$ should coincide with $\psi(r)$ (4.3.7). This gives the coefficient

$$\eta = \frac{1}{1 + (a/\sqrt{2\pi} l_0) w(\varepsilon/2\hbar\omega_0)} \tag{4.3.10}$$

and provides us with the values of the coefficients A_ν. Then, using Eq. (4.3.6) and explicit expressions $\varphi_\nu(0) = (1/2\pi l_0^2)^{1/4}(\nu-1)!!/\sqrt{\nu!}$, we immediately obtain the scattering amplitude $f_{00}(\varepsilon)$ and express all other scattering amplitudes through this quantity:

$$f_{00}(\varepsilon) = 4\pi\varphi_0^2(0) a\eta = \frac{2\sqrt{2\pi}}{l_0/a + (1/\sqrt{2\pi}) w(\varepsilon/2\hbar\omega_0)}, \tag{4.3.11}$$

$$f_{\nu\nu'}(\varepsilon) = P_{\nu\nu'} f_{00}(\varepsilon) \theta(\varepsilon - \hbar\omega_0\nu)\theta(\varepsilon - \hbar\omega_0\nu'), \tag{4.3.12}$$

where

$$P_{\nu\nu'} = \frac{\varphi_\nu(0)\varphi_{\nu'}(0)}{\varphi_0^2(0)} = \frac{(\nu-1)!!(\nu'-1)!!}{\sqrt{\nu!\nu'!}}. \tag{4.3.13}$$

One can see from Eqs. (4.3.11) and (4.3.12) that for any transition $\nu \to \nu'$ the scattering amplitude is a universal function of the parameters a/l_0 and $\varepsilon/\hbar\omega_0$. The quantity $P_{\nu\nu'}$ in Eq. (4.3.12) is nothing else than the relative probability amplitude of having an axial interparticle separation $|z| \ll l_0$ (in particular, $|z| \lesssim R_e$) for both incoming (ν) and outgoing (ν') channels of the scattering process. It is thus sufficient to study only the behavior of $f_{00}(\varepsilon)$.

We emphasize the presence of two distinct regimes of scattering. The first one, which we call quasi-2D, requires relative energies $\varepsilon \ll \hbar\omega_0$. In this case, the relative motion of particles is confined to zero point oscillations in the axial direction, and the 2D kinematics

of the relative motion at interatomic distances $\rho > l_0$ should manifest itself in the dependence of the scattering amplitude on $\varepsilon/2\hbar\omega_0$ and a/l_0. In the other regime, at energies already comparable with $\hbar\omega_0$, the 2D kinematics is no longer pronounced in the scattering process. Nevertheless, the latter is still influenced by the (tight) axial confinement. Qualitatively, the scattering amplitudes become three-dimensional, with a momentum $\sim 1/l_0$ related to the quantum character of the axial motion. Thus, we can say that this is a confinement-dominated 3D regime of scattering. With increasing the relative energy to $\varepsilon \gg \hbar\omega_0$, the momentum is increasing to $\sqrt{m\varepsilon}/\hbar$ and the confinement-dominated 3D regime continuously transforms to ordinary 3D scattering.

4.4 Quasi-2D regime

In the quasi-2D regime, due to the condition $\varepsilon \ll \hbar\omega_0$, the incident and scattered waves have quantum numbers $\nu = \nu' = 0$ for the motion in the axial harmonic potential $V_H(z)$. The relative energy $\varepsilon = \hbar^2 q^2/m$ and the inequality $ql_0 \ll 1$ is satisfied. In this case Eq. (4.3.9) gives

$$w(\varepsilon/2\hbar\omega_0) = \ln\left(B\hbar\omega_0/\pi\varepsilon\right) + i\pi, \tag{4.4.1}$$

where $B \approx 0.915$. Then our equation (4.3.11) recovers Eq. (3.1.11) of Section 3.1, obtained in this limit (In Section 3.1 the coefficient B was put equal to unity).

Using Eq. (4.4.1) we can represent $f_{00}(\varepsilon)$ (4.3.11) in the 2D form (4.2.6), with

$$d_* = (d/2)\exp C = \sqrt{\pi/B}\, l_0 \exp\left(-\sqrt{\pi/2}\, l_0/a\right). \tag{4.4.2}$$

This fact has a physical explanation. Relying on the same arguments as in the purely 2D case, one finds that in the interval of distances where $l_0 \ll \rho \ll 1/q$, the wavefunction $\psi \propto \varphi_0(z)\ln(\rho/d)$. On the other hand, for $\rho \gg l_0$ we have $\psi(\mathbf{r}) = \varphi_0(z)\psi_s(\rho)$, where ψ_s is given by the 2D expression (4.2.5) with $f(q) = f_{00}(\varepsilon)$. This follows from Eqs. (4.3.4)-(4.3.6), as all closed scattering channels ($\nu' \neq 0$) in Eq. (4.3.5) for the Green function $G_\varepsilon(\mathbf{r}, 0)$ have momenta $|q_{\nu'}| \gtrsim 1/l_0$ and will be exponentially suppressed at $\rho \gg l_0$. Matching the two expressions for the wavefunction ψ one immediately obtains the 2D equation (4.2.6). However, the parameter d_* (4.4.2) can be found only from the solution of the quasi-2D scattering problem.

We thus conclude that the scattering problem in the quasi-2D regime is equivalent to the scattering in an effective purely 2D potential which leads to the same value of d_*. For positive $a \ll l_0$, this potential can be viewed as a (low) barrier, with a height $V_0 \sim \hbar^2 a/m l_0^3$ and radius l_0. Hence, in the case of positive a we have a small (positive) scattering amplitude, in accordance with Eqs. (4.2.6) and (4.4.2). For a negative a satisfying the condition $|a| \ll l_0$, the effective potential is a shallow well which has a depth $|V_0|$ and radius l_0. This shallow well supports a weakly bound state with an exponentially small binding energy ε_0, which leads to an exponentially large d_* as follows from Eq. (4.4.2). As a result, we have a resonance energy dependence of the scattering amplitude f_{00} at a fixed ratio a/l_0, and a resonance behavior of f_{00} as a function of a/l_0 at a fixed $\varepsilon/\hbar\omega_0$.

The resonance in the energy dependence of f_{00} is quite similar to the logarithmic-scale resonance in the purely 2D case, discussed in Section 4.2. The quasi-2D resonance is also

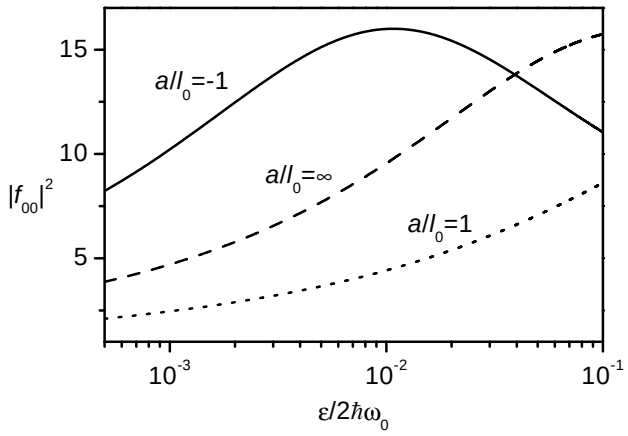

Figure 4.4.1: The function $|f_{00}|^2$ versus energy for $a/l_0 = -1$ (solid curve), $a/l_0 = \infty$ (dashed curve) and $a/l_0 = 1$ (dotted curve).

described by Eq. (4.2.6), where the length d_* is now given by Eq. (4.4.2). As expected, the dependence of f_{00} on ε is smooth.

The resonance in the dependence of the quasi-2D scattering amplitude on a/l_0 has been found and discussed in Section 3.1. Relying on the above introduced effective 2D potential for the quasi-2D scattering, we can now explain this resonance on the same grounds as the resonance in the energy dependence of f_{00}. We will do this in terms of the relative energy ε and the binding energy in the effective potential, $\varepsilon_0 = \hbar^2/md_*^2 \propto \exp(-\sqrt{\pi/2}l_0/|a|)$. For $\varepsilon/\varepsilon_0 = (qd_*)^2 \gg 1$, the scattering amplitude in Eq. (4.2.6) is real and negative. It increases in magnitude with decreasing ratio $\varepsilon/\varepsilon_0$, that is with decreasing q or l_0. In the opposite limit, where $\varepsilon/\varepsilon_0 \ll 1$, the scattering amplitude is real and positive and it increases with the ratio $\varepsilon/\varepsilon_0$. The region of energies $\varepsilon/\varepsilon_0 \sim 1$ corresponds to the resonance, where both the real and imaginary parts of f_{00} are important. The real part reaches its maximum at $\varepsilon/\varepsilon_0 = \exp(-\pi)$, drops to zero at $\varepsilon/\varepsilon_0 = 1$, and acquires the maximum negative value for $\varepsilon/\varepsilon_0 = \exp\pi$. The dependence of $\mathrm{Im}f_{00}$ on $\varepsilon/\varepsilon_0$ is the same as that of the quantity $|f_{00}|^2$. Both of them peak at $\varepsilon/\varepsilon_0 = 1$ and decrease with increasing or decreasing $\varepsilon/\varepsilon_0$.

Qualitatively, the picture remains the same for $|a| \sim l_0$. In Fig. 4.4.1 we present the dependence of $|f_{00}|^2$ on $\varepsilon/2\hbar\omega_0$ at a/l_0 equal to -1, 1, and ∞. In the two last cases we always have $\varepsilon/\varepsilon_0 \ll 1$, and $|f_{00}|^2$ increases with ε at $\varepsilon \ll \hbar\omega_0$. For $a/l_0 = -1$ we have the above described logarithmic-scale resonance in the behavior of $|f_{00}|^2$.

The quasi-2D resonance is much more pronounced in the dependence of the scattering amplitude on the parameter a/l_0. The reason is that f_{00} logarithmically depends on the particle energy, whereas the dependence on a/l_0 is a power law. For $\varepsilon \ll \hbar\omega_0$, Eq. (4.3.11) yields

$$|f_{00}|^2 = \frac{16\pi^2}{(\sqrt{2\pi}\, l_0/a + \ln(B\hbar\omega_0/\pi\varepsilon))^2 + \pi^2}. \tag{4.4.3}$$

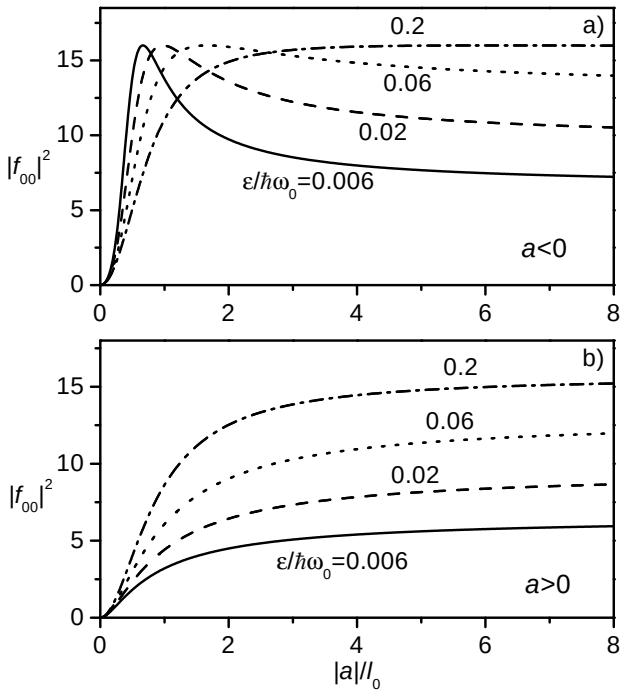

Figure 4.4.2: The function $|f_{00}|^2$ versus $|a|/l_0$ at various energies for $a < 0$ (a) and $a > 0$ (b).

The quantity $|f_{00}|^2$ differs only by a factor of $\hbar/m$ from the rate constant of elastic collisions (see Eq. (4.2.2)), and one can think of observing the resonance dependence of $|f_{00}|^2$ on a/l_0 in an experiment. For example, one can keep ε (temperature) and ω_0 constant and vary a by using Feshbach resonances. The resonance is achieved at $a = -\sqrt{2\pi} l_0 / \ln(B\hbar\omega_0/\pi\varepsilon)$. This is a striking difference from the 3D case, where the cross section and rate constant of elastic collisions monotonically increase with a^2. In Fig. 4.4.2 we present $|f_{00}|^2$ versus a/l_0 at a fixed $\varepsilon/\hbar\omega_0$. In order to extend the results to the region of energies where the validity of the quasi-2D approach is questionable, the quantity $|f_{00}|^2$ was calculated by using Eq. (4.3.11) for the scattering amplitude. The resonance is still visible at $\varepsilon/\hbar\omega_0 = 0.06$ and it disappears for $\varepsilon/\hbar\omega_0 = 0.2$.

The obtained results allow us to conclude that for $|a| \gtrsim l_0$ the approximate border line between the quasi-2D and confinement-dominated 3D regimes is $\varepsilon \approx \varepsilon_* = 0.1\hbar\omega_0$. For $|a| \ll l_0$, as we will see below, the confinement-dominated regime is practically absent.

The output of kinetic studies in thermal gases is usually related to the mean collisional frequency (the rate of interatomic collisions) $\Omega = \bar{\alpha} n$, where $\bar{\alpha}$ is the mean rate constant of elastic collisions, and n the gas density. In the quasi-2D regime, the rate constant $\bar{\alpha}$

follows directly from Eq. (4.2.2), with twice as large rhs for identical bosons:

$$\bar{\alpha} = \frac{\hbar}{m}\langle|f_{00}|^2\rangle, \tag{4.4.4}$$

where the symbol $\langle\,\rangle$ stands for the thermal average. Our numerical calculations show that the average of $|f_{00}|^2$ over the Boltzmann distribution of particles only slightly broadens the resonances in Fig. 4.4.1 and Fig. 4.4.2. Due to the logarithmic dependence of f_{00} on the relative energy, the thermal average is obtained with a good accuracy if one simply replaces ε by the gas temperature T. Thus, in order to observe the manifestation of the 2D features of the particle motion in their collisional rates one has to achieve very low temperatures $T < 0.1\hbar\omega_0$.

4.5 Confinement-dominated 3D regime

In the confinement-dominated 3D regime, where $\varepsilon \sim \hbar\omega_0$, the axial confinement influences the scattering process through the confined character of the axial motion. In order to analyze this influence, we first examine the function $w(\varepsilon/2\hbar\omega_0)$ which determines the energy dependence of the scattering amplitudes. The imaginary part of $w(x)$, following from Eq. (4.3.9), is equal to

$$\mathrm{Im}w(x) = \pi\sum_{j=0}^{[x]}\frac{(2j-1)!!}{(2j)!!} = 2\sqrt{\pi}\frac{\Gamma([x]+3/2)}{[x]!}, \tag{4.5.1}$$

where $[x]$ is the integer part of x. The function $\mathrm{Im}w(x)$ has a step-wise behavior as shown in Fig. 4.5.1. It is constant at non-integer x and undergoes a jump at each integer x, taking a larger value for larger x. With increasing x, the jumps become smaller and for $x \gg 1$ we have $\mathrm{Im}w(x) \approx 2\sqrt{\pi x}$. The real part of $w(x)$ was calculated numerically from Eq. (4.3.9) and is also given in Fig. 4.5.1. At any x we have $|\mathrm{Re}w(x)| < 1$, except for narrow intervals in the vicinity of integer x. In each of these intervals the function $\mathrm{Re}w(x)$ logarithmically goes to infinity as x approaches the corresponding integer value. This is consistent with the step-wise behavior of $\mathrm{Im}w(x)$: As one can see directly from Eq. (4.3.9), for x approaching an integer j the analytical complex function $w \propto \ln(j - x - i0)$.

The described behavior of the function $w(\varepsilon/2\hbar\omega_0)$ has a direct influence on the scattering amplitudes. For $\varepsilon/2\hbar\omega_0$ close to an integer j, the amplitude is small and it is equal to zero for $\varepsilon = 2\hbar\omega_0 j$. This phenomenon originates from the fact that for ε close to $2\hbar\omega_0 j$, a new scattering channel opens (really or virtually). For this channel the momentum $|q_{\nu'}| = \sqrt{m|\varepsilon - 2\hbar\omega_0 j|}/\hbar$ is very small. Hence, at distances $\rho \ll |1/q_{\nu'}|$ the wavefunction ψ (4.3.4) will be determined by the contribution of this low-momentum term if $\rho \gg l_0$. This is clearly seen from Eqs. (4.3.5) and (4.3.4) and makes the situation somewhat similar to that in the quasi-2D regime of scattering. In the latter case, the wavefunction ψ (4.3.4) at distances $\rho \ll 1/q$ is also determined by the contribution of the low-momentum channel as long as $\rho \gg l_0$. Then, as follows from the analysis in Section 4.4, this wavefunction and the scattering amplitude f_{00} behave as $1/\ln(\hbar\omega_0/\varepsilon)$ in the limit $\varepsilon \to 0$. In the present case, the wavefunction ψ and the scattering amplitudes are small as $1/\ln(\hbar\omega_0/|\varepsilon - 2\hbar\omega_0 j|)$ for $\varepsilon \to 2\hbar\omega_0 j$.

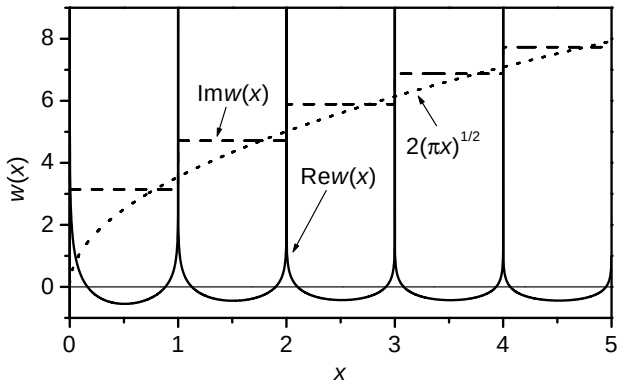

Figure 4.5.1: The functions Re$w(x)$ (solid curve) and Im$w(x)$ (dashed lines). The dotted curve shows the function $2\sqrt{\pi x}$ corresponding to the asymptotic behavior of Imw at large x.

The energy dependence of $|f_{00}|^2$ on $\varepsilon/2\hbar\omega_0$ for a/l_0 equal to -1, 1, and ∞ is displayed in Fig. 4.5.2. Outside narrow energy intervals in the vicinity of integer $\varepsilon/2\hbar\omega_0$, the quantity $|f_{00}|^2$ is a smooth function of ε. One can also see a sort of a step-wise decrease of $|f_{00}|^2$ with increasing ε, originating from the step-wise increase of the function Im$w(\varepsilon/2\hbar\omega_0)$. For $\varepsilon/2\hbar\omega_0$ close to integer values $j > 0$ we find a fine structure similar in nature to the behavior of $|f_{00}|^2$ at $\varepsilon \ll \hbar\omega_0$. For $a/l_0 = 1$ and $a/l_0 = \infty$ there are narrow dips corresponding to the logarithmic decrease of $|f_{00}|^2$ as $\varepsilon \to 2\hbar\omega_0 j$, and for $a/l_0 = -1$ these dips are accompanied by resonances. Note that the thermal distribution of particles averages out this fine structure, and the latter will not be pronounced in kinetic properties.

The difference between the confinement-dominated 3D regime and the ordinary 3D regime of scattering will manifest itself in the rate of elastic collisions (mean collisional frequency Ω). For the Boltzmann distribution of particles, one can find this quantity by turning to the thermal distribution for the relative motion of colliding partners. Collision-induced transitions between the states of the relative motion in the axial potential $V_H(z)$ are described by the rate constants

$$\alpha_{\nu\nu'}(\varepsilon) = (\hbar/m)|f_{\nu\nu'}(\varepsilon)|^2, \tag{4.5.2}$$

where the scattering amplitudes $f_{\nu\nu'}$ are given by Eqs. (4.3.11) and (4.3.12), and an extra factor 2 for identical bosons is taken into account. The collisional frequency $\Omega = \bar{\alpha}n$, where n is the (2D) density, and the mean rate constant of elastic collisions, $\bar{\alpha}$, is obtained by averaging $\alpha_{\nu\nu'}$ (4.5.2) over the thermal distribution of relative energies ε and by making the summation over all possible scattering channels. We thus have

$$\Omega = \bar{\alpha}n = \sum_{\nu\nu'} \int \frac{n\Lambda_T^2 d^2q}{(2\pi)^2} \alpha_{\nu\nu'}(\varepsilon) A \exp\left(-\frac{\varepsilon}{T}\right). \tag{4.5.3}$$

Here $\Lambda_T = (2\pi\hbar^2/mT)^{1/2}$ is the thermal de Broglie wavelength, $\varepsilon = \hbar^2 q^2/m + \hbar\omega_0\nu$,

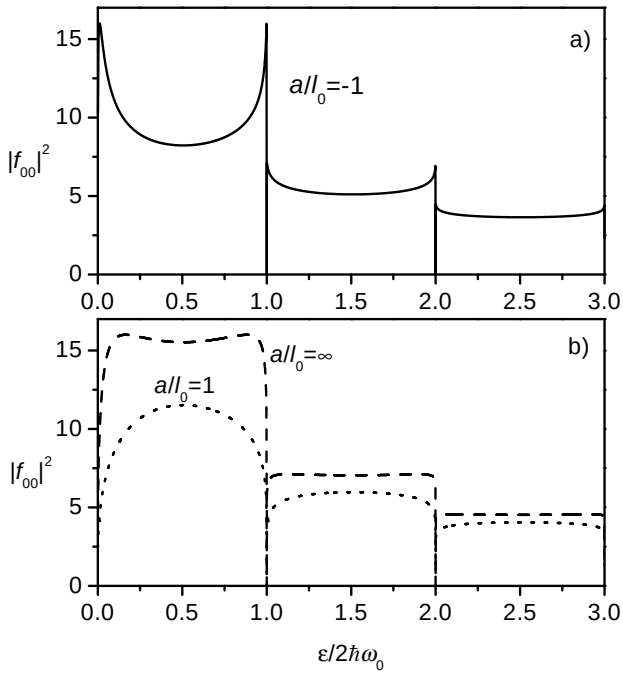

Figure 4.5.2: The function $|f_{00}|^2$ versus energy. In (a) the parameter $a/l_0 = -1$. In (b) the dashed curve corresponds to the unitarity limit ($a/l_0 = \infty$), and the dotted curve to $a/l_0 = 1$.

and the quantum numbers ν and ν' take only even values. The distribution function over ν and q is normalized to unity. The normalization coefficient A is obtained by the summation over both even and odd ν and is equal to

$$A = 2(1 - \exp(-\hbar\omega_0/T)). \tag{4.5.4}$$

Note that the number of collisions per unit time and unit surface area in the x, y plane is equal to $\bar{\alpha}n^2/2 = \Omega n/2$.

The manifestation of the tight axial confinement of the particle motion in collisional rates depends on the relation between the scattering length a and the characteristic de Broglie wavelength $\tilde{\Lambda}_\varepsilon \sim \hbar/\sqrt{m(\varepsilon + \hbar\omega_0/2)}$ accounting for the zero point axial oscillations. For the scattering length satisfying the condition $|a| \ll \tilde{\Lambda}_\varepsilon$, the scattering amplitudes are energy independent at any ε, except for extremely small energies in the quasi-2D regime. This follows directly from Eqs. (4.3.10)-(4.3.12). The condition $|a| \ll \tilde{\Lambda}_\varepsilon$ automatically leads to the inequalities $|a| \ll l_0$ and $|a| \ll \hbar/\sqrt{m\varepsilon}$. Hence, the function $w(\varepsilon/2\hbar\omega_0)$ is much smaller than $l_0/|a|$, unless $\varepsilon \lesssim \hbar\omega_0 \exp(-l_0/|a|)$ (see Eq. (4.4.1) and Fig. 4.5.1). Accordingly, Eq. (4.3.10) gives $\eta = 1$ and Eqs. (4.3.11), (4.3.12) lead to the scattering amplitudes

$$f_{\nu\nu'} = 4\pi a \varphi_\nu(0)\varphi_{\nu'}(0)\theta(\varepsilon - \hbar\omega_0\nu)\theta(\varepsilon - \hbar\omega_0\nu'). \tag{4.5.5}$$

The amplitudes (4.5.5) are nothing else than the 3D scattering amplitude averaged over the axial distribution of particles in the incoming (ν) and outgoing (ν') scattering channels. From Eqs. (4.5.2) and (4.5.5) one obtains the same rate of transitions $\nu \to \nu'$ as in the case of 3D scattering of particles harmonically confined in the axial direction and interacting with each other via the potential $V(r)$. This is what one should expect, since under the condition $|a| \ll \tilde{\Lambda}_\varepsilon$ the amplitude of 3D scattering is momentum independent. The integration over d^2q in Eq. (4.5.3) leads to the mean collisional frequency

$$\Omega = \frac{\hbar n}{2m}(4\pi a)^2 A \sum_{\nu,\nu'} \varphi_\nu^2(0)\varphi_{\nu'}^2(0) \exp\left(-\frac{\hbar\omega_0}{T}\max\{\nu,\nu'\}\right).$$

Thus, in the case where $|a| \ll \tilde{\Lambda}_T$, the tight confinement in the axial direction can manifest itself in the collisional rates only through the axial distribution of particles and the discrete structure of quantum levels in the axial confining potential. The expression for the collisional frequency Ω can be reduced to the form

$$\Omega = \frac{8\pi\hbar n}{m}\left(\frac{a}{l_0}\right)^2 \xi, \tag{4.5.6}$$

where the coefficient ξ ranges from 1 at $T \ll \hbar\omega_0$ to $2/\pi$ for $T \gg \hbar\omega_0$. The condition $|a| \ll \tilde{\Lambda}_T$ is equivalent to $|a| \ll l_0$ and $q_T|a| \ll 1$, where $q_T = \sqrt{mT}/\hbar$ is the thermal momentum of particles. For $T \gg \hbar\omega_0$, Eq. (4.5.6) gives the collisional frequency which coincides with the three-dimensional result averaged over the classical Boltzmann profile of the 3D density in the axial direction, $n_B(z)$:

$$\Omega_{3D} = \langle\sigma_{3D} v\rangle \int \frac{n_B^2(z)}{n} dz. \tag{4.5.7}$$

Here σ is the 3D elastic cross section, and v is the relative velocity of colliding particles. In other words, the quantity $(1/2)\bar{\alpha}n^2 = (1/2)\Omega n$ coincides with the number of 3D collisions per unit time and unit surface area in the x, y plane, given by $(1/2)\langle\sigma_{3D}v\rangle \int n_B^2(z)dz$.

From Eq. (4.5.6) we conclude that for $|a| \ll l_0$ the confinement-dominated 3D regime of scattering is not pronounced. At temperatures $T \lesssim \hbar\omega_0$ the collisional rate only slightly deviates from the ordinary 3D behavior. This has a simple physical explanation. For $|a| \ll \tilde{\Lambda}_T$, treating collisions as three-dimensional we have $\Omega \sim 8\pi a^2 v n_{3D}$. At low temperatures $T \lesssim \hbar\omega_0$ the velocity $v \sim \hbar/ml_0$ and the 3D density is $n_{3D} \sim n/l_0$. For $T \gg \hbar\omega_0$ we have $v \sim (T/m)^{1/2}$ and $n_{3D} \sim n(m\omega_0^2/T)^{1/2}$. In both cases the "flux" $vn_{3D} \sim \omega_0 n$, and there is only a small numerical difference between the low-T and high-T collisional frequencies.

The ultra-cold limit (4.3.2) assumes that the characteristic radius of interatomic interaction $R_e \ll l_0$. Therefore, the condition $|a| \ll l_0$ is always satisfied, unless the scattering length is anomalously large ($|a| \gg R_e$). Below we will focus our attention on this case, assuming that $|a| \gtrsim l_0$.

Let us first show how the 3D result follows from our analysis at $T \gg \hbar\omega_0$, irrespective of the relation between a and $\tilde{\Lambda}_\varepsilon$. At these temperatures the main contribution to the sum in Eq. (4.5.3) comes from $\varepsilon \gg \hbar\omega_0$ and large ν and ν'. Accordingly, we can replace the summation over ν and ν' by integration. At energies much larger than $\hbar\omega_0$ the quantity

$\sqrt{\nu}/l_0$ is nothing else than the axial momentum k_z and we have $\varepsilon = \hbar^2(q^2 + k_z^2)/m$. For these energies the function $w(\varepsilon/2\hbar\omega_0)$ in Eq. (4.3.11) takes its asymptotic form $w \approx i\sqrt{2\pi\varepsilon/\hbar\omega_0}$. Using Eq. (4.3.12), this immediately allows us to write

$$|f_{\nu\nu'}|^2 = P_{\nu\nu'}^2 \frac{8\pi a^2}{l_0^2(1+p^2a^2)} = P_{\nu\nu'}^2 \frac{\sigma_{3D}}{l_0^2}; \quad \nu' < \frac{\varepsilon}{\hbar\omega_0},$$

where $p = \sqrt{q^2 + k_z^2}$ is the 3D momentum of the relative motion, and $\sigma_{3D} = 8\pi a^2/(1 + p^2a^2)$ is the cross section for the 3D elastic scattering. For large ν and ν', Eq. (4.3.13) gives $P_{\nu\nu'} = (4/\pi^2\nu\nu')^{1/4}$, and the integration over ν' in Eq. (4.5.3) multiplies σ_{3D} by the relative 3D velocity v. Then, turning from the integration over ν to the integration over the axial momentum, we reduce Eq. (4.5.3) to

$$\Omega = \int \frac{n\Lambda_T^2 d^3p}{(2\pi)^3}(\sigma_{3D}v)A\exp\left(-\frac{\hbar^2p^2}{mT}\right), \tag{4.5.8}$$

and one can easily check that Eq. (4.5.8) coincides with the three-dimensional result Ω_{3D} (4.5.7).

In the limiting case, where the thermal momentum of particles satisfies the inequality $q_T|a| \gg 1$, we obtain

$$\Omega_{3D} = \frac{16\hbar n}{m}\left(\frac{\hbar\omega_0}{T}\right); \quad q_T|a| \gg 1. \tag{4.5.9}$$

In the opposite limit, where $q_T|a| \ll 1$, at temperatures $T \gg \hbar\omega_0$ we automatically have $|a| \ll \Lambda_T$ and, accordingly, recover Eq. (4.5.6) with $\xi = 2/\pi$:

$$\Omega_{3D} = \frac{16\hbar n}{m}\left(\frac{a}{l_0}\right)^2; \quad q_T|a| \ll 1. \tag{4.5.10}$$

As mentioned in Section 4.4, for $|a| \gtrsim l_0$ the approximate border line between the quasi-2D and confinement-dominated 3D regimes is $\varepsilon_* \approx 0.1\hbar\omega_0$. In the temperature interval $\varepsilon_* < T < \hbar\omega_0$, the leading scattering channel will be the same as in the quasi-2D case, that is $\nu = \nu' = 0$. However, the expression for the scattering amplitude f_{00} is different. From Fig. 4.5.1 and Eq. (4.3.11) one concludes that the real part of the function w can be neglected and the scattering amplitude takes the form

$$f_{00} = \frac{2\sqrt{2\pi}}{l_0/a + i\sqrt{\pi/2}}.$$

Then, retaining only the scattering channel $\nu = \nu' = 0$, Eqs. (4.5.2) and (4.5.3) yield

$$\Omega = \frac{8\pi\hbar n}{m}\left(\frac{a}{l_0}\right)^2 \frac{1 - \exp(-\hbar\omega_0/T)}{1 + \pi a^2/2l_0^2}. \tag{4.5.11}$$

The difference of Eq. (4.5.11) from the quasi-2D result of Eqs. (4.4.3) and (4.4.4) is related to the absence of the logarithmic term in the denominator. This follows from the fact that now we omitted the real part of the function w, which is logarithmically large in the quasi-2D regime.

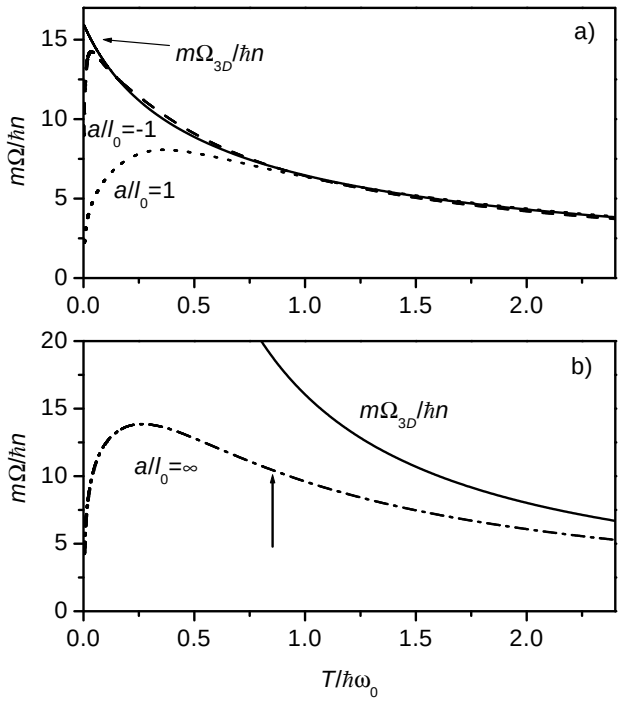

Figure 4.5.3: The quantity $m\Omega/\hbar n$ versus temperature. In (a) the parameter $a/l_0 = -1$ (dashed curve), and $a/l_0 = 1$ (dotted curve). In (b) $a/l_0 = \infty$ (unitarity limit). The solid curves in (a) and (b) show the 3D result (4.5.7). The arrow in (b) indicates the lowest ratio $T/\hbar\omega_0$ in the Stanford and ENS experiments.

It is worth to note that for $l_0 \gg |a|$, Eq. (4.5.11) is only slightly different from the 3D result (4.5.10). This is consistent with the above given analysis leading to Eq. (4.5.6).

On the other hand, for large $|a|/l_0$ the difference between Eq. (4.5.11) and the 3D result (4.5.9) is significant. This originates from the fact that for a large scattering length a the 3D amplitude of scattering in the ultra-cold limit depends on the particle momenta. For a tight axial confinement, treating collisions as three-dimensional, the relative momentum of colliding particles at temperatures $T \lesssim \hbar\omega_0$ is $\sim 1/l_0$ and it no longer depends on temperature. Hence, the scattering rate is quite different from that in 3D. Given these arguments, one expects a strongly pronounced confinement-dominated 3D regime of scattering if the ratio $|a|/l_0 \gg 1$.

This is confirmed by our numerical calculations for the temperature dependence of Ω from Eq. (4.5.3). In Fig. 4.5.3 we present the results for a/l_0 equal to -1, 1, and ∞. The largest deviation from the 3D regime is observed in the unitarity limit ($a \to \infty$). From Fig. 4.5.3 we see that in the Stanford [27] and ENS [29; 30] experiments performed in this limit[3] one should have significant deviations of collisional rates from the ordinary

[3]In the Stanford experiment [27] the unitarity limit for collisions between Cs atoms in the hyperfine

3D behavior.

4.6 Thermalization rates

We will now discuss the collision-induced energy exchange between axial and radial degrees of freedom of the particle motion in an ultra-cold Bose gas tightly confined in the axial direction of a pancake-shaped trap. It is assumed that the radial confinement is shallow and it does not influence the scattering amplitudes. In this geometry, using degenerate Raman sideband cooling, the Stanford [73; 27] and ENS [74; 75; 29; 30] groups created Cs gas clouds with different axial (T_z) and radial (T_ρ) temperatures. After switching off the cooling, interatomic collisions lead to energy exchange between the axial and radial particle motion and the temperatures T_z and T_ρ start to approach each other. Ultimately, the gas reaches a new equilibrium state, with a temperature in between the initial T_z and T_ρ. The corresponding (thermalization) rate has been measured at Stanford [27] and ENS [29; 30] and it provides us with the information on the regimes of interatomic collisions in the gas.

The radial motion of particles is classical. Therefore, we will calculate the rate of energy exchange between the radial and axial degrees of freedom for a given value of the radial coordinate $\boldsymbol{\rho}$ and then average the result over the Boltzmann density profile in the radial direction. The latter is given by

$$n(\rho) = n(0)\exp\left(-\frac{m\omega^2\rho^2}{2T}\right), \tag{4.6.1}$$

where $n(0) = m\omega^2 N/2\pi T$ is the 2D density for $\rho = 0$, ω the radial frequency, and N the total number of particles. Collision-induced transitions $\nu \to \nu'$ change the energy of the axial motion by $\hbar\omega_0(\nu' - \nu)$. We will assume that in the course of evolution the axial and radial distribution of particles remain Boltzmann, with instantaneous values of T_z and T_ρ. Then the rate of energy transfer from the radial to axial motion can be written on the same grounds as Eq. (4.5.3) and reads

$$\dot{E}_z = -\dot{E}_\rho = \frac{1}{2}\int n^2(\rho)d^2\rho \sum_{\nu\nu'}\int \frac{\Lambda_T^2 d^2q}{(2\pi)^2}\hbar\omega_0(\nu'-\nu)\frac{\hbar}{m}|f_{\nu\nu'}(\varepsilon)|^2 A\exp\left(-\frac{\hbar^2q^2}{mT_\rho} - \frac{\hbar\omega_0\nu}{T_z}\right), \tag{4.6.2}$$

where $\varepsilon = \hbar^2q^2/m + \hbar\omega_0\nu$, and the normalization coefficient A depends now on both T_z and T_ρ.

The radial energy of the gas is $E_\rho = 2NT_\rho$, and the axial energy is given by $E_z = N\hbar\omega_0[\exp(\hbar\omega_0/T) - 1]^{-1}$. The time derivatives of these energies take the form

$$\dot{E}_z = \frac{N\hbar^2\omega_0^2\dot{T}_z}{4T_z^2\sinh^2(\omega_0/2T_z)}; \quad \dot{E}_\rho = 2N\dot{T}_\rho. \tag{4.6.3}$$

state $F = 3$, $m_F = 3$ has been achieved by tuning the magnetic field to the Feshbach resonance at 30 G. In the ENS experiment [29; 30] the magnetic field was very small. According to the recent calculations [122], this corresponds to a large and negative scattering length ($a \sim -1500$ Å) for collisions between Cs atoms in $F = 3$ states. For the ENS axial frequency $\omega_0 = 80$ kHz we have $l_0 \approx 200$ Å . Hence, the ratio $|a|/l_0$ in this experiment was approximately equal to 7, which is already rather close to the unitarity limit.

Given the initial values of T_z and T_ρ, Eqs. (4.6.2) and (4.6.3) provide us with the necessary information on the evolution of $T_z(t)$ and $T_x(t)$.

For a small difference $\delta T = T_\rho - T_z$, these equations can be linearized with respect to δT. As the total energy is conserved, Eqs. (4.6.3) reduce to

$$\delta\dot{T} = \frac{\dot{E}_z}{N}\left(\frac{1}{2} + \frac{4T^2\sinh^2(\hbar\omega_0/2T)}{\hbar^2\omega_0^2}\right). \tag{4.6.4}$$

In Eq. (4.6.2) we represent the exponent as $-(\varepsilon/T + \delta T\hbar\omega_0\nu/T^2)$ and turn from the integration over dq to integration over $d\varepsilon$. The zero order term of the expansion in powers of δT vanishes. The (leading) linear term, being substituted into Eq. (4.6.4), leads to the differential equation for $\delta T(t)$:

$$\delta\dot{T} = -\Omega_{th}(T)\delta T, \tag{4.6.5}$$

where the thermalization rate $\Omega_{th}(T)$ is given by

$$\Omega_{th} = \frac{n(0)\Lambda_T^2 A}{16\pi\hbar}\left[\frac{\hbar^2\omega_0^2}{2T^2} + 4\sinh^2\left(\frac{\hbar\omega_0}{2T}\right)\right]\sum_{\nu>\nu'}(\nu-\nu')^2\int_{\hbar\omega_0\nu}^{\infty} d\varepsilon|f_{\nu\nu'}(\varepsilon)|^2\exp\left(-\frac{\varepsilon}{T}\right). \tag{4.6.6}$$

The degeneracy parameter is $n(0)\Lambda_T^2 = N(\hbar\omega/T)^2$ and it is small as the gas obeys the Boltzmann statistics. The normalization coefficient A is again given by Eq. (4.5.4).

The quantum numbers ν and ν' take only even values and, hence, in order to change the state of the axial motion one should have a relative energy $\varepsilon > 2\hbar\omega_0$. Therefore, at temperatures lower than $\hbar\omega_0$ the rate of transitions changing the axial and radial energy is $\propto \exp(-2\hbar\omega_0/T)$. On the other hand, the axial energy $E_z \propto \exp(-\hbar\omega_0/T)$ and thus the thermalization rate $\Omega_{th} \propto \exp(-\hbar\omega_0/T)$. This can be easily found from Eq. (4.6.6) and shows that the quantum character of the axially confined particle motion exponentially suppresses the thermalization process at temperatures $T \ll \hbar\omega_0$. In particular, this is the case for the quasi-2D regime.

In the most interesting part of the confinement-dominated 3D regime, where $\varepsilon_* < T < \hbar\omega_0$, the energy exchange between the axial and radial motion of particles is mostly related to transitions between the states with $\nu' = 0$ and $\nu = 2$. The relative energy ε should be larger than $2\hbar\omega_0$ and, at the same time, this energy is well below $4\hbar\omega_0$. Hence, the scattering amplitude $f_{20}(\varepsilon)$ is determined by Eqs. (4.3.11 and (4.3.12) in which one can put $w(\varepsilon/2\hbar\omega_0) \approx i3\pi/2$ (see Eq. (4.5.1) and Fig. 4.5.1). This gives

$$f_{20} = \frac{2\sqrt{2\pi}}{l_0/a + i(3/2)\sqrt{\pi/2}},$$

and from Eq. (4.6.6) we obtain

$$\Omega_{th} = \frac{16\hbar\omega_0}{9\pi T}\Omega_0\frac{\exp(-\hbar\omega_0/T)}{1+8l_0^2/9\pi a^2}(1-\exp(-\hbar\omega_0/T))^3. \tag{4.6.7}$$

The characteristic frequency Ω_0 is given by

$$\Omega_0 = \omega^2 N/\omega_0. \tag{4.6.8}$$

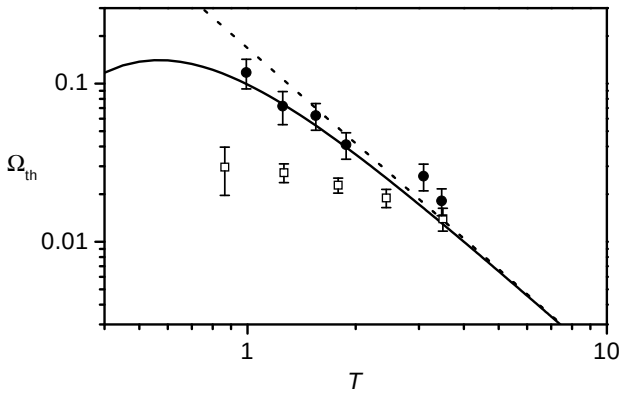

Figure 4.6.1: Thermalization rate versus temperature in the unitarity limit ($a = \infty$). The solid curve shows the result of our calculations for Ω_{th}/Ω_0, and the dotted line the 3D result $\Omega_{th}^{3D}/\Omega_0$. Squares and circles show the data of the Stanford and ENS experiments.

At temperatures $T \gg \hbar\omega_0$, Eq. (4.6.6) leads to the 3D result for the thermalization rate:

$$\Omega_{th}^{3D} = \frac{8}{15\pi}\left(\frac{\hbar\omega_0}{T}\right)^2 \Omega_0; \quad q_T|a| \gg 1, \tag{4.6.9}$$

$$\Omega_{th}^{3D} = \frac{16}{15\pi}\left(\frac{a}{l_0}\right)^2 \left(\frac{\hbar\omega_0}{T}\right) \Omega_0; \quad q_T|a| \ll 1. \tag{4.6.10}$$

Comparing Eqs. (4.6.9) and (4.6.10) with Eq. (4.6.7) one sees that Ω_{th} should acquire its maximum value at $T \sim \hbar\omega_0$. For $|a| \gtrsim l_0$ this maximum value is on the order of $\Omega_0/2\pi$.

As one expects from the discussion in Section 4.5, the difference of the thermalization rate from Ω_{th}^{3D} is pronounced for large values of a. For example, in the unitarity limit Eq. (4.6.9) gives $\Omega_{th}^{3D} \propto 1/T^2$, whereas in the confinement-dominated regime we have $\Omega_{th} \propto (1/T)\exp(-\hbar\omega_0/T)$.

It should be emphasized that for any T, ω_0, and a the ratio Ω_{th}/Ω_0 depends only on the parameters $T/\hbar\omega_0$ and a/l_0. This can be found directly from Eq. (4.6.6). In Fig. 4.6.1 we present the temperature dependence of Ω_{th} in the unitarity limit, obtained numerically from Eq. (4.6.6), and compare our results with the data of the Stanford [27] and ENS [29; 30] experiments. With the current error bars, the ENS results do not show significant deviations from the classical 3D behavior. These results agree fairly well with our calculations. The Stanford experiment gives somewhat lower values of Ω_{th}/Ω_0 at the lowest temperatures of the experiment.

In the hydrodynamic regime for the gas cloud, where the characteristic collisional frequency greatly exceeds the radial frequency ω, our assumption of quasiequilibrium at instantaneous (time-dependent) values of T_z and T_ρ may not be valid. Nevertheless, the shape of the curve $\Omega_{th}(T)$ qualitatively remains the same, including the exponential decrease with temperature at $T < \hbar\omega_0$ and power law decrease with increasing T at

temperatures larger than $\hbar\omega_0$. However, the maximum value of Ω_{th} will be somewhat lower (in particular, of the order of ω [27]).

The number of particles (per "2D" sheet of atoms) in the Stanford experiment [27] was $N \sim 10^4$ [123], which is by a factor of 20 higher than at ENS for $T \approx \hbar\omega_0$ [29; 30]. We then estimate the 2D density of atoms for these temperatures to be $n \sim 2.5\times10^8$ cm^{-2} at Stanford ($\omega \approx 90$ Hz), and $n \sim 0.5\times10^8$ cm^{-2} at ENS ($\omega \approx 180$ Hz). For these densities, the ratio of the collisional frequency Ω in Fig. 4.5.3 to the radial frequency is $\Omega/\omega \sim 0.3$ in the ENS experiment, and $\Omega/\omega \sim 3$ in the experiment at Stanford. At temperatures $T > \hbar\omega_0$ the density n and the ratio Ω/ω are smaller in both experiments. We thus see that the ENS experiment [29; 30] was in the collisionless regime, although rather close to the hydrodynamic regime at temperatures $T \approx \hbar\omega_0$. For these temperatures, the Stanford experiment [27] has already achieved the hydrodynamic regime, and this can explain the discrepancy between our calculations and the Stanford results in Fig. 4.6.1.

4.7 Inelastic 2-body processes

Inelastic scattering of atoms is also influenced by the tight axial confinement of the particle motion. In this section we will consider the inelastic 2-body processes, such as spin relaxation, in which the internal states of colliding atoms are changing, and the released internal-state energy of the atoms is transferred to their kinetic energy. Our goal is to establish a relation between the inelastic rates in 3D and those in the (tightly) axially confined geometry. The analysis given below relies on two important conditions widely met for the 2-body spin relaxation [124]:

i)The energy release per collision greatly exceeds the gas temperature and the frequency of the axial confinement. Accordingly, the inelastic transitions occur at comparatively short interparticle distances $\sim R_{in}$ which are much smaller than the characteristic de Broglie wavelength of particles.

ii)The inelastic transitions are caused by weak (spin-dipole, spin-orbit, etc.) interatomic interactions and can be treated with perturbation theory.

To first order in perturbation theory the amplitude of inelastic scattering, defined in the same way as in the previous sections, is given by a general expression [125]

$$f_{in}(\varepsilon) = \frac{m}{\hbar^2}\int \psi_i(\mathbf{r})U_{int}(\mathbf{r})\psi_f(\mathbf{r})d^3r. \tag{4.7.1}$$

Here $\psi_i(\mathbf{r})$ and $\psi_f(\mathbf{r})$ are the true wavefunctions of the initial and final states of the relative motion of colliding atoms, and $U_{int}(\mathbf{r})$ is the (weak) interatomic potential responsible for inelastic transitions. This potential is the same as in the 3D case. The function ψ_f is also the same as in 3D, since the relative energy in the final state is much larger than $\hbar\omega_0$. Thus, the only difference of the amplitude f_{in} (4.7.1) from the amplitude of inelastic scattering in the 3D case is related to the form of the wavefunction ψ_i.

The characteristic interatomic distance R_{in} at which the inelastic transitions occur, satisfies the inequality $R_{in} \ll \tilde{\Lambda}_\varepsilon$ (see item ii). Therefore, we are in the ultra-cold limit similar to that determined by Eq. (4.3.2) in the case of elastic scattering, and the conditions $qR_{in} \ll 1$ and $R_{in} \ll l_0$ are satisfied. The former ensures a dominant contribution of the s-wave (of the initial wavefunction ψ_i) to the scattering amplitude

f_{in} (4.7.1). Due to the condition $R_{in} \ll l_0$, at distances $r \sim R_{in}$ the wavefunction ψ_i has a three-dimensional character: $\psi_i(r) \propto \tilde{\psi}_{3D}(r)$, where $\tilde{\psi}_{3D}(r)$ is the wavefunction of the 3D relative motion at zero energy. For $r \gg R_e$ we have $\tilde{\psi}_{3D}(r) = (1 - a/r)$, and in order to be consistent with Eq. (4.3.7) we should write

$$\psi_i(r) = \eta(\varepsilon)\varphi_\nu(0)\tilde{\psi}_{3D}(r), \tag{4.7.2}$$

where the coefficient $\eta(\varepsilon)$ is given by Eq. (4.3.10), and ν is the quantum number of the initial state of the relative motion in the axial harmonic potential $V_H(z)$.

In the 3D case, the amplitude f_0 of inelastic scattering at zero initial energy is determined by Eq. (4.7.1) with ψ_i replaced by $\tilde{\psi}_{3D}$. Hence, Eq. (4.7.2) directly gives a relation between the two scattering amplitudes:

$$f_{in} = \eta(\varepsilon)\varphi_\nu(0)f_0. \tag{4.7.3}$$

Due to the high relative kinetic energy of particles in the final state of the inelastic channel, the density of final states in this channel is independent of the axial confinement. Therefore, relying on Eq. (4.7.3) the mean rate constant $\bar{\alpha}_{in}$ of inelastic collisions in the axially confined geometry and the corresponding collisional frequency can be represented in the form

$$\bar{\alpha}_{in} = \langle|\eta(\varepsilon)|^2\varphi_\nu^2(0)\theta(\varepsilon - \hbar\omega_0\nu)\rangle\alpha_0; \quad \Omega_{in} = \bar{\alpha}_{in}n, \tag{4.7.4}$$

where α_0 is the 3D inelastic rate constant at zero energy.

Note that in the ultra-cold limit the 3D inelastic rate constant is temperature independent and equal to α_0 if the scattering length $|a| \lesssim R_e$. For $|a| \gg R_e$, the wavefunction of the relative motion in the region of interatomic interaction takes the form $\psi_i(r) = \eta_{3D}\tilde{\psi}_{3D}(r)$, where $|\eta_{3D}|^2 = (1 + p^2a^2)^{-1}$ and p is the 3D relative momentum of colliding particles (see, e.g. [126]). Hence, for the inelastic rate constant we have $\langle\alpha_0(1 + p^2a^2)^{-1}\rangle$. In the presence of axial confinement, averaging the frequency of inelastic collisions over the (quantum) axial density profile $n_{3D}(z)$, we obtain

$$\Omega_{in} = \left\langle \frac{\alpha_0}{(1 + p^2a^2)} \right\rangle \int \frac{n_{3D}^2(z)}{n} dz. \tag{4.7.5}$$

The density profile $n_{3D}(z)$ accounts for the discrete structure of quantum levels in the axial confining potential and for the quantum spatial distribution of particles. Therefore, Eq. (4.7.5) gives the ordinary 3D result only at temperatures $T \gg \hbar\omega_0$, where $n_{3D}(z)$ becomes the Boltzmann distribution $n_B(z)$.

We first analyze the influence of axial confinement on Ω_{in} (4.7.4) for the case where $|a| \ll \tilde{\Lambda}_T$ or, equivalently, $|a| \ll l_0$ and $q_T|a| \ll 1$. In this case we may put $\eta = 1$ at any T, except for extremely low temperatures in the quasi-2D regime. Then Eq. (4.7.4) gives

$$\Omega_{in} = \langle\varphi_\nu^2(0)\rangle\alpha_0 n = \frac{\alpha_0 n}{\sqrt{2\pi}\, l_0} \tanh^{1/2}\left(\frac{\hbar\omega_0}{T}\right). \tag{4.7.6}$$

One can easily check that Eq. (4.7.6) coincides with Eq. (4.7.5) in which $p|a| \ll 1$. The reason for this coincidence is that, similarly to the case of elastic scattering described by Eq. (4.5.5), for $\eta = 1$ the scattering amplitude f_{in} (4.7.3) is independent of the relative

energy ε. Hence, the inelastic rate is influenced by the axial confinement only through the axial distribution of particles. However, this influence is significant, in contrast to the case of elastic scattering under the same conditions (see Eq. (4.5.6)). Qualitatively, for $q_T|a| \ll 1$ we have $\Omega_{in} \sim \alpha_0 n_{3D}$. At temperatures $T \ll \hbar\omega_0$, a characteristic value of the 3D density is $n_{3D} \sim n/l_0$ and we obtain $\Omega_{in} \sim \alpha_0 n/l_0$. For $T \gg \hbar\omega_0$, the 3D density $n_{3D} \sim n(m\omega_0^2/T)^{1/2}$ and hence the frequency of inelastic collisions is $\Omega_{in} \sim (\alpha_0 n/l_0)(\hbar\omega_0/T)^{1/2}$.

We now discuss the temperature dependence of the inelastic rate for the case where $|a| \gtrsim l_0$, which in the ultra-cold limit (4.3.2) assumes that $|a| \gg R_e$. In the quasi-2D regime and in the temperature interval $\varepsilon_* < T < \hbar\omega_0$ of the confinement-dominated 3D regime, the most important contribution to the inelastic rate in Eq. (4.7.4) comes from collisions with the axial quantum number $\nu = 0$. Then, using Eq. (4.3.11) we express the parameter η through the elastic amplitude f_{00} and obtain a relation between Ω_{in} and the mean frequency of elastic collisions $\Omega(T)$:

$$\Omega_{in}(T) = \langle |f_{00}(\varepsilon)|^2 \rangle \frac{\alpha_0 n}{(4\pi a \varphi_0(0))^2} = \Omega(T)\beta, \tag{4.7.7}$$

where $\beta = (1/128\pi^3)^{1/2}(ml_0\alpha_0/\hbar a^2)$ is a dimensionless parameter independent of temperature. The temperature dependence of Ω is displayed in Fig. 4.4.1 and Fig. 4.5.3 and was discussed in Sections 4.4 and 4.5. Note that the parameter β is not equal to zero for $|a| \to \infty$. In this case, since the amplitude f_0 is calculated with the wavefunction $\tilde{\psi}_{3D}$ which behaves as a/r for $r \to \infty$, we have $\alpha_0 \propto a^2$ and $\beta = \text{const}$.

At temperatures $T \gg \hbar\omega_0$, using the same method as in Section 4.5 for the case of elastic scattering, from Eq. (4.7.4) we recover the 3D result Ω_{in}^{3D} given by Eq. (4.7.5) with $n_{3D}(z) = n_B(z)$. In the limiting case, where $q_T|a| \gg 1$, we find

$$\Omega_{in}^{3D} = \frac{8\hbar n}{m}\beta \left(\frac{2\hbar\omega_0}{T}\right)^{3/2} = \Omega_{3D}(T)\beta \left(\frac{2\hbar\omega_0}{T}\right)^{1/2}. \tag{4.7.8}$$

Comparing Eq. (4.7.8) with Eq. (4.7.7), we see that in the confinement-dominated 3D regime the deviation of the inelastic rate from the ordinary 3D behavior should be larger than that in the case of elastic scattering.

As follows from Eq. (4.7.7) and Fig. 4.5.3, for $|a| \gtrsim l_0$ the inelastic frequency Ω_{in} reaches its maximum at temperatures near the border between the quasi-2D and confinement-dominated 3D regimes. The maximum value of Ω_{in} is close to

$$\tilde{\Omega}_{in} = \frac{16\hbar}{m}\beta. \tag{4.7.9}$$

From Eq. (4.7.4) one finds that at any T the ratio $\Omega_{in}/\tilde{\Omega}_{in}$ depends only on two parameters: $T/\hbar\omega_0$ and a/l_0. In Fig. 4.7.1 we present our numerical results for $\Omega_{in}/\tilde{\Omega}_{in}$ as a function of $T/\hbar\omega_0$ for a/l_0 equal to -1, 1, and ∞. As expected, the deviations from the 3D behavior are the largest in the unitarity limit.

The inelastic rate of spin relaxation in a tightly (axially) confined gas of atomic cesium has been measured for the unitarity limit in the Stanford experiment [27]. Due to a shallow radial confinement of the cloud in this experiment, the 2D density $n \sim 1/T$

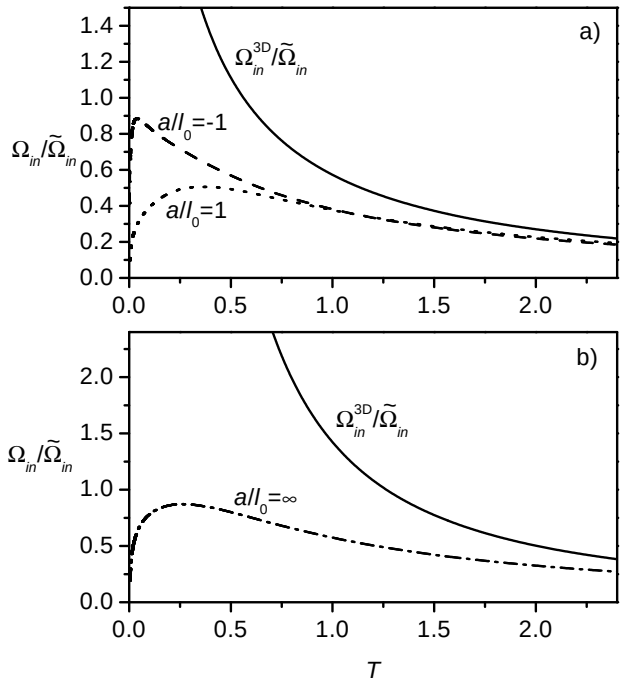

Figure 4.7.1: The quantity $\Omega_{in}/\tilde{\Omega}_{in}$ versus temperature. In (a) the parameter $a/l_0 = -1$ (dashed curve), and $a/l_0 = 1$ (dotted curve). In (b) $a/l_0 = \infty$ (unitarity limit). The solid curves in (a) and (b) show the 3D result (4.7.7).

(see Eq. (4.6.1)). Then, Eq. (4.7.8) gives the 3D inelastic frequency $\Omega_{in}^{3D} \sim 1/T^{5/2}$, whereas in the temperature interval $\varepsilon_* < T < \hbar\omega_0$ of the confinement-dominated regime Eqs. (4.5.11) and (4.7.7) lead to $\Omega_{in} \sim (1/T)(1 - \exp(-\hbar\omega_0/T))$. In order to compare our calculations with the data of the Stanford experiment on spin relaxation, in Fig. 4.7.2 we display the ratio of $\Omega_{in}(T/\hbar\omega_0)$ to Ω_{in} at $T = 3\hbar\omega_0$ which was the highest temperature in the experiment. The temperature dependence of the inelastic rate, following from the Stanford results, agrees fairly well with the calculations and shows significant deviations from the 3D behavior. It should be noted that, in contrast to thermalization rates, the inelastic decay rate is not sensitive to whether the gas is in the collisionless or hydrodynamic regime [27].

4.8 Concluding remarks

In conclusion, we have developed a theory which describes the influence of a tight axial confinement of the particle motion on the processes of elastic and inelastic scattering. The most interesting case turns out to be the one in which the 3D scattering length a exceeds the extension of the wavefunction in the axial direction, l_0. In the ultra-

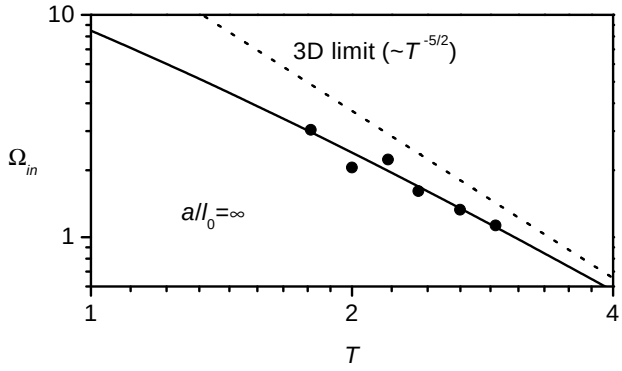

Figure 4.7.2: The ratio of $\Omega_{in}(T/\hbar\omega_0)$ to Ω_{in} at $T = 3\hbar\omega_0$ versus temperature in the unitarity limit ($a = \infty$). The solid curve shows the result of our numerical calculations, and the dotted line the 3D limit. Circles show the data of the Stanford experiment.

cold limit defined by Eq. (4.3.2), the condition $|a| > l_0$ automatically requires large $|a|$ compared to the radius of interatomic interaction R_e. Then we have a pronounced confinement-dominated 3D regime of scattering at temperatures on the order of $\hbar\omega_0$. Treating interatomic collisions as three-dimensional, the relative momentum of colliding atoms is related to the quantum character of the axial motion in the confining potential and becomes of the order of $1/l_0$. As a result, the scattering rate can strongly deviate from the ordinary 3D behavior. The axial extension of the wavefunction, achieved in the experiments at Stanford and ENS [73; 27; 74; 75; 29; 30], is $l_0 \approx 200$ Å. The required value of the scattering length, $|a| > l_0$ and $|a| \gg R_e$, is characteristic for Cs atoms ($R_e \approx 100$Å) and can also be achieved for other alkali atoms by using Feshbach resonances.

In order to observe the 2D features of the particle motion in the rates of interatomic collisions one has to reach the quasi-2D regime of scattering, which requires much lower temperatures, at least by an order of magnitude smaller than $\hbar\omega_0$. For $\omega_0 \approx 80$kHz ($\hbar\omega_0 \approx 4$ μK) as in the Stanford [73; 27] and ENS [74; 75; 29; 30] experiments, these are temperatures below 400nK. As one can see from Fig. 4.5.3, the rate of elastic collisions is still rather large for these temperatures and, hence, one can think of achieving them by evaporative cooling. Moreover, for realistic radial frequencies $\omega \sim 100$Hz there is a hope to achieve quantum degeneracy and observe a cross-over to the BEC regime. The cross-over temperature is $T_c \approx N^{1/2}\hbar\omega$ (see [32] and the discussion in Section 3.1), and for $N \sim 1000$ particles in a quasi-2D layer we find $T_c \approx 100$nK.

Another approach to reach BEC in the quasi-2D regime will be to prepare initially a 3D trapped condensate and then adiabatically slowly turn on the tight axial confinement. Manipulating the obtained (quasi-)2D condensate and inducing the appearance of thermal clouds with temperatures $T < T_c$, one can observe interesting phase coherence phenomena originating from the phase fluctuations of the condensate in quasi-2D (see Section 3.1).

Interestingly, at temperatures $T \sim T_c$ the collisional frequency Ω can be on the

order of the cross-over temperature if $|a| \gtrsim l_0$. This follows directly from Fig. 4.4.1 and Eq. (4.4.4) which give $\Omega \sim \pi\hbar n/m$ even at temperatures by two orders of magnitude smaller than $\hbar\omega_0$. As the 2D density of thermal particles is $n \sim Nm\omega^2/T$, we immediately obtain $\hbar\Omega(T_c) \sim N^{1/2}\hbar\omega \approx T_c$. This condition means that the trapped gas becomes a strongly interacting system. The mean free path of a particle, $v/\Omega(T_c)$, is already on the order of its de Broglie wavelength $\hbar/\sqrt{mT_c}$. At the same time, the system remains dilute, since the mean interparticle separation is still much larger than the radius of interatomic interaction R_e. In this respect, the situation is similar to the 3D case with a large scattering length $a \gg R_e$ at densities where $na^3 \sim 1$. The investigation of the cross-over to the BEC regime in such strongly interacting quasi-2D gases should bring in analogies with condensed matter systems or dense 2D gases. Well-known examples of dense 2D systems in which the Kosterlitz-Thouless phase transition [47; 48] has been found experimentally, are monolayers of liquid helium [14; 15] and the quasi-2D gas of atomic hydrogen on liquid helium surface [16].

On the other hand, for $|a| \ll l_0$ the collisional frequency near the BEC cross-over, $\Omega(T_c) \ll T_c/\hbar$, and the (quasi-)2D gas remains weakly interacting. Then, the nature of the cross-over is questionable (see Section 3.1). Generally speaking, one can have both the ordinary BEC cross-over like in an ideal trapped gas [32] and the Kosterlitz-Thouless type [47; 48] of a cross-over. We thus see that axially confined Bose gases in the quasi-2D regime are remarkable systems where by tuning a or l_0 one can modify the nature of the BEC cross-over.

Chapter 5 Regimes of quantum degeneracy in trapped 1D gases

We discuss the regimes of quantum degeneracy in a trapped 1D gas and obtain the diagram of states. Three regimes have been identified: the BEC regimes of a true condensate and quasicondensate, and the regime of a trapped Tonks gas (gas of impenetrable bosons). The presence of a sharp cross-over to the BEC regime requires extremely small interaction between particles. We discuss how to distinguish between true and quasicondensates in phase coherence experiments.

Low-temperature 1D Bose systems attract a great deal of interest as they show a remarkable physics not encountered in 2D and 3D. In particular, the 1D Bose gas with repulsive interparticle interaction (the coupling constant $g > 0$) becomes more non-ideal with decreasing 1D density n [56; 57]. The regime of a weakly interacting gas requires the correlation length $l_c = \hbar/\sqrt{mng}$ (m is the atom mass) to be much larger than the mean interparticle separation $1/n$. For small n or large interaction, where this condition is violated, the gas acquires Fermi properties as the wavefunction strongly decreases at short interparticle distances [54; 56; 57]. In this case it is called a gas of impenetrable bosons or Tonks gas (cf. [127]).

Spatially homogeneous 1D Bose gases with repulsive interparticle interaction have been extensively studied in the last decades. For the delta-functional interaction, Lieb and Liniger [56; 57] have calculated the ground state energy and the spectrum of elementary excitations which at low momenta turns out to be phonon-like. Generalizing the Lieb-Liniger approach, Yang and Yang [128] have proved the analyticity of thermodynamical functions at any finite temperature T, which indicates the absence of a phase transition. However, at sufficiently low T the correlation properties of a 1D Bose gas are qualitatively different from classical high-T properties. In the regime of a weakly interacting gas ($nl_c \gg 1$) the density fluctuations are suppressed [44; 129], whereas at finite T the long-wave fluctuations of the phase lead to exponential decay of the one-particle density matrix at large distances [44; 129; 130]. A similar picture, with a power-law decay of the density matrix, was found at $T = 0$ [51; 52]. Therefore, the Bose-Einstein condensate is absent at any T, including $T = 0$. From a general point of view, the absence of a true condensate in 1D at finite T follows from the Bogolyubov k^{-2} theorem as was expounded in [10; 11] (for the $T = 0$ case see [53]). Earlier studies of 1D Bose systems are reviewed in [12]. They allow us to conclude that in 1D gases the decrease of temperature leads to a continuous transformation of correlation properties from ideal-gas classical to interaction/statistics dominated. A 1D classical field model for calculating correlation functions in the conditions, where both the density and phase fluctuations are important, was developed in [131] and for Bose gases in [132]. Interestingly, 1D gases can posses the property of superfluidity at $T = 0$ [133; 12]. Moreover, at finite T one can have metastable supercurrent states which decay on a time scale independent of the size of the system [134].

The earlier discussion of 1D Bose gases was mostly academic as there was no possible realization of such a system. Fast progress in evaporative and optical cooling of trapped atoms and the observation of Bose-Einstein condensation (BEC) in trapped clouds of alkali atoms [3; 4; 5] stimulated a search for non-trivial trapping geometries. At present, there are significant efforts to create (quasi-)1D trapped gases [135; 62], where the radial motion of atoms in a cylindrical trap is (tightly) confined to zero point oscillations. Then, kinematically the gas is 1D, and the difference from purely 1D gases is only related to the value of the interparticle interaction which now depends on the radial confinement. The presence of the axial confinement allows one to speak of a trapped 1D gas.

Ketterle and van Druten [33] considered a trapped 1D ideal gas and have revealed a BEC-like behavior of the cloud. They have established that at temperatures $T < N\hbar\omega/\ln 2N$, where N is the number of particles and ω the trap frequency (we use the Boltzmann constant $k_B = 1$), the population of the ground state rapidly grows with decreasing T and becomes macroscopic.

A fundamental question concerns the influence of interparticle interaction on the presence and character of BEC. In this chapter we discuss the regimes of quantum degeneracy in a trapped 1D gas with repulsive interparticle interaction. We find that the presence of a sharp cross-over to the BEC regime, predicted in [33], requires extremely small interaction between particles. Otherwise, the decrease of temperature leads to a continuous transformation of a classical gas to quantum degenerate. We identify 3 regimes at $T \ll T_d$, where $T_d \approx N\hbar\omega$ is the degeneracy temperature. For a sufficiently large interparticle interaction and the number of particles much smaller than a characteristic value N_*, at any $T \ll T_d$ one has a trapped Tonks gas characterized by a Fermi-gas density profile. For $N \gg N_*$ we have a weakly interacting gas. The presence of the trapping potential introduces a finite size of the sample and drastically changes the picture of long-wave fluctuations of the phase compared to the uniform case. We calculate the density and phase fluctuations and find that well below T_d there is a quasicondensate, i.e. the BEC state where the density fluctuations are suppressed but the phase still fluctuates. At very low T the long-wave fluctuations of the phase are suppressed due to a finite size of the system, and we have a true condensate. The true condensate and the quasicondensate have the same Thomas-Fermi density profile and local correlation properties, and we analyze how to distinguish between these BEC states in an experiment.

We first discuss the coupling constant g for possible realizations of 1D gases. These realizations imply particles in a cylindrical trap, which are tightly confined in the radial (ρ) direction, with the confinement frequency ω_0 greatly exceeding the mean-field interaction. Then, at sufficiently low T the radial motion of particles is essentially "frozen" and is governed by the ground-state wavefunction of the radial harmonic oscillator. If the radial extension of the wavefunction, $l_0 = (\hbar/m\omega_0)^{1/2} \gg R_e$, where R_e is the characteristic radius of the interatomic potential, the interaction between particles acquires a 3D character and will be characterized by the 3D scattering length a. In this case, assuming $l_0 \gg |a|$, we have

$$g = 2\hbar^2 a/ml_0^2. \tag{5.0.1}$$

This result follows from the analysis in [136] and can also be obtained by averaging the 3D interaction over the radial density profile. Thus, statistical properties of the sample are the same as those of a purely 1D system with the coupling constant given by Eq. (5.0.1).

In the regime of a weakly interacting gas, where $nl_c \gg 1$, we have a small parameter

$$\gamma = 1/(nl_c)^2 = mg/\hbar^2 n \ll 1. \tag{5.0.2}$$

For particles trapped in a harmonic (axial) potential $V(z) = m\omega^2 z^2/2$, one can introduce a complementary dimensionless quantity $\alpha = mgl/\hbar^2$ which provides a relation between the interaction strength g and the trap frequency ω ($l = \sqrt{\hbar/m\omega}$ is the amplitude of axial zero point oscillations).

At $T = 0$ one has a true condensate: In the Thomas-Fermi (TF) regime the mean square fluctuations of the phase do not exceed $\sim \gamma^{1/2}$ and, hence, they are small under the condition (5.0.2) (see [43]). The condensate wavefunction is determined by the Gross-Pitaevskii equation which gives the TF parabolic density profile $n_0(z) = n_{0\mathrm{m}}(1 - z^2/R_{TF}^2)$. The maximum density $n_{0\mathrm{m}} = \mu/g$, the TF size of the condensate $R_{TF} = (2\mu/m\omega^2)^{1/2}$, and the chemical potential $\mu = \hbar\omega(3N\alpha/4\sqrt{2})^{2/3}$. For $\alpha \gg 1$ we are always in the TF regime ($\mu \gg \hbar\omega$). In this case, Eq. (5.0.2) requires a sufficiently large number of particles:

$$N \gg N_* = \alpha^2. \tag{5.0.3}$$

Note that under this condition the ratio $\mu/T_d \sim (\alpha^2/N)^{1/3} \ll 1$. For $\alpha \ll 1$ the criterion (5.0.2) of a weakly interacting gas is satisfied at any N, and the condensate is in the TF regime if $N \gg \alpha^{-1}$. In the opposite limit the mean-field interaction is much smaller than the level spacing in the trap $\hbar\omega$. Hence, one has a macroscopic occupation of the ground state of the trap, i.e. there is an ideal gas condensate with a Gaussian density profile.

At this point, we briefly discuss the cross-over to the BEC regime, predicted by Ketterle and van Druten for a trapped 1D ideal gas [33]. They found that the decrease of T to below $T_c = N\hbar\omega/\ln 2N$ strongly increases the population of the ground state, which rapidly becomes macroscopic. This sharp cross-over originates from the discrete structure of the trap levels and is not observed in quasiclassical calculations [32]. We argue that the presence of the interparticle interaction changes the picture drastically. One can distinguish between the (lowest) trap levels only if the interaction between particles occupying a particular level is much smaller than the level spacing. Otherwise the interparticle interaction smears out the discrete structure of the levels. For T close to T_c the occupation of the ground state is $\sim T_c/\hbar\omega \approx N/\ln 2N$ [33] and, hence, the mean-field interaction between the particles in this state (per particle) is $Ng/l\ln 2N$. The sharp BEC cross-over requires this quantity to be much smaller than $\hbar\omega$, and we arrive at the condition $N/\ln 2N \ll \alpha^{-1}$. For a realistic number of particles ($N \sim 10^3 - 10^4$) this is practically equivalent to the condition at which one has the ideal gas Gaussian condensate (see above).

As we see, the sharp BEC cross-over requires small α. For possible realizations of 1D gases, using the coupling constant g (5.0.1), we obtain $\alpha = 2al/l_0^2$. Then, even for the ratio $l/l_0 \sim 10$ and moderate radial confinement with $l_0 \sim 1\mu$m, we have $\alpha \sim 0.1$ for Rb atoms ($a \approx 50$ Å). Clearly, for a reasonably large number of particles the cross-over condition $N \ll \alpha^{-1}$ can only be fulfilled at extremely small interparticle interaction. One can think of reducing a to below 1Å and achieving $\alpha < 10^{-3}$ by using Feshbach resonances as in the MIT and JILA experiments [82; 120]. In this case one can expect the sharp BEC cross-over already for $N \sim 10^3$.

We now turn to the case of large α. For $\gamma \gg 1$ one has a Tonks gas [56; 57] (the realization of the axially uniform Tonks gas in a square-well (axial) potential was discussed in [136]). The one-to-one mapping of this system to a gas of free fermions [54] ensures the fermionic spectrum and density profile of a trapped Tonks gas. For (axial) harmonic trapping the condition $\gamma \gg 1$ requires $N \ll N_*$. The chemical potential is equal to $N\hbar\omega$, and the density distribution is $n(z) = (\sqrt{2N}/\pi l)\sqrt{1-(z/R)^2}$, where the size of the cloud $R = \sqrt{2N}l$. The density profile $n(z)$ is different from both the profile of the zero-temperature condensate and the classical distribution of particles, which provides a root for identifying the trapped Tonks gas in experiments. The interference effects and dynamical properties of this system are now a subject of theoretical studies [137; 138]. In Rb and Na this regime can be achieved for $N \lesssim 10^3$ by the Feshbach increase of a to ~ 500 Å and using $\omega \sim 1$Hz and $\omega_0 \sim 10$kHz ($\alpha \sim 50$).

Large α and N satisfying Eq. (5.0.3), or small α and $N \gg \alpha^{-1}$, seem most feasible in experiments with trapped 1D gases. In this case, at any $T \ll T_d$ one has a weakly interacting gas in the TF regime. Similarly to the uniform 1D case, the decrease of temperature to below T_d continuously transforms a classical 1D gas to the regime of quantum degeneracy. At $T = 0$ this weakly interacting gas turns to the true TF condensate (see above). It is then subtle to understand how the correlation properties change with temperature at $T \ll T_d$. For this purpose, we analyze the behavior of the one-particle density matrix by calculating the fluctuations of the density and phase. We *a priori* assume small density fluctuations and prove this statement relying on the zero-temperature equations for the mean density $n_0(z)$ and excitations. The operator of the density fluctuations is (see, e.g. [71])

$$\hat{n}'(z) = n_0^{1/2}(z) \sum_{j=1}^{\infty} i f_j^-(z) \hat{a}_j + h.c., \tag{5.0.4}$$

where $\hat{a}_j$ is the annihilation operator of the excitation with quantum number j and energy ϵ_j, $f_j^{\pm} = u_j \pm v_j$, and the u, v functions of the excitations are determined by the same Bogolyubov-de Gennes equations (generalization of the Bogolyubov method for spatially inhomogeneous systems see in [37]) as in the presence of the TF condensate.

The solution of these equations gives the spectrum $\epsilon_j = \hbar\omega\sqrt{j(j+1)/2}$ [43; 42] and the wavefunctions

$$f_j^{\pm}(x) = \left(\frac{j+1/2}{R_{TF}}\right)^{1/2} \left[\frac{2\mu}{\epsilon_j}(1-x^2)\right]^{\pm 1/2} P_j(x), \tag{5.0.5}$$

where j is a positive integer, P_j are Legendre polynomials, and $x = z/R_{TF}$. For the mean square fluctuations of the density, $\langle \delta\hat{n}^2_{zz'} \rangle = \langle (\hat{n}'(z) - \hat{n}'(z'))^2 \rangle$, we have

$$\frac{\langle \delta\hat{n}^2_{zz'} \rangle}{n_{0m}^2} = \sum_{j=1}^{\infty} \frac{\epsilon_j (j+1/2)}{2\mu n_{0m} R_{TF}} (P_j(x) - P_j(x'))^2 (1 + 2N_j),$$

with $N_j = [\exp(\epsilon_j/T) - 1]^{-1}$ being the occupation numbers for the excitations. At $T \gg \hbar\omega$ the main contribution to the density fluctuations comes from quasiclassical excitations ($j \gg 1$). The vacuum fluctuations are small: $\langle \delta\hat{n}^2_{zz'} \rangle_0 \sim n_{0m}^2 \gamma^{1/2}$. For the thermal fluctuations on a distance scale $|z - z'| \gg l_c$, we obtain

$$\langle \delta n^2_{zz'} \rangle_T \approx n_{0m}^2 (T/T_d) \min\{(T/\mu), 1\}. \tag{5.0.6}$$

We see that the density fluctuations are strongly suppressed at temperatures $T \ll T_d$. Then, one can write the total field operator as $\hat{\psi}(z) = \sqrt{n_0(z)}\exp(i\hat{\phi}(z))$, where $\hat{\phi}(z)$ is the operator of the phase fluctuations, and the one-particle density matrix takes the form (see, e.g. [12]) which is a generalization of Eq. (2.3.1) for the inhomogeneous case

$$\langle\hat{\psi}^\dagger(z)\hat{\psi}(z')\rangle = \sqrt{n_0(z)n_0(z')}\exp\{-\langle\delta\hat{\phi}^2_{zz'}\rangle/2\}, \tag{5.0.7}$$

with $\delta\hat{\phi}_{zz'} = \hat{\phi}(z) - \hat{\phi}(z')$. The operator $\hat{\phi}(z)$ is given by (we count only phonon part (see Overview))

$$\hat{\phi}(z) = [4n_0(z)]^{-1/2}\sum_{j:\ \epsilon_j<\mu} f_j^+(z)\hat{a}_j + h.c., \tag{5.0.8}$$

and for the mean square fluctuations we have

$$\langle\delta\hat{\phi}^2_{zz'}\rangle = \sum_{j:\ \epsilon_j<\mu}\frac{\mu(j+1/2)}{2\epsilon_j n_{0m}R_{TF}}(P_j(x) - P_j(x'))^2(1+2N_j).$$

For the vacuum fluctuations we find (c.f. [139; 43])

$$\langle\delta\hat{\phi}^2_{zz'}\rangle_0 \approx (\gamma^{1/2}/\pi)\ln(|z-z'|/l_c),$$

and they are small for any realistic size of the gas cloud. The thermal fluctuations of the phase are mostly provided by the contribution of the lowest excitations and the restriction $\epsilon_j < \mu$ is not important. A direct calculation, with $N_j = T/\epsilon_j$, yields

$$\langle\delta\hat{\phi}^2_{zz'}\rangle_T = \frac{4T\mu}{3T_d\hbar\omega}\left|\log\left[\frac{(1-x')}{(1+x')}\frac{(1+x)}{(1-x)}\right]\right|. \tag{5.0.9}$$

In the inner part of the gas sample the logarithm in Eq. (5.0.9) is of order unity.

Thus, we can introduce a characteristic temperature

$$T_{ph} = T_d\hbar\omega/\mu \tag{5.0.10}$$

at which the quantity $\langle\delta\hat{\phi}^2_{zz'}\rangle \approx 1$ on a distance scale $|z-z'| \sim R_{TF}$. The characteristic radius of phase fluctuations is $R_\phi \approx R_{TF}(T_{ph}/T) \propto N^{2/3}/T$, and for $T < T_{ph}$ it exceeds the sample size R_{TF}. This means that at $T \ll T_{ph}$ both the density and phase fluctuations are suppressed, and there is a true condensate. The condition (5.0.3) always provides the ratio $T_{ph}/\hbar\omega \approx (4N/\alpha^2)^{1/3} \gg 1$.

In the temperature range, where $T_d \gg T \gg T_{ph}$, the density fluctuations are suppressed, but the phase fluctuates on a distance scale $R_\phi \ll R_{TF}$. Thus, similarly to the quasi-2D case (see Section 3.1), we have a quasicondensate. The radius of the phase fluctuations greatly exceeds the correlation length: $R_\phi \approx l_c(T_d/T) \gg l_c$. Hence, the quasicondensate has the same density profile as the true condensate. Correlation properties at distances smaller than R_ϕ are also the same. However, the phase fluctuations lead to a drastic difference in the phase coherence properties.

In Fig. 5.0.1 we present the state diagram of the trapped 1D gas for $\alpha = 10$ ($N_* = 100$). For $N \gg N_*$, the decrease of temperature to below T_d leads to the appearance

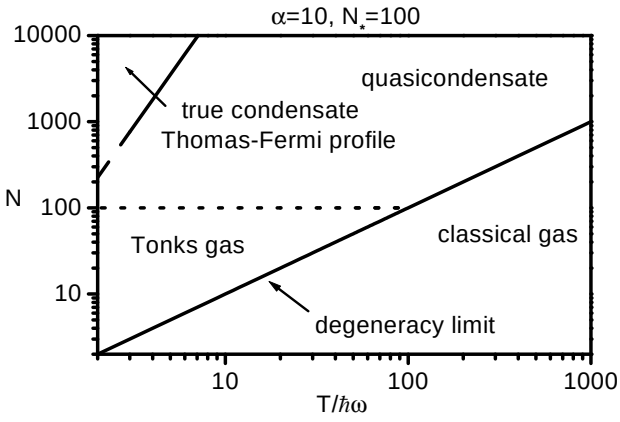

Figure 5.0.1: Diagram of states for a trapped 1D gas.

of a quasicondensate which at $T < T_{ph}$ turns to the true condensate. In the $T - N$ plane the approximate border line between the two BEC regimes is determined by the equation $(T/\hbar\omega) = (32N/9N_*)^{1/3}$. For $N < N_*$ the system can be regarded as a trapped Tonks gas (for an infinitely long atom waveguide, the approximate border line between the Tonks and weakly interacting regimes is given in terms of density and temperature in [140]).

Phase coherence properties of trapped 1D gases can be studied in 'juggling' experiments similar to those with 3D condensates at NIST and Munich [141; 142]. Small clouds of atoms are ejected from the main cloud by stimulated Raman or RF transitions. Observing the interference between two clouds, simultaneously ejected from different parts of the sample, allows the reconstruction of the spatial phase correlation properties. Similarly, temporal correlations of the phase can be studied by overlapping clouds ejected at different times from the same part of the sample. In this way juggling experiments provide a direct measurement of the one-particle density matrix. Repeatedly juggling clouds of a small volume Ω from points z and z' of the sample, for equal time of flight to the detector we have the averaged detection signal $I = \Omega[n_0(z) + n_0(z') + 2\langle\hat{\psi}^\dagger(z)\psi(z')\rangle]$.

At $T \ll T_{ph}$ the phase fluctuations are small and one has a true condensate. In this case, for $z' = -z$ we have $\langle\hat{\psi}^\dagger(z)\hat{\psi}(z')\rangle = n_0(z)$ and $I = 4\Omega n_0(z)$, and there is a pronounced interference effect: The detected signal is twice as large as the number of atoms in the ejected clouds. The phase fluctuations grow with T and for $T > T_{ph}$, where the true condensate turns to a quasicondensate, the detection signal decreases as described by $\langle\hat{\psi}^\dagger(z)\hat{\psi}(z')\rangle$ from Eqs. (5.0.7) and (5.0.9). For $T \gg T_{ph}$ the phase fluctuations completely destroy the interference between the two ejected clouds, and $I = 2\Omega n_0(z)$.

In conclusion, we have identified 3 regimes of quantum degeneracy in a trapped 1D gas: the BEC regimes of a quasicondensate and true condensate, and the regime of a trapped Tonks gas. The creation of 1D gases will open handles on interesting phase coherence studies and the studies of "fermionization" in Bose systems.

Chapter 6 Phase-fluctuating 3D Bose-Einstein condensates

6.1 Phase-fluctuating 3D condensates in elongated traps

We find that in very elongated 3D trapped Bose gases, even at temperatures far below the BEC transition temperature T_c, the equilibrium state will be a 3D condensate with fluctuating phase (quasicondensate). At sufficiently low temperatures the phase fluctuations are suppressed and the quasicondensate turns into a true condensate. The presence of the phase fluctuations allows for extending thermometry of Bose-condensed gases well below those established in current experiments.

Phase coherence properties are among the most interesting aspects of Bose-condensed gases. Since the discovery of Bose-Einstein condensation (BEC) in trapped ultra-cold clouds of alkali atoms [3; 4; 5], various experiments have proved the presence of phase coherence in trapped condensates. The MIT group [76] has found the interference of two independently prepared condensates, once they expand and overlap after switching off the traps. The MIT [143], NIST [141] and Munich [142] experiments provide evidence for the phase coherence of trapped condensates through the measurement of the phase coherence length and/or single particle correlations.

These results support the usual picture of BEC in 3D gases. In equilibrium, the fluctuations of density and phase are important only in a narrow temperature range near the BEC transition temperature T_c. Outside this region, the fluctuations are suppressed and the condensate is phase coherent. This picture precludes the interesting physics of phase-fluctuating condensates, which is present in 2D and 1D systems (see Section 3.1, Chapter 5 and refs. therein).

In this section we show that the phase coherence properties of 3D Thomas-Fermi (TF) condensates depend on their shape. In very elongated 3D condensates, the axial phase fluctuations are found to manifest themselves even at temperatures far below T_c. Then, as the density fluctuations are suppressed, the equilibrium state will be a *condensate with fluctuating phase* (quasicondensate) similar to that in 1D trapped gases (see Chapter 5). Decreasing T below a sufficiently low temperature, the 3D quasicondensate gradually turns into a true condensate.

The presence and the temperature dependence of axial phase fluctuations in sufficiently elongated 3D condensates suggests a principle of thermometry for Bose-condensed gases with indiscernible thermal clouds. The idea is to extract the temperature from a measurement of the axial phase fluctuations, for example by measuring the single-particle correlation function. This principle works for quasicondensates or for any condensate that can be elongated adiabatically until the phase fluctuations become observable.

So far, axial phase fluctuations have not been measured in experiments with cigar-

shaped condensates. We discuss the current experimental situation and suggest how one should select the parameters of the cloud in order to observe the phase-fluctuating 3D condensates.

We first consider a 3D Bose gas in an elongated cylindrical harmonic trap and analyze the behavior of the single-particle correlation function. The natural assumption of the existence of a true condensate at $T = 0$ automatically comes out of these calculations. In the TF regime, where the mean-field (repulsive) interparticle interaction greatly exceeds the radial (ω_ρ) and axial (ω_z) trap frequencies, the density profile of the zero-temperature condensate has the well-known shape $n_0(\rho, z) = n_{0m}(1 - \rho^2/R^2 - z^2/L^2)$, where $n_{0m} = \mu/g$ is the maximum condensate density, with μ being the chemical potential, $g = 4\pi\hbar^2 a/m$, m the atom mass, and $a > 0$ the scattering length. Under the condition $\omega_\rho \gg \omega_z$, the radial size of the condensate, $R = (2\mu/m\omega_\rho^2)^{1/2}$, is much smaller than the axial size $L = (2\mu/m\omega_z^2)^{1/2}$.

Fluctuations of the density and phase of the condensate, in particular at finite T, are related to elementary excitations of the cloud. The density fluctuations are dominated by the excitations with energies of the order of μ. The wavelength of these excitations is much smaller than the radial size of the condensate. Hence, the density fluctuations have the ordinary 3D character and are small. Therefore, one can write the total field operator of atoms as $\hat{\psi}(\mathbf{r}) = \sqrt{n_0(\mathbf{r})}\exp(i\hat{\phi}(\mathbf{r}))$, where $\hat{\phi}(\mathbf{r})$ is the operator of the phase. The single-particle correlation function is then expressed through the mean square fluctuations of the phase (see, e.g. [12]):

$$\langle\hat{\psi}^\dagger(\mathbf{r})\hat{\psi}(\mathbf{r}')\rangle = \sqrt{n_0(\mathbf{r})n_0(\mathbf{r}')}\exp\{-\langle[\delta\hat{\phi}(\mathbf{r},\mathbf{r}')]^2\rangle/2\}, \tag{6.1.1}$$

with $\delta\hat{\phi}(\mathbf{r},\mathbf{r}') = \hat{\phi}(\mathbf{r}) - \hat{\phi}(\mathbf{r}')$. The operator $\hat{\phi}(\mathbf{r})$ is given by (see, e.g., [71])

$$\hat{\phi}(\mathbf{r}) = [4n_0(\mathbf{r})]^{-1/2}\sum_\nu f_\nu^+(\mathbf{r})\hat{a}_\nu + h.c., \tag{6.1.2}$$

where $\hat{a}_\nu$ is the annihilation operator of the excitation with quantum number(s) ν and energy ϵ_ν, $f_\nu^+ = u_\nu + v_\nu$, and the u, v functions of the excitations are determined by the Bogolyubov-de Gennes equations.

The excitations of elongated condensates can be divided into two groups: "low energy" axial excitations with energies $\epsilon_\nu < \hbar\omega_\rho$, and "high energy" excitations with $\epsilon_\nu > \hbar\omega_\rho$. The latter have 3D character as their wavelengths are smaller than the radial size R. Therefore, as in ordinary 3D condensates, these excitations can only provide small phase fluctuations. The low-energy axial excitations have wavelengths larger than R and exhibit a pronounced 1D behavior. Hence, one expects that these excitations give the most important contribution to the long-wave axial fluctuations of the phase.

The solution of the Bogolyubov-de Gennes equations for the low-energy axial modes gives the spectrum $\epsilon_j = \hbar\omega_z\sqrt{j(j+3)/4}$ [42], where j is a positive integer. The wavefunctions f_j^+ of these modes have the form

$$f_j^+(\mathbf{r}) = \sqrt{\frac{(j+2)(2j+3)gn_0(\mathbf{r})}{4\pi(j+1)R^2L\epsilon_j}}P_j^{(1,1)}\left(\frac{z}{L}\right), \tag{6.1.3}$$

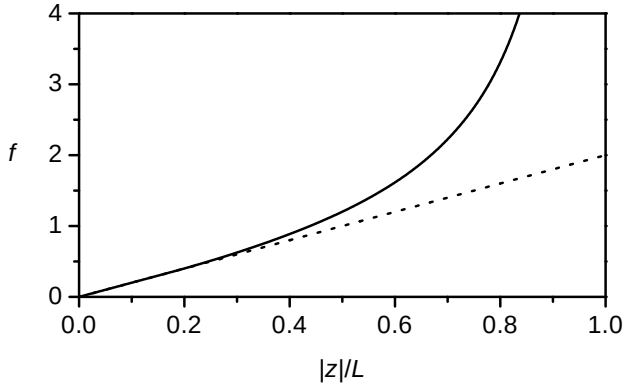

Figure 6.1.1: The function $f(z/L)$. The solid curve shows the result of our numerical calculation, and the dotted line is $f(z) = 2|z|/L$ following from Eq. (6.1.5).

where $P_j^{(1,1)}$ are Jacobi polynomials. Note that the contribution of the low-energy axial excitations to the phase operator (6.1.2) is independent of the radial coordinate ρ.

Relying on Eqs. (6.1.2) and (6.1.3), we now calculate the mean square axial fluctuations of the phase at distances $|z - z'| \ll R$. As in 1D trapped gases (see Chapter 5), the vacuum fluctuations are small for any realistic axial size L. The thermal fluctuations are determined by the equation (we count only the "low energy" excitations)

$$\langle[\delta\hat{\phi}(z,z')]^2\rangle_T = \sum_{j:\ \epsilon_j<\hbar\omega_\rho} \frac{\mu(j+2)(2j+3)}{15(j+1)\epsilon_j N_0}\left(P_j^{(1,1)}\left(\frac{z}{L}\right) - P_j^{(1,1)}\left(\frac{z'}{L}\right)\right)^2 N_j\,, \quad (6.1.4)$$

with $N_0 = (8\pi/15)n_{0m}R^2L$ being the number of Bose-condensed particles, and N_j the equilibrium occupation numbers for the excitations. The main contribution to the sum over j in Eq. (6.1.4) comes from several lowest excitation modes, and at temperatures $T \gg \hbar\omega_z$ we may put $N_j = T/\epsilon_j$. Then, in the central part of the cloud ($|z|, |z'| \ll L$) a straightforward calculation yields

$$\langle[\delta\hat{\phi}(z,z')]^2\rangle_T = \delta_L^2|z - z'|/L, \quad (6.1.5)$$

where the quantity δ_L^2 represents the phase fluctuations on a distance scale $|z - z'| \sim L$ and is given by

$$\delta_L^2(T) = 32\mu T/15N_0(\hbar\omega_z)^2. \quad (6.1.6)$$

Note that at any z and z' the ratio of the phase correlator (6.1.4) to δ_L^2 is a universal function of z/L and z'/L:

$$\langle[\delta\hat{\phi}(z,z')]^2\rangle_T = \delta_L^2(T)f(z/L, z'/L). \quad (6.1.7)$$

In Fig. 6.1.1 we present the function $f(z/L) \equiv f(z/L, -z/L)$ calculated numerically from Eq. (6.1.4).

The phase fluctuations decrease with temperature. As the TF chemical potential is $\mu = (15N_0\, g/\pi)^{2/5}(m\bar{\omega}^2/8)^{3/5}$ ($\bar{\omega} = \omega_\rho^{2/3}\omega_z^{1/3}$), Eq. (6.1.6) can be rewritten in the form

$$\delta_L^2 = (T/T_c)(N/N_0)^{3/5}\delta_c^2, \tag{6.1.8}$$

where $T_c \approx N^{1/3}\hbar\bar{\omega}$ is the BEC transition temperature, and N the total number of particles. The presence of the 3D BEC transition in elongated traps requires the inequality $T_c \gg \hbar\omega_\rho$ and, hence, limits the aspect ratio to $\omega_\rho/\omega_z \ll N$. The parameter δ_c^2 is given by

$$\delta_c^2 = \frac{32\mu(N_0 = N)}{15N^{2/3}\hbar\bar{\omega}}\left(\frac{\omega_\rho}{\omega_z}\right)^{4/3} \propto \frac{a^{2/5}m^{1/5}\omega_\rho^{22/15}}{N^{4/15}\omega_z^{19/15}}. \tag{6.1.9}$$

Except for a narrow interval of temperatures just below T_c, the fraction of non-condensed atoms is small and Eq. (6.1.8) reduces to $\delta_L^2 = (T/T_c)\delta_c^2$. Thus, the phase fluctuations can be important at large values of the parameter δ_c^2, whereas for $\delta_c^2 \ll 1$ they are small on any distance scale and one has a true Bose-Einstein condensate. In Fig. 6.1.2 we present the quantity δ_c^2 for the parameters of various experiments with elongated condensates.

In the Konstanz [144] and Hannover [145] experiments the ratio T/T_c was smaller than 0.5. In the recent experiment [65] the value $\delta_c^2 \approx 3$ has been reached, but the temperature was very low. Hence, the axial phase fluctuations were rather small in these experiments and they were dealing with true condensates. The last statement also holds for the ENS experiment [146] where T was close to T_c and the Bose-condensed fraction was $N_0/N \approx 0.75$.

The single-particle correlation function is determined by Eq. (6.1.1) only if the condensate density n_0 is much larger than the density of non-condensed atoms, n'. Otherwise, this equation should be completed by terms describing correlations in the thermal cloud. However, irrespective of the relation between n_0 and n', Eq. (6.1.1) and Eqs. (6.1.4)-(6.1.6) correctly describe phase correlations in the condensate as long as the fluctuations of the condensate density are suppressed. This is still the case for T close to T_c and $N_0 \ll N$, if we do not enter the region of critical fluctuations. Then, Eq. (6.1.8) gives $\delta_L^2 = (N/N_0)^{3/5}$. At the highest temperatures of the Bose-condensed cloud in the MIT sodium experiment [147], the condensed fraction was $N_0/N \sim 0.1$ and the phase fluctuations were still small.

On the contrary, for $N_0/N \approx 0.06$ in the hydrogen experiment [148], with δ_c^2 from Fig. 6.1.2 we estimate $\delta_L^2 \approx 1$. The same or even larger value of δ_L^2 was reached in the Munich Rb experiment [142] where the gas temperature was varying in a wide interval around T_c. In the Rb experiment at AMOLF [149], the smallest observed Bose-condensed fraction was $N_0/N \approx 0.03$, which corresponds to $\delta_L^2 \approx 5$. However, axial fluctuations of the phase have not been measured in these experiments.

We will focus our attention on the case where $N_0 \approx N$ and the presence of the axial phase fluctuations is governed by the parameter δ_c^2. For $\delta_c^2 \gg 1$, the nature of the Bose-condensed state depends on temperature. In this case we can introduce a characteristic temperature

$$T_\phi = 15(\hbar\omega_z)^2 N/32\mu \tag{6.1.10}$$

at which the quantity $\delta_L^2 \approx 1$ (for $N_0 \approx N$). In the temperature interval $T_\phi < T < T_c$, the phase fluctuates on a distance scale smaller than L. Thus, as the density fluctuations are suppressed, the Bose-condensed state is a condensate with fluctuating phase or

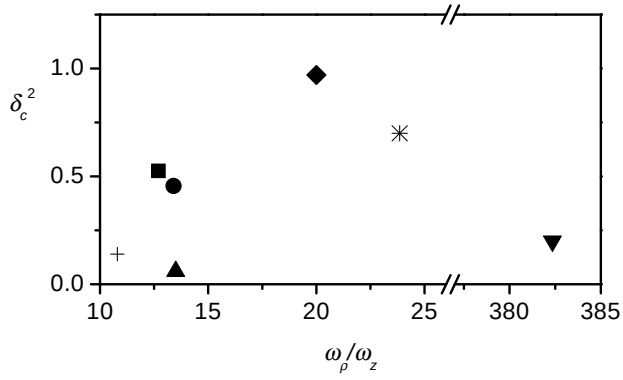

Figure 6.1.2: The parameter δ_c^2 for experiments with elongated condensates. The up and down triangles stand for δ_c^2 in the sodium [147] and hydrogen [148] MIT experiments, respectively. Square, cross, diamond, circle, and star show δ_c^2 for the rubidium experiments at Konstanz [144], Munich [142], Hannover [145], ENS [146], and AMOLF [149].

quasicondensate. The expression for the radius of phase fluctuations (phase coherence length) follows from Eq. (6.1.5) and is given by

$$l_\phi \approx L(T_\phi/T). \tag{6.1.11}$$

The phase coherence length l_ϕ greatly exceeds the correlation length $l_c = \hbar/\sqrt{m\mu}$. Eqs. (6.1.11) and (6.1.10) give the ratio $l_\phi/l_c \approx (T_c/T)(T_c/\hbar\omega_\rho)^2 \gg 1$. Therefore, the quasicondensate has the same density profile and local correlation properties as the true condensate. However, the phase coherence properties of quasicondensates will be drastically different (see below).

The decrease of temperature to well below T_ϕ makes the phase fluctuations small ($\delta_L^2 \ll 1$) and continuously transforms the quasicondensate into a true condensate.

It is interesting to compare the described behavior of the interacting gas for $\delta_c^2 \gg 1$, with the two-step BEC predicted for the ideal Bose gas in elongated traps [150]. In both cases, at T_c the particles Bose-condense in the ground state of the radial motion. However, the ideal gas remains non-condensed (thermal) in the axial direction for $T > T_{1D} = N\hbar\omega_z/\ln 2N$ (assuming $T_{1D} < T_c$), and there is a sharp cross-over to the axial BEC regime at $T \approx T_{1D}$. The interacting Bose gas below T_c forms the 3D TF (non-fluctuating) density profile, and the spatial correlations become non-classical in all directions. For $\delta_c^2 \gg 1$, the axial phase fluctuations at $T \sim T_c$ are still large, and one has a quasicondensate which continuously transforms into a true condensate at T below T_ϕ. Note that T_ϕ is quite different from T_{1D} of the ideal gas.

Let us now demonstrate that 3D elongated quasicondensates can be achieved for realistic parameters of trapped gases. As found above, the existence of a quasicondensate requires large values of the parameter δ_c^2 given by Eq. (6.1.9). Most important is the dependence of δ_c^2 on the aspect ratio of the cloud ω_ρ/ω_z, whereas the dependence on the number of atoms and on the scattering length is comparatively weak. Fig. 6.1.3

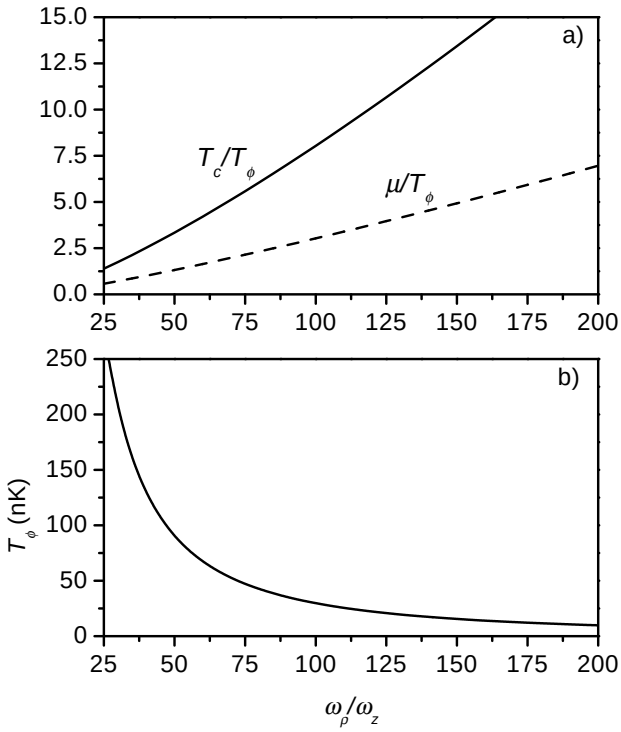

Figure 6.1.3: The ratios $T_c/T_\phi = \delta_c^2$ and μ/T_ϕ in (a) and the temperature T_ϕ in (b), versus the aspect ratio ω_ρ/ω_z for trapped Rb condensates with $N = 10^5$ and $\omega_\rho = 500$ Hz.

shows $T_c/T_\phi = \delta_c^2$, μ/T_ϕ, and the temperature T_ϕ as functions of ω_ρ/ω_z for rubidium condensates at $N = 10^5$ and $\omega_\rho = 500$ Hz. Comparing the results for δ_c^2 in Fig. 6.1.3 with the data in Fig. 6.1.2, we see that 3D quasicondensates can be obtained by transforming the presently achieved BEC's to more elongated geometries corresponding to $\omega_\rho/\omega_z \gtrsim 50$.

One can distinguish between quasicondensates and true BEC's in various types of experiments. By using the Bragg spectroscopy method developed at MIT one can measure the momentum distribution of particles in the trapped gas and extract the coherence length l_ϕ[143]. The use of two (axially) counter-propagating laser beams to absorb a photon from one beam and emit it into the other one, results in axial momentum transfer to the atoms which have momenta at Doppler shifted resonance with the beams. These atoms form a small cloud which will axially separate from the rest of the sample provided the mean free path greatly exceeds the axial size L. The latter condition can be assured by applying the Bragg excitation after abruptly switching off the radial confinement of the trap. The axial momentum distribution is then conserved if the dynamic evolution of the cloud does not induce axial velocities. According to the scaling approach [67; 68], this is the case for the axial frequency decreasing as $\omega_z(t) = \omega_z(0)[1 + \omega_\rho^2 t^2]^{-1/2}$.

In "juggling" experiments described in Chapter 5 and similar to those at NIST and Munich [141; 142], one can directly measure the single-particle correlation function. The latter is obtained by repeatedly ejecting small clouds of atoms from the parts z and z' of the sample and averaging the pattern of interference between them in the detection region over a large set of measurements. As follows from Eqs. (6.1.6) and (6.1.7), for $z' = -z$ the correlation function depends on temperature as $\exp\{-\delta_L^2(T) f(z/L)/2\}$, where $f(z/L)$ is given in Fig. 6.1.1.

The phase fluctuations are very sensitive to temperature. From Fig. 6.1.3 we see that one can have $T_\phi/T_c < 0.1$, and the phase fluctuations are still significant at $T < \mu$, where only a tiny indiscernible thermal cloud is present.

This suggests a principle for thermometry of 3D Bose-condensed gases with indiscernible thermal clouds. If the sample is not an elongated quasicondensate by itself, it is first transformed to this state by adiabatically increasing the aspect ratio ω_ρ/ω_z. This does not change the ratio T/T_c as long as the condensate remains in the 3D TF regime. Second, the phase coherence length l_ϕ or the single-particle correlation function are measured. These quantities depend on temperature if the latter is of the order of T_ϕ or larger. One thus can measure the ratio T/T_c for the initial cloud, which is as small as the ratio T_ϕ/T_c for the elongated cloud.

We believe that the studies of phase coherence in elongated condensates will reveal many new interesting phenomena. The measurement of phase correlators will allow one to study the evolution of phase coherence in the course of the formation of a condensate out of a non-equilibrium thermal cloud.

6.2 Observation of phase fluctuations in Bose-Einstein condensates

We describe a method of observing phase fluctuations through the measurement of the density profile after releasing the gas from the trap. It is shown how the phase fluctuations of an elongated BEC transform into the density modulations in the course of free expansion. The average value of the modulations is found as a function of the number of particles, temperature, time of flight, and trap frequencies.

Fluctuations of the phase of a Bose condensate are related to thermal excitations and always appear at finite temperature. However, as shown in Section 6.1, the fluctuations depend not only on temperature but also on the trap geometry and on the particle number. Typically, fluctuations in spherical traps are strongly suppressed as the wavelengths of excitations are smaller than the size of the atomic cloud. In contrast, wavelengths of the excitations in strongly elongated traps can be larger than the *radial* size of the cloud. In this case, the low-energy *axial* excitations acquire a 1D character and can lead to more pronounced phase fluctuations, although the density fluctuations of the equilibrium state are still suppressed. Because of the pronounced phase fluctuations, the coherence properties of elongated condensates can be significantly altered as compared with previous observations. In particular, the axial coherence length can be much smaller than the size of the condensate, which can have dramatic consequences for practical applications.

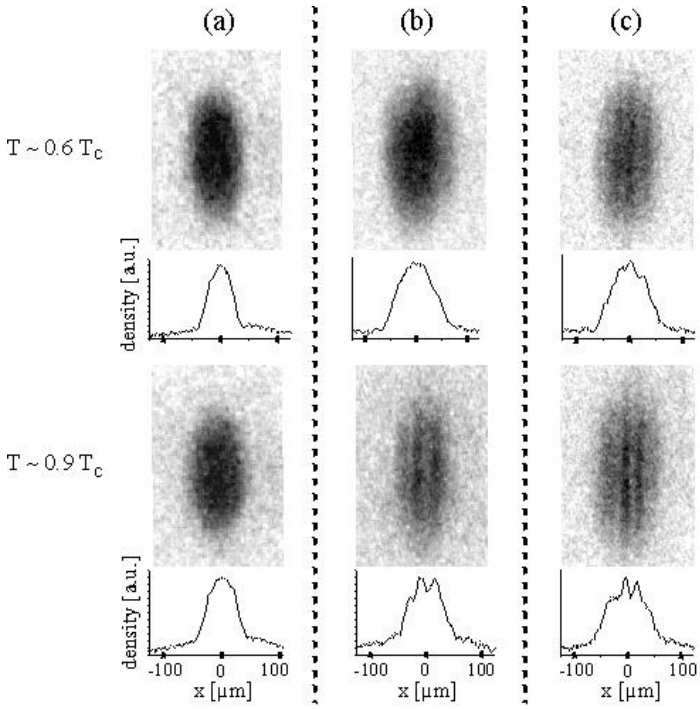

Figure 6.2.1: Absorption images and corresponding density profiles of BECs after 25 ms time-of-flight taken for various temperatures T and aspect ratios [$\lambda = 10$ (a), 26 (b), 51 (c)].

This section provides a theoretical basis for the experiment on observation of phase fluctuations carried out at the University of Hannover (see [151; 152]). The experiment is performed with Bose-Einstein condensates of up to $N_0 = 5 \times 10^5$ rubidium atoms in the $|F = 2, m_F = +2\rangle$ state of a cloverleaf-type magnetic trap. The fundamental frequencies of the magnetic trap are $\omega_x = 2\pi \times 14\,\mathrm{Hz}$ and $\omega_\rho = 2\pi \times 365\,\mathrm{Hz}$ along the axial and radial direction, respectively. Due to the highly anisotropic confining potential with an aspect ratio $\lambda = \omega_\rho/\omega_x$ of 26, the condensate is already elongated along the horizontal x axis. In addition, further radial compression of the ensemble by means of a superimposed blue detuned optical dipole trap is possible [65]. The measurements are performed for radial trap frequencies ω_ρ between $2\pi \times 138\,\mathrm{Hz}$ and $2\pi \times 715\,\mathrm{Hz}$ corresponding to aspect ratios λ between 10 and 51. After rf evaporative cooling to the desired temperature, the system is allowed to reach an equilibrium state by waiting for 1 sec (with rf "shielding"). Then, within $200\,\mu$s the trapping potential is switched off and the density profile of the cloud is detected after a variable time-of-flight.

Figure 6.2.1 shows examples of experimental data for various temperatures $T < T_c$ and aspect ratios λ. The usual anisotropic expansion of the condensate related to the anisotropy of the confining potential is clearly visible in the absorption images. The

line density profiles below reflect the parabolic shape of the BEC density distribution. Remarkably, pronounced stripes in the density distribution are observed in some cases. On average these stripes are more pronounced at high aspect ratios of the trapping potential [Fig. 6.2.1(c)], high temperatures (bottom row of Fig. 6.2.1), and low atom numbers.

The appearance of stripes in the process of ballistic expansion can be understood qualitatively as follows. As mentioned in Section 6.1, in the equilibrium state of a BEC in a trap the density distribution remains largely unaffected even if the phase fluctuates. The reason is that the mean-field interparticle interaction prevents the transformation of local velocity fields provided by the phase fluctuations into modulations of the density. However, after switching off the trap, the mean-field interaction rapidly decreases and the axial velocity field is then converted into a particular density distribution.

The stripes and their statistical properties can be described analytically using the scaling theory (see e.g. [66; 67; 68]). The condensate without initial fluctuations evolve according to the scaling solution

$$\psi = \frac{\sqrt{n_0}(\rho, x)}{b_\rho^2(t)} e^{i\phi_0}, \tag{6.2.1}$$

where $\phi_0 = (m/2\hbar)(\dot{b}_\rho/b_\rho)\rho^2$, ρ is the radial coordinate, and n_0 is the initial Thomas-Fermi density profile. The scaling parameter $b_\rho(t)$ is the ratio of the radial size at time t to the initial size. This parameter is determined by the scaling equations [66; 67; 68]). For initially elongated condensate, on a time scale $t \ll \omega_\rho^2/\omega_z$ we have $b_\rho^2(t) = 1 + \omega_\rho^2 t^2$, whereas the axial size of the released cloud remains unchanged.

Equations determining the ballistic expansion in the presence of the density and phase fluctuations, δn and ϕ, are obtained from the Gross-Pitaevskii equation linearized with regard to δn, $\nabla\phi$ around the solution (6.2.1). This gives two coupled equations:

$$\dot{\delta n} = \frac{1}{b_\rho^2}\hat{\xi}\phi - \frac{\hbar\nabla_x^2(n_0\phi)}{m}, \tag{6.2.2}$$

$$-n_0\dot{\phi} = \frac{gn_0\delta n}{\hbar b_\rho^2} + \frac{1}{4b_\rho^2}\hat{\xi}\left(\frac{\delta n}{n_0}\right) - \frac{\hbar\nabla_x^2\delta n}{4m}, \tag{6.2.3}$$

where $\hat{\xi} = -(\hbar/m)(\vec{\nabla}_{\rho'} n_0 \cdot \vec{\nabla}_{\rho'} + n_0\nabla_{\rho'}^2)$, and $\rho' = \rho/b_\rho$. Combining Eqs. (6.2.2) and (6.2.3), we find:

$$\ddot{\delta n} - \frac{g\nabla_x^2(n_0\delta n)}{mb_\rho^2} + \frac{\hbar^2\nabla_x^4\delta n}{4m^2} = \frac{\partial}{\partial t}\left(\frac{\hat{\xi}\phi}{b_\rho^2}\right) + \frac{\hbar}{4b_\rho^2 m}\nabla_x^2\hat{\xi}\frac{\delta n}{n_0}. \tag{6.2.4}$$

In the Thomas-Fermi limit ($\mu/\hbar\omega_\rho \gg 1$) the last term in the rhs of Eq. (6.2.4) can be neglected. For the axial excitations the quantities ϕ and δn are independent of the radial coordinate (see [42], and Eq. (6.1.2) in the previous section). This allows us to average Eq. (6.2.4) over the radial coordinate. The averaging procedure nullifies the first term in the rhs and yields

$$\ddot{\delta n} - \frac{\nabla_x^2(\mu(x)\delta n)}{2mb_\rho^2} + \frac{\hbar^2}{4m^2}\nabla_x^4\delta n = 0, \tag{6.2.5}$$

with $\mu(x) = \mu(1 - x^2/L^2)$, and L being the axial size. At $t = 0$ we have $b_\rho = 1$, and Eq. (6.2.5) is nothing else than the eigenmode equation for the axial excitations of trapped elongated condensates. For low-energy excitations the third term in the lhs of the eigenmode equation (quantum pressure term) can be omitted and one has the energy spectrum $\epsilon_j = \hbar\omega_x\sqrt{j(j+3)/4}$, where j is a positive integer (see [42] and the previous section).

The main contribution to the density modulations in the expanding cloud comes from quasiclassical excitations ($j \gg 1$), at least on a time scale $t \gg 1/\omega_\rho$. Therefore, we will rely on the local density approximation and neglect spatial derivatives of $\mu(x)$. Then Eq. (6.2.5) transforms to the equation for (local) Bogolyubov eigenmodes characterized by the axial momentum k:

$$\hbar^2\ddot{\delta n}_k + \tilde{\epsilon}_k^2(t)\delta n_k = 0\,, \tag{6.2.6}$$

where

$$\tilde{\epsilon}_k(t) = \sqrt{\frac{\mu(x)\hbar^2k^2}{2mb_\rho^2} + \frac{\hbar^4k^4}{4m^2}} \tag{6.2.7}$$

is the "local Bogolyubov spectrum". For short times, namely $t \lesssim 1/\omega_\rho$, the phonon part of this spectrum is dominant and $\tilde{\epsilon}_k(t) \approx \hbar c(x)k/b_\rho(t)$, where $c(x) = \sqrt{\mu(x)/2m}$ is the local velocity of axially propagating phonons in the initial cloud. Then Eq. (6.2.6) is solved in terms of hypergeometric functions of the variable $-\tau^2 = -\omega_\rho^2 t^2$. For larger times we have $b_\rho \approx \omega_\rho t$ and Eq. (6.2.6) can be solved in terms of Bessel functions of the variable $\tilde{t} = \tilde{\epsilon}_k^2(0)t/\hbar\mu(x)$. The two regimes may be matched by using the asymptotic expression for the hypergeometric function at $\tau \gg 1$, and for the Bessel function at $\tilde{t} \ll 1$. In this way we obtain an analytic expression for the density fluctuations $\delta n(x,t) = \sum_k \delta n_k(x,t)$. Since the momentum k and the quantum number j are related to each other as $k = \omega_x j/2c(x)$, the relative density fluctuations for $\tau \gg 1$ can be represented in the form:

$$\frac{\delta n(x,t)}{n_0(x)} = 2\sum_j \phi_j \exp\left\{-(\epsilon_j/\hbar\omega_\rho)^2 \ln\tau\right\} \sin\left(\frac{\epsilon_j^2\tau}{\mu(x)\hbar\omega_\rho}\right), \tag{6.2.8}$$

where ϕ_j is the initial (t=0) contribution of the j-th mode to the phase operator in Eq. (6.1.2) (with $\nu = j$).

From Eq. (6.2.8) one obtains a closed relation for the mean square density fluctuations σ^2 by averaging $(\delta n/n_0)^2$ over different realizations of the initial phase. Taking into account that $\langle(\hat{a}_j + \hat{a}_j^\dagger)(\hat{a}_{j'} + \hat{a}_{j'}^\dagger)\rangle/4 = N_j\delta_{jj'}/2$, using the quasiclassical average $(P_j^{(1,1)}(x))^2 \simeq 4(1-x^2)^{-3/2}/\pi j$, and transforming the sum over j into an integral we obtain:

$$\left\langle\left(\frac{\delta n(x,t)}{n_0(x,t)}\right)^2\right\rangle = \frac{4}{\pi(1-(x/L)^2)^{3/2}}\frac{T}{T_\phi}\int_{j=0}^{\infty}\frac{\mathrm{d}j}{j^2}\sin^2\left(\frac{\hbar\omega_x^2\tau j^2}{4\mu(x)\omega_\rho}\right)\exp\left[-\left(\frac{\omega_x j}{\omega_\rho}\right)^2\frac{\ln\tau}{2}\right]. \tag{6.2.9}$$

In the central part of the cloud ($x \approx 0$) the integration of Eq. (6.2.9) gives

$$\left\langle\left(\frac{\delta n(0,t)}{n_0(0,t)}\right)^2\right\rangle = \left(\frac{\sigma_{BEC}}{n_0}\right)^2 = \frac{\omega_x}{\omega_\rho}\frac{T}{T_\phi}\sqrt{\frac{\ln\tau}{\pi}}\left(\sqrt{1+\sqrt{1+\left(\frac{\hbar\omega_\rho\tau}{\mu\ln\tau}\right)^2}} - \sqrt{2}\right). \tag{6.2.10}$$

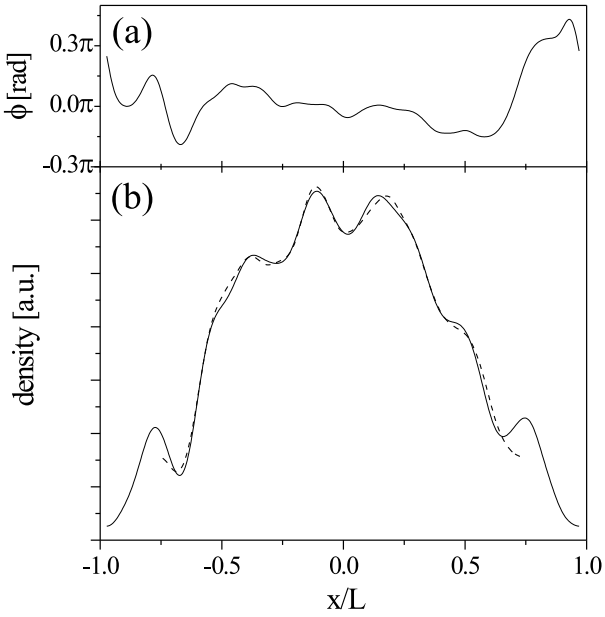

Figure 6.2.2: (a) A typical initial phase distribution calculated for $\omega_x = 2\pi \times 14\,\mathrm{Hz}$, $\omega_\rho = 2\pi \times 508\,\mathrm{Hz}$, $N_0 = 2 \times 10^5$, and $T = 0.5\,T_c$. (b) Corresponding density profile after 25 ms time-of-flight from a direct solution of the Gross-Pitaevskii equation (solid line) and analytical theory (dashed line).

Note that Eq. (6.2.10) provides a direct relation between the observed density fluctuations and temperature, and thus can be used for thermometry at very low T.

In the experiment [151; 152] Eq. (6.2.10) has been used to compare directly the averaged measured value of $[\overline{(\sigma_{\mathrm{BEC}}/n_0)^2}\,]^{1/2}_{\mathrm{exp}}$ to the predicted value of $(\sigma_{\mathrm{BEC}}/n_0)_{\mathrm{theory}}$ for various values of $T, N_0, \omega_x, \omega_\rho$, and t (see Fig. 6.2.3). The theoretical value takes into account the limited experimental imaging resolution.

The experimental results follow the expected general dependence very well. With the direct link of the phase fluctuations in the magnetic trap to the observed density modulation given by Eq. (6.2.10), the data therefore confirm the predicted general behavior of phase fluctuations in elongated BECs. However, the measured values are approximately by a factor of 2 smaller than those predicted by theory. This discrepancy could be due to, for example, a reduction of the observed contrast caused by a small tilt in the detection laser beam with respect to the radial stripes. Most of the observed experimental data, which exhibit fluctuations well above the noise limit, correspond to $T > T_\phi$. This implies that the measurements were performed in the regime of quasicondensation; i.e., the phase coherence length $l_\phi = LT_\phi/T$ of the initial condensate was smaller than the axial size L. For instance, for $\lambda = 51$, $T = 0.5\,T_c$, and $N_0 = 3 \times 10^4$, one obtains $l_\phi \approx L/3$.

Recently, theoretical predictions of this chapter have been experimentally tested by Gerbier et al. [153]. They have measured the temperature-dependent coherence length of

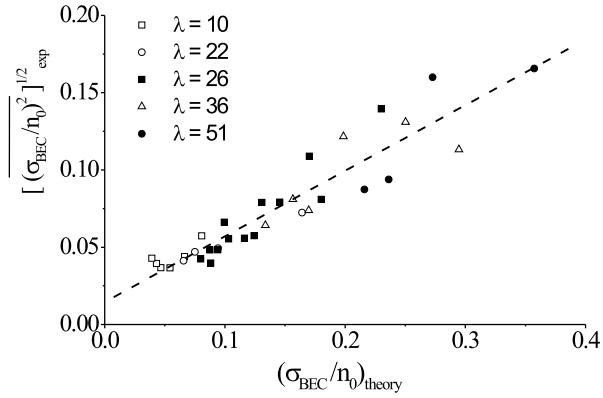

Figure 6.2.3: Average standard deviation of the measured line densities $[\overline{(\sigma_{\rm BEC}/n_0)^2}]^{1/2}_{\rm exp}$ compared to the theoretical value of $(\sigma_{\rm BEC}/n_0)_{\rm theory}$ obtained from Eq. (6.2.10). The dashed line is a fit to the experimental data.

an elongated Bose condensate by using Bragg spectroscopy and have found quantitative agreement between their measurements and our theoretical results. The measurements are consistent with the absence of density fluctuations, even when the phase fluctuations are strong, and confirm the existence of the regime of quasicondensate – novel phenomenon in the physics of elongated 3D BECs.

Bibliography

[1] S. Bose, Z. Phys. **26**, 178 (1924).

[2] A. Einstein, Sitzber. Kgl. Preuss. Akad. Wiss. 261 (1924).

[3] M. H. Anderson *et al.*, Science **269**, 198 (1995).

[4] K. B. Davis *et al.*, Phys. Rev. Lett. **75**, 3969 (1995).

[5] C. C. Bradley, C. A. Sackett, J. J. Tolett, and R. G. Hulet, Phys. Rev. Lett. **75**, 1687 (1995).

[6] A. Görlitz *et al.*, Phys. Rev. Lett. **87**, 130402 (2001).

[7] S. Burger *et al.*, Europhys. Lett. **57**, 1 (2002).

[8] F. Schreck *et al.*, Phys. Rev. Lett. **87**, 080403 (2001).

[9] M. Greiner *et al.*, Phys. Rev. Lett. **87**, 160405 (2001).

[10] N. D. Mermin and H. Wagner, Phys. Rev. Lett. **17**, 1133 (1966).

[11] P. C. Hohenberg, Phys. Rev. **158**, 383 (1967).

[12] V. N. Popov, *Functional Integrals in Quantum Field Theory and Statistical Physics* (D. Reidel Pub., Dordrecht, 1983).

[13] Y. Kagan, B. V. Svistunov, and G. V. Shlyapnikov, Sov. Phys. JETP **66**, 480 (1987).

[14] D. J. Bishop and J. D. Reppy, Phys. Rev. Lett. **40**, 1727 (1978).

[15] D. J. Bishop and J. D. Reppy, Phys. Rev. B **22**, 5171 (1980).

[16] A. I. Safonov *et al.*, Phys. Rev. Lett. **81**, 4545 (1998).

[17] E. Hanamura and H. Huag, Phys. Rep. **33**, 209 (1977).

[18] C. Comte and P. Nozières, J. Phys. (Paris) **43**, 1069 (1982).

[19] A. Mysyrowicz, J. Phys. (Paris) **41**, 281 (1980).

[20] A. Griffin, D. W. Snoke, and S. Stringari, *Bose-Einstein Condensation of Excitons and Biexcitons* (Cambridge Univ. Pess, Cambridge, 1995).

[21] D. W. Snoke, J. P. Wolfe, and A. Mysyrowicz, Phys. Rev. Lett. **64**, 2543 (1990).

[22] D. Snoke *et al.*, Nature **418**, 754 (2002).

[23] L. V. Butov *et al.*, Nature **417**, 47 (2002).

[24] L. V. Butov, A. C. Gossard, and D. S. Chemla, Nature **418**, 751 (2002).

[25] *Proceedings of the International Conference on High-T_c Superconductors and Materials and Mechanisms of Superconductivity, Interlaken, Switzerland*, edited by J. Müller and J. L. Olsen, Physica (Amsterdam) **153-155C**, Pts. I and II (1988).

[26] R. Brusetti *et al.*, Physica C **153-155**, 459 (1988).

[27] V. Vuletić, A. J. Kerman, C. Chin, and S. Chu, Phys. Rev. Lett. **82**, 1406 (1999).

[28] V. Vuletić, C. Chin, A. J. Kerman, and S. Chu, Phys. Rev. Lett. **83**, 943 (1999).

[29] I. Bouchoule, Ph.D. thesis, LKB ENS, Paris, 2000.

[30] I. Bouchoule, M. Morinaga, C. Salomon, and D. S. Petrov, Phys. Rev. A **65**, 033402 (2002).

[31] M. Hammes *et al.*, physics/0208065.

[32] V. Bagnato and D. Kleppner, Phys. Rev. A **44**, 7439 (1991).

[33] W. Ketterle and N. J. van Druten, Phys. Rev. A **54**, 656 (1996).

[34] W. J. Mullin, J. Low Temp. Phys. **106**, 615 (1997).

[35] E. B. Sonin, Sov. Phys. JETP **29**, 520 (1969).

[36] L. D. Landau and E. M. Lifshitz, *Quantum Mechanics, Non-relativistic Theory* (Butterworth-Heinemann, Oxford, 1999).

[37] P. G. de Gennes, *Superconductivity of Metals and Alloys* (Benjamin, New York, 1966).

[38] S. Stringari, Phys. Rev. Lett. **77**, 2360 (1996).

[39] P. Öhberg *et al.*, Phys. Rev. A **56**, R3346 (1997).

[40] M. Fliesser, A. Csordás, P. Szépfalusy, and R. Graham, Phys. Rev. A **56**, R2533 (1997).

[41] F. Dalfovo, S. Giorgini, L. P. Pitaevskii, and S. Stringari, Rev. Mod. Phys. **71**, 463 (1999).

[42] S. Stringari, Phys. Rev. A **58**, 2385 (1998).

[43] T.-L. Ho and M. Ma, J. Low Temp. Phys. **115**, 61 (1999).

[44] W. Kane and L. Kadanoff, Phys. Rev. **155**, 80 (1967).

[45] V. L. Berezinskii, Sov. Phys. JETP **32**, 493 (1971).

[46] V. L. Berezinskii, Sov. Phys. JETP **34**, 610 (1972).

[47] J. M. Kosterlitz and D. J. Thouless, J. Phys. C **6**, 1181 (1973).

[48] J. M. Kosterlitz, J. Phys. C **7**, 1046 (1974).

[49] N. Prokof'ev, O. Ruebenacker, and B. Svistunov, Phys. Rev. Lett. **87**, 270402 (2001).

[50] N. Prokof'ev and B. Svistunov, Phys. Rev. A **66**, 043608 (2002).

[51] M. Schwartz, Phys. Rev. B **15**, 1399 (1977).

[52] F. D. M. Haldane, Phys. Rev. Lett. **47**, 1840 (1981).

[53] L. P. Pitaevskii and S. Stringari, J. Low Temp. Phys. **85**, 377 (1991).

[54] M. Girardeau, J. Math. Phys. **1**, 516 (1960).

[55] M. Girardeau, Phys. Rev. **139**, B500 (1965).

[56] E. H. Lieb and W. Liniger, Phys. Rev. **130**, 1605 (1963).

[57] E. H. Lieb, Phys. Rev. **130**, 1616 (1963).

[58] J. Fortagh, A. Grossmann, C. Zimmermann, and T. W. Hänsch, Phys. Rev. Lett. **81**, 5310 (1998).

[59] J. Reichel, W. Hänsel, and T. W. Hänsch, Phys. Rev. Lett. **83**, 3398 (1999).

[60] D. Müller *et al.*, Phys. Rev. Lett. **83**, 5194 (1999).

[61] N. H. Dekker *et al.*, Phys. Rev. Lett. **84**, 1124 (2000).

[62] M. Key *et al.*, Phys. Rev. Lett. **84**, 1371 (2000).

[63] R. Folman *et al.*, Phys. Rev. Lett. **84**, 4749 (2000).

[64] T. Kuga *et al.*, Phys. Rev. Lett. **78**, 4713 (1997).

[65] K. Bongs *et al.*, Phys. Rev. A **63**, 031602(R) (2001).

[66] Y. Kagan, E. L. Surkov, and G. V. Shlyapnikov, Phys. Rev. A **54**, R1753 (1996).

[67] Y. Castin and R. Dum, Phys. Rev. Lett. **77**, 4315 (1996).

[68] Y. Kagan, E. L. Surkov, and G. V. Shlyapnikov, Phys. Rev. A **55**, R18 (1997).

[69] E. M. Lifshitz and L. P. Pitaevskii, *Statistical Physics, Part 2* (Pergamon Press, Oxford, 1980).

[70] J. T. M. Walraven, in *Atomic Hydrogen on Liquid Helium Surfaces*, *Fundamental Systems in Quantum Optics, Proceedings of the Les Houches Summer School, Session LIII*, edited by J. Dalibard, J. M. Raimond, and J. Zinn-Justin (Elsevier Science Publishers, Amsterdam, 1992).

[71] S. I. Shevchenko, Sov. J. Low Temp. Phys. **18**, 223 (1992).

[72] H. Gauck *et al.*, Phys. Rev. Lett. **81**, 5298 (1998).

[73] V. Vuletić, C. Chin, A. J. Kerman, and S. Chu, Phys. Rev. Lett. **81**, 5768 (1998).

[74] I. Bouchoule *et al.*, Phys. Rev. A **59**, R8 (1999).

[75] M. Morinaga, I. Bouchoule, J.-C. Karam, and C. Salomon, Phys. Rev. Lett. **83**, 4037 (1999).

[76] M. R. Andrews *et al.*, Science **275**, 637 (1997).

[77] A. A. Abrikosov, L. P. Gorkov, and I. E. Dzyaloshinski, *Methods of Quantum Field Theory in Statistical Physics* (Dover Publications Inc., New York, 1975).

[78] R. P. Feynman and A. R. Hibbs, *Quantum Mechanics and Path Integrals* (McGraw-Hill, New York, 1965).

[79] S. J. J. M. F. Kokkelmans, B. J. Verhaar, and K. Gibble, Phys. Rev. Lett. **81**, 951 (1998).

[80] D. Guery-Odelin, J. Soding, P. Desbiolles, and J. Dalibard, Optics Express **2**, 323 (1998).

[81] S. A. Hopkins *et al.*, Phys. Rev. A **61**, 032707 (2000).

[82] J. Stenger *et al.*, Phys. Rev. Lett. **82**, 2422 (1999).

[83] L. Pricoupenko and M. Olshanii, cond-mat/0205210.

[84] P. O. Fedichev, M. W. Reynolds, and G. V. Shlyapnikov, Phys. Rev. Lett. **77**, 2921 (1996).

[85] B. D. Esry, C. H. Greene, and J. P. B. Jr., Phys. Rev. Lett. **83**, 1751 (1999).

[86] B. DeMarco and D. Jin, Science **285**, 1703 (1999).

[87] T. Loftus *et al.*, Phys. Rev. Lett. **88**, 173201 (2002).

[88] G. Roati, F. Riboli, G. Modugno, and M. Inguscio, Phys. Rev. Lett. **89**, 150403 (2002).

[89] G. Modugno *et al.*, Science **297**, 2240 (2002).

[90] A. Truscott *et al.*, Science **291**, 2570 (2001).

[91] S. Granade, M. E. Gehm, K. M. O'Hara, and J. E. Thomas, Phys. Rev. Lett. **88**, 120405 (2002).

[92] K. M. O'Hara *et al.*, Phys. Rev. A **66**, 041401(R) (2002).

[93] Z. Hadzibabic *et al.*, Phys. Rev. Lett. **88**, 160401 (2002).

[94] K. Dieckmann *et al.*, Phys. Rev. Lett. **89**, 203201 (2002).

[95] K. O'Hara *et al.*, Science **298**, 2179 (2002).

[96] K. Miyake, Progr. Theor. Phys. **69**, 1794 (1983).

[97] M. Randeria, J.-M. Duan, and L.-Y. Shieh, Phys. Rev. Lett. **62**, 981 (1989).

[98] S. Schmitt-Rink, C. M. Varma, and A. E. Ruckenstein, Phys. Rev. Lett. **63**, 445 (1989).

[99] M. Drechsler and W. Zwerger, Ann. Phys. **1**, 15 (1992).

[100] L. P. Gor'kov and T. K. Melik-Barkhudarov, Sov. Phys. JETP **13**, 1018 (1961).

[101] A. J. Leggett, Rev. Mod. Phys. **47**, 331 (1975).

[102] M. Randeria, *Bose-Einstein Condensation*, edited by A. Griffin, D. Snoke, and S. Stringari (Cambridge University Press, Cambridge, 1995).

[103] M. Y. Kagan, Sov. Phys. Uspekhi **37**, 69 (1994).

[104] D. M. Eagles, Phys. Rev. **186**, 456 (1969).

[105] A. J. Leggett, *Modern Trends in the Theory of Condensed Matter*, edited by A. Pekalski and J. Przystawa (Springer, Berlin, 1980).

[106] P. Nozieres and S. Schmitt-Rink, J. Low Temp. Phys. **59**, 195 (1985).

[107] M. Holland, S. J. J. M. F. Kokkelmans, M. L. Chiofalo, and R. Walser, Phys. Rev. Lett. **87**, 120406 (2001).

[108] E. Timmermans, K. Furuya, P. W. Milonni, and A. K. Kerman, Phys. Lett. A **285**, 228 (2001).

[109] D. S. Petrov, Phys. Rev. A **67**, 010703 (2003).

[110] D. J. Heinzen *et al.*, workshop on Cold Molecules, Les Houches, 2002.

[111] V. Efimov, Sov. J. Nucl. Phys. **12**, 589 (1971).

[112] V. Efimov, Nucl. Phys. A **210**, 157 (1973).

[113] E. Nielsen, D. V. Fedorov, and A. S. Jensen, Phys. Rev. A **56**, 3287 (1997).

[114] E. Tiesinga, A. J. Moerdijk, B. J. Verhaar, and H. T. C. Stoof, Phys. Rev. A **46**, R1167 (1992).

[115] E. Tiesinga, B. J. Verhaar, and H. T. C. Stoof, Phys. Rev. A **47**, 4114 (1993).

[116] S. Inouye *et al.*, Nature **392**, 151 (1998).

[117] P. Courteille *et al.*, Phys. Rev. Lett. **81**, 69 (1998).

[118] C. Chin, V. Vuletič, A. J. Kerman, and S. Chu, Phys. Rev. Lett. **85**, 2717 (2000).

[119] J. L. Roberts, N. R. Claussen, S. L. Cornish, and C. E. Wieman, Phys. Rev. Lett. **85**, 728 (2000).

[120] S. L. Cornish *et al.*, Phys. Rev. Lett. **85**, 1795 (2000).

[121] Y. Kagan, G. V. Shlyapnikov, I. A. Vartan'yantz, and N. A. Glukhov, JETP Lett. **35**, 477 (1982).

[122] P. J. Leo, C. J. Williams, and P. S. Julienne, Phys. Rev. Lett. **85**, 2721 (2000).

[123] V. Vuletić, private communication.

[124] J. Weiner, V. S. Bagnato, S. Zilio, and P. S. Julienne, Rev. Mod. Phys. **71**, 1 (1999).

[125] A. S. Davydov, *Quantum mechanics* (Pergamon, Oxford, 1976).

[126] P. O. Fedichev, M. W. Reynolds, U. M. Rahmanov, and G. V. Shlyapnikov, Phys. Rev. A **53**, 1447 (1996).

[127] L. Tonks, Phys. Rev. **50**, 955 (1936).

[128] C. N. Yang and C. P. Yang, J. Math. Phys. **10**, 1115 (1969).

[129] J. W. Kane and L. P. Kadanoff, J. Math. Phys. **6**, 1902 (1965).

[130] L. Reatto and G. V. Chester, Phys. Rev. **155**, 88 (1967).

[131] D. J. Scolapino, M. Sears, and R. A. Ferrell, Phys. Rev. B **6**, 3409 (1972).

[132] Y. Castin *et al.*, J. Mod. Opt. **47**, 2671 (2000).

[133] E. B. Sonin, Sov. Phys. JETP **32**, 773 (1971).

[134] Y. Kagan, N. V. Prokof'ev, and B. V. Svistunov, Phys. Rev. A **61**, 045601 (2000).

[135] J. Denschlag, D. Cassettari, and J. Schmiedmayer, Phys. Rev. Lett. **82**, 2014 (1999).

[136] M. Olshanii, Phys. Rev. Lett. **81**, 938 (1998).

[137] E. B. Kolomeisky, T. J. Newman, J. P. Straley, and X. Y. Qi, Phys. Rev. Lett. **85**, 1146 (2000).

[138] M. D. Girardeau and E. M. Wright, Phys. Rev. Lett. **84**, 5239 (2000).

[139] H. Monien, M. Linn, and N. Elstner, Phys. Rev. A **58**, R3395 (1998).

[140] J. H. Thywissen *et al.*, Eur. Phys. J. D **7**, 361 (1999).

[141] E. W. Hagley *et al.*, Science **283**, 1706 (1999).

[142] I. Bloch, T. W. Hänsch, and T. Esslinger, Nature (London) **403**, 166 (2000).

[143] J. Stenger *et al.*, Phys. Rev. Lett. **82**, 4569 (1999).

[144] U. Ernst *et al.*, Europhys. Lett. **41**, 1 (1998).

[145] K. Bongs *et al.*, Phys. Rev. Lett. **83**, 3577 (1999).

[146] J. Söding *et al.*, Appl. Phys. B **69**, 257 (1999).

[147] D. M. Stamper-Kurn *et al.*, Phys. Rev. Lett. **81**, 500 (1998).

[148] D. G. Fried *et al.*, Phys. Rev. Lett. **81**, 3811 (1998).

[149] K. Dieckmann, Ph.D. thesis, FOM Institute for Atomic and Molecular Physics, Amsterdam, 2001.

[150] N. J. van Druten and W. Ketterle, Phys. Rev. Lett. **79**, 549 (1997).

[151] S. Dettmer *et al.*, Phys. Rev. Lett. **87**, 160406 (2001).

[152] D. Hellweg *et al.*, Appl. Phys. B **73**, 781 (2001).

[153] F. Gerbier *et al.*, cond-mat/0210206.

Summary

This Thesis is devoted to theoretical investigation of trapped low-dimensional quantum gases.

In Chapter 2 we review theoretical grounds of the physics of degenerate low-dimensional Bose gases. We discuss Bose-Einstein condensation (BEC) in ideal low-dimensional gases, macroscopic description of an interacting quantum Bose gas, elementary excitations and their description in terms of Bogolyubov-de Gennes equations, phase fluctuations and coherence, and the phenomenon of quasicondenstaion.

Then, in Chapter 3 we investigate quasi-2D Bose and Fermi gases. In the first section we discuss BEC in quasi-2D trapped gases and arrive at two key conclusions. First, well below the temperature of quantum degeneracy T_d the phase fluctuations are small, and the equilibrium state is a true condensate. At intermediate temperatures the phase fluctuates on a distance scale smaller than the Thomas-Fermi size of the gas, and one has a quasicondensate. Second, in quasi-2D the coupling constant is sensitive to the frequency of the tight confinement ω_0 and, for negative 3D scattering length a, one can switch the mean-field interaction from attractive to repulsive by increasing ω_0.

In the second section of Chapter 3 we show that quasi-2D atomic Fermi gases can strongly compete with 3D gases in achieving superfluidity. In the regime of BCS pairing for weak attraction we calculate the critical temperature T_c to the second order in perturbation theory and analyze possibilities of increasing the ratio T_c/ε_F, where ε_F is the Fermi energy. In the opposite limit, where a strong coupling leads to the formation of weakly bound quasi-2D dimers, we find that the interaction between the dimers is repulsive and their collisional relaxation and decay are strongly suppressed. We thus conclude that a Bose-Einstein condensate of these composite bosons will be stable on a rather long time scale.

In Chapter 4 we consider a Bose gas tightly confined in one (axial) direction and discuss how the axial confinement manifests itself in elastic and inelastic pair collisions. We identify two regimes of scattering. At temperatures $T \ll \hbar\omega_0$ one has a quasi-2D regime in which the 2D character of the relative motion of particles manifests itself in a logarithmic energy dependence of the scattering amplitude. At temperatures $T \sim \hbar\omega_0$ we have a confinement-dominated 3D regime of scattering, where the 2D character of the particle motion is no longer pronounced in the scattering process, but the axial confinement can strongly influence the energy (temperature) dependence of the scattering rate. For a large 3D scattering length, the tight confinement provides a much weaker temperature dependence of the elastic collisional rate than in the 3D case and suppresses its resonant enhancement at low energies. We have employed our theory for explaining the Stanford and ENS experiments with tightly confined Cs clouds.

In Chapter 5 we discuss the regimes of quantum degeneracy in a trapped 1D gas with repulsive interparticle interaction. We find that the presence of a sharp crossover to the BEC regime requires extremely small interaction between particles. Otherwise, the decrease of temperature leads to a continuous transformation of a classical gas to a quantum degenerate. We identify three regimes at $T \ll T_d$. For a sufficiently large interparticle

interaction and the number of particles much smaller than a characteristic value N_*, at any $T \ll T_d$ one has a trapped Tonks gas characterized by a Fermi-gas density profile. For $N \gg N_*$ we have a weakly interacting gas. In this case we calculate the density and phase fluctuations and find that even well below T_d there is a quasicondensate. At very low T the long-wave fluctuations of the phase are suppressed due to a finite size of the system, and we have a true condensate. The true condensate and the quasicondensate have the same Thomas-Fermi density profile and local correlation properties, and we analyze how to distinguish between these BEC states in an experiment.

Finally, in Chapter 6, we show that phase coherence properties of 3D Thomas-Fermi condensates depend on their shape. In very elongated 3D condensates, the axial long-wave fluctuations of the phase manifest themselves even at temperatures far below the BEC transition temperature. Then the equilibrium state is a quasicondensate similar to that in 1D trapped gases. At sufficiently low temperatures, the 3D quasicondensate gradually transforms into a true condensate with decreasing T. In the second section we investigate the influence of equilibrium phase fluctuations on the density profile of an elongated 3D Thomas-Fermi condensate after switching off the trap. We find a relation between the phase fluctuations in the trap and density modulations in the expanding cloud. The results of this chapter have been used for explaining experiments with elongated condensates in Hannover and have been confirmed by experiments in Orsay.

Samenvatting

Dit proefschrift is gewijd aan de theoretische onderzoek van opgesloten laag-dimensionale kwantumgassen.

In hoofdstuk 2 geven we een overzicht van de theoretische basis van de natuurkunde van laag-dimensionale Bose gassen in het ontaarde kwantumgebied. We bespreken de Bose-Einstein-condensatie (BEC) van een ideaal gas in lage dimensies, de makroscopische beschrijving van een wisselwerkend kwantum Bose gas, de elementaire excitaties en hun beschrijving in termen van Bogolyubov-de-Gennes-vergelijkingen, de fase fluctuaties en de coherente eigenschappen van het condensaat, en het fenomeen van quasicondensatie.

Vervolgens, in hoofdstuk 3 onderzoeken we quasi-twee-dimensionale Bose en Fermi gassen. In het eerste deel bespreken we BEC in quasi-2D opgesloten gassen en komen tot twee sleutelconclusies. Ten eerste, de fase fluctueert weinig bij temperaturen veel lager dan de temperatuur T_d van de kwantum ontaarding. Bij tussenliggende temperaturen fluctueert de fase op een schaal kleiner dan de Thomas-Fermi lengte van het gas: men heeft een quasicondensaat. De tweede conclusie is dat in het quasi-2D geval de interactiekonstante gevoelig is voor de frequentie van de sterke opsluiting ω_0. Daarnaast kan men bij een systeem met negatieve 3D verstrooiingslengte a, de mean-field wisselwerking veranderen van aantrekkend tot afstotend door ω_0 te verhogen.

In het tweede deel van hoofdstuk 3 laten we zien dat atomaire quasi-2D Fermi gassen sterk met 3D gassen kunnen concureren als het gaat om het bereiken van superfluïditeit. In het geval van BCS paring bij zwakke aantrekking berekenen we de kritieke temperatuur T_c tot de tweede orde in storingsrekening en analyseren we de mogelijkheden om de ratio T_c/ε_F te vergroten; hier is ε_F de Fermi energie. In het tegenovergesteld geval, waarin sterke interactie tot vorming van zwak-gebonden quasi-2D dimeren leidt, vinden we dat de wisselwerking tussen de dimeren afstotend is en dat hun verval en relaxatie door botsingen sterk zijn onderdrukt. Wij concluderen daarom dat een Bose-Einstein condensaat van deze samengestelde bosonen over langere tijd stabiel zal zijn.

In hoofdstuk 4 beschouwen we een Bose gas, dat in één (axiale) richting sterk opgesloten is. Ook beschrijven wij hoe de axiale opsluiting zich in elastische en inelastische paarbotsingen uit. We identificeren twee verschillende verstrooiingsgebieden. Bij temperaturen van $T \ll \hbar\omega_0$ vindt men een quasi-2D gebied waarbij het 2D karakter van de relatieve beweging van deeltjes zichzelf manifesteert in een logaritmische energie afhankelijkheid van de verstrooiingsamplitude. Bij temperaturen $T \sim \hbar\omega_0$ vinden we een 3D regime waarbij de opsluiting het verstrooiingsgedrag domineert. Het 2D karakter van de deeltjesbeweging is dan niet meer belangrijk in het verstrooiingsproces, maar de energie (temperatuur) afhankelijkheid van de verstrooingsfrequentie zal sterk door de axial opsluiting worden beïnvloed. De nauwe opsluiting maakt de temperatuurafhankelijkheid van de elastische botsingsfrequentie voor grote 3D verstrooiingslengtes veel zwakker dan in het 3D geval. Ook wordt de resonante verstrooiing bij lage energieën onderdrukt. Wij hebben onze theorie toegepast op experimenten die op Stanford en bij de ENS zijn gedaan met sterk opgesloten Cs.

In hoofdstuk 5 bespreken we de gebieden van de kwantumontaarding in een opgeslo-

ten 1D gas met afstotende wisselwerking tussen de deeltjes. Wij vinden dat voor een scherpe BEC-overgang de wisselwerking tussen de atomen bijzonder zwak moet zijn. In het tegenovergesteld geval lijdt de verlaging van de temperatuur tot een onafgebroken vervorming van een klassiek tot een kwantum ontaard gas. We onderscheiden drie gebieden voor $T \ll T_d$. Als de wisselwerking tussen de deeltjes sterk genoeg is en het aantal atomen veel kleiner is dan de karakteristieke waarde N_*, dan heeft men een opgesloten Tonks gas voor willekeurige $T \ll T_d$. Het Tonks gas heeft een dichtheidprofiel gelijk aan die van een ideaal Fermi gas. Voor $N \gg N_*$ hebben wij een zwak wisselwerkende gas. Voor dit geval berekenen we de dichtheid en fase fluctuaties. Wij vinden dat men zelfs voor temperaturen ver onder T_d een quasicondensaat krijgt. Voor zeer lage temperaturen T zijn de langegolf fluctuaties van de fase onderdrukt wegens de eindige lengte van het systeem. Dit resulteert in een echt condensaat. Het echte condensaat en het quasicondensaat hebben dezelfde Thomas-Fermi dichtheidsprofielen en lokale correlatie eigenschappen. Wij analyseren hoe men het verschil tussen deze BEC-toestanden in een experiment zichtbaar kan maken.

Tenslotte, in hoofdstuk 6 laten we zien dat fase coherente eigenschappen van een 3D Thomas-Fermi condensaat afhankelijk zijn van zijn vorm. In zeer lange 3D condensaten manifesteren de axiale langegolf fase fluctuaties zich bij temperaturen veel lager dan de kritieke temperatuur voor BEC. Het thermische evenwicht van het systeem is dan een quasicondensaat vergelijkbaar met 1D opgesloten gassen. Voor voldoende lage temperaturen vervormt het 3D condensaat geleidelijk tot een echt condensaat met kleiner wordende T. In het tweede deel onderzoeken we hoe de fase fluctuaties van de evenwichtstoestand het dichtheidsprofiel van een lang 3D Thomas-Fermi condensaat beïnvloeden na het uitzetten van de val. Wij vinden een relatie tussen de fase fluctuaties die de wolk had tijdens de opsluiting in de val en de dichtheidsmodulaties van de expanderende wolk. De resultaten van dit hoofdstuk zijn gebruikt om experimenten met lange condensaten in Hannover te verklaren. Ook zijn deze resultaten door experimenten in Orsay bevestigd.

Acknowledgments

There is quite a number of people that contributed to this Thesis either explicitly or implicitly.

I was lucky to have been doing physics under the guidance of two outstanding scientists – Gora Shlyapnikov and Jook Walraven. Thanks to them I gained an invaluable experience from which I will benefit in the years to come.

It was a gift to share an office with a very good friend Igor Shvarchuck. I much appreciated his company and support. Thank you, Igor.

I will never forget a friendly atmosphere of the Quantum Gases group at AMOLF. Kai Dieckmann, Martin Zielonkowski, Wolf von Klitzing, Christian Buggle, Lorenzo Vichi, Mark Kemmann, Tobias Tiecke and Imogen Colton greatly helped my research. I wish them all good luck.

Colleagues from the neighboring office were always open for my questions. Ruediger Lang helped me with TeX and provided me with a useful information which affected the style of this book. I am grateful to Annemieke Petrignani for the translation of the summary of this Thesis into Dutch.

Infrastructure of AMOLF and people working there made the institute a perfect place to do research. I thank our travel and accommodation guru Roudy van der Wijk for her kindness and for a wonderful apartment that she found for me. Thanks to personnel officers Wouter Harmsen and Daniëlle de Vries I was never lost in the labyrinth of dutch bureaucracy. Jan van Elst helped me a lot with Linux configuration.

During my PhD period I enjoyed the good company of many people all over the world. In particular, I would like to thank colleagues with whom I worked on various projects or just discussed physics. These are Isabelle Bouchoule, Christophe Salomon, Yvan Castin, Subhasis Sinha, Jean Dalibard, David Guery-Odélin, Maciej Lewenstein, Luis Santos, Jason Ho, Yuri Kagan, Boris Svistunov, Maxim Olshanii, Allard Mosk, Markus Holzmann, Klaus Sengstock, Jan Arlt and many others. Conversations with my friends Peter Fedichev, Misha Baranov and Andrey Muryshev always brought fresh waves of motivation.

With great pleasure I recollect the times of fishing, playing tennis, and cycling to the seaside with Pavel Bouchev, Peter Fedichev and Yaroslav Usenko. It was a real pity that Pavel and Peter moved to Innsbruck. However, thanks to them we spent a marvelous skiing vacation in Austria.

I am infinitely grateful to my parents Sergei and Tatiana and my wife Anna for their enormous tolerance and encouragement. It would not be an exaggeration to say that without their help this Thesis would have never been written.